

Supporting Information

Analyses of Sizable ZFS and Magnetic Tensors of High Spin Metallo-porphyrins, Fe^{III}(Cl)OEP and Co^{II}OEP and A Pseudo-Octahedral Re^{III,IV} Dinuclear Complexes by X-Band CW/Pulsed ESR and Electron Spin Nutation Spectroscopy: Exact Analytical and Zeeman Perturbation Treatments, and Quantum Chemical Calculations

Takeshi Yamane,^a Kenji Sugisaki,^a Tomoki Nakagawa,^a Hideto Matsuoka,^{a,#} Takahisa Nishio,^a Shigemori Kinjyo,^a Nobuyuki Mori,^a Satoshi Yokoyama,^a Chika Kawashima,^a Naoki Yokokura,^a Kazunobu Sato,^{a,*} Yuki Kanzaki,^a Daisuke Shiomi,^a Kazuo Toyota,^a David H. Dolphin,^b Wei-Ching Lin,^b the late Charles A. McDowell,^b Makoto Tadokoro,^c and Takeji Takui,^{a,d,*}

^aDepartment of Chemistry and Molecular Materials Science, Graduate School of Science, Osaka City University, Osaka 558-8585, Japan

^bDepartment of Chemistry, The University of British Columbia, Vancouver, British Columbia, V6T 1Z1 Canada

^cDepartment of Chemistry, Tokyo University of Science, Tokyo 162-0825, Japan

^dResearch Support/URA Center, University Administration Department, Osaka City University, 3-3-138 Sugimoto, Sumiyoshi-ku, Osaka 558-8585, Japan

[#]Present Address: Institute of Physical and Theoretical Chemistry, University of Bonn, Wegelerstrasse 12, 53115 Bonn, Germany

E-mail: sato@sci.osaka-cu.ac.jp, takui@sci.osaka-cu.ac.jp

Contents

1. Analytical formulas for spin-triplet states

1.1 Derivation of the $g^{\text{eff}}-g^{\text{true}}$ relationships as a function of $|E/D|$ in spin-triplet states ($S = 1$)..... S4

1.2 The $g^{\text{eff}}-g^{\text{true}}$ relationships by using of the genuine Zeeman perturbation approach in the case of spin-triplet states ($S = 1$)..... S7

2. Analytical formulas for spin-quartet states

2.1 Derivation of the $g^{\text{eff}}-g^{\text{true}}$ relationships as a function of $|E/D|$ in spin-quartet states ($S = 3/2$)..... S9

2.2 The $g^{\text{eff}}-g^{\text{true}}$ relationships by using of the genuine Zeeman perturbation approach in the case of spin-quartet states ($S = 3/2$)..... S12

2.3 Global permutation rules for the ZFS energy in the case of $S = 3/2$ S14

3. Analytical formula for spin-quintet states

3.1 Derivation of the $g^{\text{eff}}-g^{\text{true}}$ relationships as a function of $|E/D|$ in spin-quintet case ($S = 2$)..... S15

3.2 The $g^{\text{eff}}-g^{\text{true}}$ relationships by using of the genuine Zeeman perturbation approach in the case of spin-quintet states ($S = 2$) S18

3.3 Global permutation for the ZFS energies in the case of $S = 2$ S21

4. Analytical formulas for spin-sextet states

4.1 Derivation of the $g^{\text{eff}}-g^{\text{true}}$ relationships as a function of $|E/D|$ in spin-sextet case ($S = 5/2$) S22

4.2 The $g^{\text{eff}}-g^{\text{true}}$ relationships by using of the genuine Zeeman perturbation approach in the case of spin-sextet case ($S = 5/2$).....	S24
4.3 Global permutation rules for the ZFS energy in the case of $S = 5/2$	S32
4.4 Derivation of approximate $g^{\text{eff}}-g^{\text{true}}$ relationships in the spin sextet case ($S = 5/2$)	S33
5. Analytical formulas for spin-septet states	
5.1 Derivation of the $g^{\text{eff}}-g^{\text{true}}$ relationships as a function of $ E/D $ in spin-septet states ($S = 3$)	S36
5.2 The $g^{\text{eff}}-g^{\text{true}}$ relationships by using of the genuine Zeeman perturbation approach in the case of spin-septet states ($S = 3$).....	S39
5.3 Global permutation for ZFS energy in the case of $S = 3$	S44
6. Analytical formulas for spin-octet states	
6.1 Derivation of the $g^{\text{eff}}-g^{\text{true}}$ relationships as a function of $ E/D $ in spin-octet states ($S = 7/2$).....	S46
6.2 The $g^{\text{eff}}-g^{\text{true}}$ relationships by using of the genuine Zeeman perturbation approach in the case of spin-octet case ($S = 7/2$)	S49
7. Single-crystal cw ESR/ENDOR and pulsed ESR spectroscopy of Fe^{III}(Cl)OEP	
7.1 Angular dependence of cw ESR spectra of Fe ^{III} (Cl)OEP diluted in Ni ^{II} OEP single-crystals in the crystallographic <i>abc</i> axis system.....	S53
7.2 Typical ESR spectra of Fe ^{III} (Cl)OEP observed at liquid helium temperature.....	S54
7.3 Temperature dependence of the spin-lattice relaxation time T_1 of Fe ^{III} (Cl)OEP determined by an inversion recovery method based on pulsed ESR spectroscopy.....	S55
7.4 Angular dependences of both the spin-lattice relaxation time T_1 and spin-spin relaxation time T_2 of Fe ^{III} (Cl)OEP	S56
7.5 ¹⁴ N-ENDOR spectroscopy of Fe ^{III} (Cl)OEP diluted in Ni ^{II} OEP single-crystals	S57
7.6 Pulse-based electron spin nutation spectroscopy of Fe ^{III} (Cl)OEP diluted in Ni ^{II} OEP single-crystal	S58
8. Single-crystal and powder-pattern ESR spectroscopy of Co^{II}OEP diluted in diamagnetic Ni^{II}OEP single crystals	
8.1 Principal values and direction cosine of the magnetic tensors of Co ^{II} OEP experimentally determined by the fictitious spin-1/2 Hamiltonian approach	S60
8.2 Principal values and direction cosine of the magnetic tensors of ¹⁴ N nuclei of Co ^{II} OEP experimentally determined by the fictitious spin-1/2 Hamiltonian approach	S61
8.3 Angular dependence of the ESR spectra of Co ^{II} OEP with the static magnetic field in the principal <i>zx</i> plane; Simulated in terms of the fictitious spin and ZFS/e-Zeeman spin Hamiltonian parameters.....	S63
8.4 Simulation of the powder-pattern fine-structure/hyperfine ESR spectra of Co ^{II} OEP/Ni ^{II} OEP	S67
8.5 Simulation of the powder-pattern ESR spectra composed of the forbidden transitions of Co ^{II} OEP/Ni ^{II} OEP.....	S68
8.6 The powder-pattern ESR spectra observed at a liquid nitrogen temperature showing the dynamic Jahn-Teller distortion	S69

8.7 2D electron spin transient nutation spectroscopy of Co ^{II} OEP diluted in the Ni ^{II} OEP single-crystal	S70
9. Single-crystal ESR spectroscopy of a Re^{III,IV} dinuclear complex	
9.1 ESR experiments in the principal-axis system of the Re ^{III,IV} dinuclear complex	S71
9.2 Angular dependence of the single-crystal ESR spectra of the Re ^{III,IV} dinuclear complex.....	S72
9.3 Magnetic measurement (<i>M-H</i> plot) for the Re ^{III,IV} dinuclear complex.....	S73
10. Quantum chemical calculations for magnetic tensors	
10.1 Quantum chemical calculations for the spin Hamiltonian parameters of Fe ^{III} (Cl)OEP and Co ^{II} OEP	S74
10.2 Quantum chemical calculations for the spin Hamiltonian parameters of Re ^{IV} -monomer	S79
11. Experiments	S81
References	S82

1. Analytical formulas for spin-triplet states

1.1 Derivation of the $g^{\text{eff}}-g^{\text{true}}$ relationships as a function of $|E/D|$ in spin-triplet states ($S = 1$)

The spin Hamiltonian having electron-Zeeman (abbreviated to eZ) and zero-field splitting (ZFS) terms is given in the matrix form as follows;

$$\mathcal{H}_{\text{ZFS+eZ}} = \tilde{\mathbf{S}} \cdot \mathbf{D} \cdot \mathbf{S} + \beta \tilde{\mathbf{S}} \cdot \mathbf{g} \cdot \mathbf{B}$$

where \mathbf{S} is a spin operator, \mathbf{g} and \mathbf{D} denote the \mathbf{g} - and \mathbf{D} -tensor, respectively, and β is the Bohr magneton and \mathbf{B} is an external magnetic field. In the principal axis system, this Hamiltonian (termed as ZFS/e-Zeeman spin Hamiltonian in MS) can be represented by using of the zero-field splitting parameters D and E and the components of \mathbf{S} , \mathbf{g} and \mathbf{B} as

$$\mathcal{H}_{\text{ZFS+eZ}} = D[S_z^2 - S(S+1)/3] + E(S_x^2 - S_y^2) + \beta(g_x S_x B_x + g_y S_y B_y + g_z S_z B_z),$$

where the collinearity between the tensors is assumed.

In the triplet case with the static magnetic field along the principal z -axis, the matrix representation of $\mathcal{H}_{\text{ZFS+eZ}}$ is as follows;

$$H_{\text{ZFS+eZ}}^{\text{triplet}} = \begin{pmatrix} \langle +1| & \langle 0| & \langle -1| \\ \frac{D}{3} + g_z^{\text{true}} \beta B & 0 & E \\ 0 & -\frac{2D}{3} & 0 \\ E & 0 & \frac{D}{3} - g_z^{\text{true}} \beta B \end{pmatrix} \begin{matrix} | +1 \rangle \\ | 0 \rangle \\ | -1 \rangle \end{matrix}$$

The number in the bra-kets denotes M_S ($M_S = S, S-1, \dots, -S$; S is a spin quantum number of the system under study). The diagonalized eigenenergies E_{M_S} and corresponding wavefunctions Ψ_{M_S} are in the following.

$$E_{+1} = \frac{D}{3} + \sqrt{E^2 + (g_z^{\text{true}} \beta B)^2} \quad (\text{S1a})$$

$$E_{-1} = \frac{D}{3} - \sqrt{E^2 + (g_z^{\text{true}} \beta B)^2} \quad (\text{S1b})$$

$$E_0 = -\frac{2D}{3} \quad (\text{S1c})$$

$$\Psi_{+1} = \left(\sqrt{E^2 + (g_z^{\text{true}} \beta B)^2} + g_z^{\text{true}} \beta B \right) | +1 \rangle + E | -1 \rangle \quad (\text{S2a})$$

$$\Psi_{-1} = -E | +1 \rangle + \left(\sqrt{E^2 + (g_z^{\text{true}} \beta B)^2} + g_z^{\text{true}} \beta B \right) | -1 \rangle \quad (\text{S2b})$$

$$\Psi_0 = | 0 \rangle \quad (\text{S2c})$$

Equalizing the energy difference between E_{+1} and E_{-1} to $g_z^{\text{eff}} \beta B$ gives

$$E_{+1} - E_{-1} = 2\sqrt{E^2 + (g_z^{\text{true}} \beta B)^2} = g_z^{\text{eff}} \beta B$$

$$4E^2 + 4(g_z^{\text{true}} \beta B)^2 = (g_z^{\text{eff}} \beta B)^2, \quad (\text{S3})$$

where g_z^{eff} denotes the effective g_z -value. Comparing the coefficient of equation (S3) with respect to B , we obtain $g_z^{\text{eff}}/g_z^{\text{true}} = 2$ if and only if $E = 0$. Otherwise the general relationship of $g_z^{\text{eff}}/g_z^{\text{true}}$ does not hold.

It is worth calculating the transition probability $|\langle \Psi_{-M_S} | S_i | \Psi_{+M_S} \rangle|^2$ ($i = x, y, z$) between the $M_S = \pm 1$ dominant transition. According to the spin functions, only S_z components have non-zero values;

$$|\langle \Psi_{-1} | S_z | \Psi_{+1} \rangle|^2 = \frac{4E^2}{N^4} \left(\sqrt{E^2 + (g_z^{\text{true}} \beta B)^2} + g_z^{\text{true}} \beta B \right)^2,$$

where N denotes the normalization factor.

When the magnetic field is along the x -axis, the energy eigenvalues and eigenfunctions are given by exploiting the cyclic permutation relationship between the principal axes, ^[S1-S4]

$$E_{x,+1} = \frac{1}{6}(3E - D) + \frac{1}{2} \sqrt{(E + D)^2 + 4(g_x^{\text{true}} \beta B)^2} \quad (\text{S4a})$$

$$E_{x,-1} = \frac{1}{6}(3E - D) - \frac{1}{2} \sqrt{(E + D)^2 + 4(g_x^{\text{true}} \beta B)^2} \quad (\text{S4b})$$

$$E_{x,0} = \frac{D}{3} - E \quad (\text{S4c})$$

$$\Psi_{x,+1} = | +1 \rangle - \frac{E + D - \sqrt{(E + D)^2 + 4(g_x^{\text{true}} \beta B)^2}}{\sqrt{2} g_x^{\text{true}} \beta B} | 0 \rangle + | -1 \rangle \quad (\text{S5a})$$

$$\Psi_{x,-1} = | +1 \rangle - \frac{E + D + \sqrt{(E + D)^2 + 4(g_x^{\text{true}} \beta B)^2}}{\sqrt{2} g_x^{\text{true}} \beta B} | 0 \rangle + | -1 \rangle \quad (\text{S5b})$$

$$\Psi_{x,0} = | +1 \rangle - | -1 \rangle \quad (\text{S5c})$$

where the subscripts $\pm 1, 0$ are taken over from those of the eigenenergies/eigenfunctions with the principal z -axis, and the normalization factor was omitted for simplicity. To equalize the energy difference between $E_{x,\pm 1}$ to $g_x^{\text{eff}} \beta B$,

$$E_{x,+1} - E_{x,-1} = \sqrt{(E + D)^2 + 4(g_x^{\text{true}} \beta B)^2} = g_x^{\text{eff}} \beta B$$

$$(E + D)^2 + 4(g_x^{\text{true}} \beta B)^2 = (g_x^{\text{eff}} \beta B)^2. \quad (\text{S6})$$

In this case, there is no special solution in the range of $0 \leq E/D \leq 1/3$.

Under $\mathbf{B} // x$, the transition probability $|\langle \Psi_{-M_S} | S_i | \Psi_{+M_S} \rangle|^2$ ($i = x, y, z$) between the $M_S = \pm 1$ dominant transition is different from that in $\mathbf{B} // z$.

$$|\langle \Psi_{x,-1} | S_x | \Psi_{x,+1} \rangle|^2 = \frac{1}{N'^4} \left[\frac{3E + 3D + \sqrt{(E + D)^2 + 4(g_x^{\text{true}} \beta B)^2}}{2B} \right]^2,$$

where N' denotes the normalization factor.

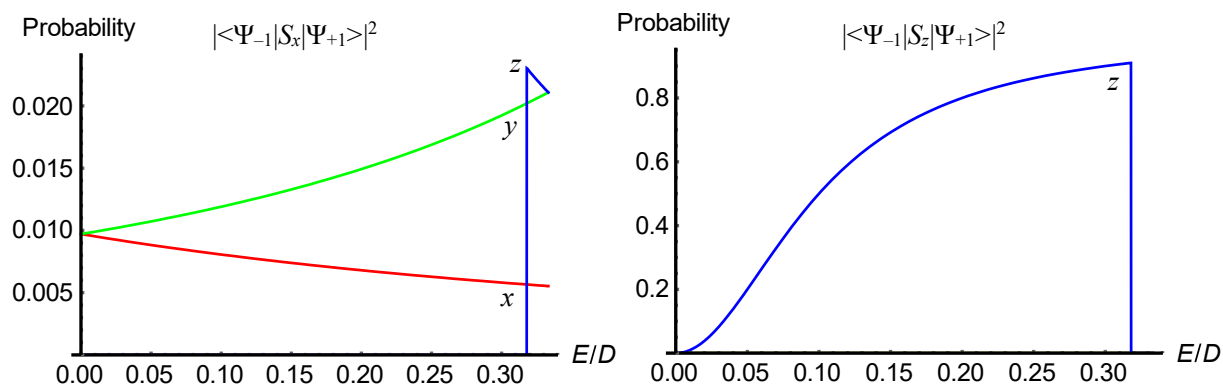


Figure S1 Transition probabilities between the $|M_S = \pm 1\rangle$ -dominant transitions for the principal axes. ($g^{\text{true}}\beta B/D = 0.1$) Transition probabilities for the parallel transition (right) in the case of $B//x$ or y are zero for all the range of E/D .

1.2 The g^{eff} - g^{true} relationships by using of the genuine Zeeman perturbation approach in the case of spin-triplet states ($S = 1$)

In the genuine Zeeman perturbation approach, the ZFS Hamiltonian ($\mathcal{H}_{\text{ZFS}} = \tilde{\mathbf{S}} \cdot \mathbf{D} \cdot \mathbf{S}$) is taken as the unperturbed term and the others (here only the electron-Zeeman Hamiltonian, $\mathcal{H}_{eZ} = \beta \tilde{\mathbf{S}} \cdot \mathbf{g} \cdot \mathbf{B}$) are considered as the perturbed term. Based on this procedure, we derive the perturbed energies to the second order. The unperturbed Hamiltonian and the corresponding matrix representation ($H_{\text{ZFS}}^{\text{triplet}}$) in the $|M_S\rangle$ basis are

$$H_{\text{ZFS}}^{\text{triplet}} = \begin{pmatrix} \langle +1| & \langle 0| & \langle -1| \\ \frac{D}{3} & 0 & E \\ 0 & -\frac{2D}{3} & 0 \\ E & 0 & \frac{D}{3} \end{pmatrix} \begin{matrix} | +1\rangle \\ | 0\rangle \\ | -1\rangle \end{matrix}$$

The eigenenergies $\varepsilon_{M_S}^{(0)}$ and the eigenfunctions $\varphi_{M_S}^{(0)}$ are

$$\varepsilon_{+1}^{(0)} = \frac{D}{3} + E, \quad \varphi_{+1}^{(0)} = \frac{|+1\rangle + |-1\rangle}{\sqrt{2}} \quad (\text{S7a})$$

$$\varepsilon_{-1}^{(0)} = \frac{D}{3} - E, \quad \varphi_{-1}^{(0)} = \frac{|+1\rangle - |-1\rangle}{\sqrt{2}} \quad (\text{S7b})$$

$$\varepsilon_0^{(0)} = -\frac{2D}{3}, \quad \varphi_0^{(0)} = |0\rangle. \quad (\text{S7c})$$

The electron-Zeeman term expanded with the new basis $\{\varphi_{M_S}^{(0)}\}$ are with \mathbf{B}/z

$$H_{eZ}^{\text{triplet}} = g_z^{\text{true}} \beta B \begin{pmatrix} 1 & 0 & 0 \\ 0 & 0 & 0 \\ 0 & 0 & -1 \end{pmatrix} \rightarrow H'_{eZ} = g_z^{\text{true}} \beta B \begin{pmatrix} 0 & 0 & 1 \\ 0 & 0 & 0 \\ 1 & 0 & 0 \end{pmatrix}$$

Since the perturbed electron-Zeeman Hamiltonian includes only non-diagonal terms, the interaction with respect to the magnetic field will be taken to the second-order energy.

$$E'_{+1} = \frac{D}{3} + E + \frac{(g_z^{\text{true}} \beta B)^2}{2E} \quad (\text{S8a})$$

$$E'_{-1} = \frac{D}{3} - E - \frac{(g_z^{\text{true}} \beta B)^2}{2E} \quad (\text{S8b})$$

In a similar manner to the exact treatment, the g_z^{eff} - g_z^{true} relationship is obtained.

$$E'_{+1} - E'_{-1} = 2E + \frac{(g_z^{\text{true}} \beta B)^2}{E} = g_z^{\text{eff}} \beta B$$

$$g_z^{\text{eff}} \beta B E = 2E^2 + (g_z^{\text{true}} \beta B)^2 \quad (\text{S9})$$

Comparing the coefficient in Equation (S9) does not give any general and specific g_z^{eff} - g_z^{true} relationship.

The permutation of the subscripts x, y, z gives rise to the following ZFS formulas.

$$-\frac{2D}{3} \xrightarrow{\mathbf{B}\parallel x} -\frac{2}{3} \left[\frac{1}{2} (3E - D) \right] = \frac{D}{3} - E$$
$$-\frac{2D}{3} \xrightarrow{\mathbf{B}\parallel y} -\frac{2}{3} \left[-\frac{1}{2} (3E + D) \right] = \frac{D}{3} + E$$

2. Analytical formulas for spin-quartet states

2.1 Derivation of the g^{eff} - g^{true} relationships as a function of $|E/D|$ in spin-triplet states ($S = 3/2$)

The spin Hamiltonian in the presence of the electron-Zeeman term is represented in the matrix form in the principal-axis system with \mathbf{B}/z as follows;

$$H_{eZ+ZFS}^{\text{quartet}} = \begin{pmatrix} \langle +3/2 | & \langle +1/2 | & \langle -1/2 | & \langle -3/2 | \\ D + \frac{3}{2}g_z^{\text{true}}\beta B & 0 & \sqrt{3}E & 0 \\ 0 & -D + \frac{1}{2}g_z^{\text{true}}\beta B & 0 & \sqrt{3}E \\ \sqrt{3}E & 0 & -D - \frac{1}{2}g_z^{\text{true}}\beta B & 0 \\ 0 & \sqrt{3}E & 0 & D - \frac{3}{2}g_z^{\text{true}}\beta B \end{pmatrix} \begin{matrix} | +3/2 \rangle \\ | +1/2 \rangle \\ | -1/2 \rangle \\ | -3/2 \rangle \end{matrix}$$

This matrix can be divided into two 2×2 conjugate matrixes in which the basis set is $\{|+3/2\rangle, |-1/2\rangle\}$ (and $\{|-3/2\rangle, |+1/2\rangle\}$):

$$H_{eZ+ZFS,1}^{\text{quartet}} = \begin{pmatrix} \langle +3/2 | & \langle -1/2 | \\ D + \frac{3}{2}g_z^{\text{true}}\beta B & \sqrt{3}E \\ \sqrt{3}E & -D - \frac{1}{2}g_z^{\text{true}}\beta B \end{pmatrix} \begin{matrix} | +3/2 \rangle \\ | -1/2 \rangle \end{matrix}$$

For the basis of $\{|-3/2\rangle, |+1/2\rangle\}$, the sign of the Zeeman terms are required to change. The diagonalized eigenenergies and eigenfunctions for the former conjugate matrix are

$$E_{+\frac{3}{2}} = \frac{1}{2}g_z^{\text{true}}\beta B + \sqrt{(D + g_z^{\text{true}}\beta B)^2 + 3E^2}, \quad \Psi_{+\frac{3}{2}} = \cos \theta_+ \left| +\frac{3}{2} \right\rangle + \sin \theta_+ \left| -\frac{1}{2} \right\rangle \quad (\text{S10a})$$

$$E_{-\frac{1}{2}} = \frac{1}{2}g_z^{\text{true}}\beta B - \sqrt{(D + g_z^{\text{true}}\beta B)^2 + 3E^2}, \quad \Psi_{-\frac{1}{2}} = \cos \theta_+ \left| -\frac{1}{2} \right\rangle - \sin \theta_+ \left| +\frac{3}{2} \right\rangle \quad (\text{S10b})$$

where

$$\tan 2\theta_+ = \frac{\sqrt{3}E}{D + g_z^{\text{true}}\beta B}$$

Algebraic expressions without trigonometric functions are available for accurate numerical computations.

It should be noted that E_{M_S} denotes the energy eigenvalue of the M_S -sublevel dominant admixed state in the presence of the Zeeman terms. The other eigenvalues corresponding to the latter conjugate spin states $\{|-3/2\rangle, |+1/2\rangle\}$ are derived by replacing B with $-B$. This arises from the intrinsic nature of double-groups to which half-integer spins belong. Equalizing the energy differences between $|\pm 3/2\rangle$ states to $g_z^{\text{eff}}\beta B$ gives

$$E_{+\frac{3}{2}} - E_{-\frac{3}{2}} = g_z^{\text{true}}\beta B + \sqrt{(D + g_z^{\text{true}}\beta B)^2 + 3E^2} - \sqrt{(D - g_z^{\text{true}}\beta B)^2 + 3E^2} = g_z^{\text{eff}}\beta B$$

$$\sqrt{(D + g_z^{\text{true}}\beta B)^2 + 3E^2} - \sqrt{(D - g_z^{\text{true}}\beta B)^2 + 3E^2} = (g_z^{\text{eff}} - g_z^{\text{true}})\beta B.$$

Squaring the both side and collecting the terms with the integer indices of B .

$$\begin{aligned}
& 2D^2 + 6E^2 + 2(g_z^{\text{true}}\beta B)^2 - (g_z^{\text{eff}} - g_z^{\text{true}})^2(\beta B)^2 \\
& = 2\sqrt{(D + g_z^{\text{true}}\beta B)^2 + 3E^2}\sqrt{(D - g_z^{\text{true}}\beta B)^2 + 3E^2}
\end{aligned}$$

Then, we obtain the following.

$$\begin{aligned}
& \left[2D^2 + 6E^2 + 2(g_z^{\text{true}}\beta B)^2 - (g_z^{\text{eff}} - g_z^{\text{true}})^2(\beta B)^2\right]^2 \\
& = 4[(D + g_z^{\text{true}}\beta B)^2 + 3E^2][(D - g_z^{\text{true}}\beta B)^2 + 3E^2] \\
(D^2 + 3E^2)(g_z^{\text{eff}})^2 - 2(D^2 + 3E^2)g_z^{\text{eff}}g_z^{\text{true}} - 3(D^2 - E^2)(g_z^{\text{true}})^2 & = 0 \\
\frac{g_z^{\text{eff}}}{g_z^{\text{true}}} & = \frac{D^2 + 3E^2 \pm 2D\sqrt{D^2 + 3E^2}}{D^2 + 3E^2} \\
& = 1 \pm \frac{2D}{\sqrt{D^2 + 3E^2}} \\
& = 1 \pm \frac{2}{\sqrt{1 + 3\lambda^2}} \tag{S11}
\end{aligned}$$

where $\lambda = E/D$. For the other principal-axis orientations, as well known, the cyclic permutation of the subscripts for the axes, $D_z \rightarrow D_x, D_x \rightarrow D_y, D_y \rightarrow D_z$ gives the corresponding values and functions; i.e., for the static magnetic field \mathbf{B} parallel to the principal x -axis, the transformation of $D \rightarrow 1/2(3E - D)$ and $E \rightarrow -1/2(E + D)$, and for \mathbf{B}/y , $D \rightarrow -1/2(3E + D)$ and $E \rightarrow 1/2(E - D)$ under the definition of the D - and E -values give the corresponding expressions, respectively.^[S1-S4]

It is worth calculating the transition probabilities of the $|M_S = \pm 1/2\rangle$ and $|\pm 3/2\rangle$ -dominant transitions. We consider only the ‘‘quantum-mechanical/group-theoretic’’ transition probabilities $P_{M_S} = |\langle \Psi_{-M_S} | S_x | \Psi_{+M_S} \rangle|^2$ and exclude the Boltzmann factor depending on the energy differences for simplicity. For the $|M_S = \pm 1/2\rangle$ -dominant transition,

$$\begin{aligned}
P_{\pm\frac{1}{2}} & = \left[\left(\cos \theta_- \left\langle +\frac{1}{2} \right| - \sin \theta_- \left\langle -\frac{3}{2} \right| \right) \left(S_x \cos \theta_+ \left| -\frac{1}{2} \right\rangle - S_x \sin \theta_+ \left| +\frac{3}{2} \right\rangle \right) \right]^2 \\
& = \left[\left(\cos \theta_- \left\langle +\frac{1}{2} \right| - \sin \theta_- \left\langle -\frac{3}{2} \right| \right) \left(2 \cos \theta_+ \left| +\frac{1}{2} \right\rangle + \frac{\sqrt{3}}{2} \cos \theta_+ \left| -\frac{3}{2} \right\rangle - \frac{\sqrt{3}}{2} \sin \theta_+ \left| +\frac{1}{2} \right\rangle \right) \right]^2 \\
& = \left[2 \cos \theta_+ \cos \theta_- - \frac{\sqrt{3}}{2} \sin \theta_+ \cos \theta_- - \frac{\sqrt{3}}{2} \cos \theta_+ \sin \theta_- \right]^2,
\end{aligned}$$

and for the $|M_S = \pm 3/2\rangle$ -dominant transition,

$$\begin{aligned}
P_{\pm\frac{3}{2}} & = \left[\left(\cos \theta_- \left\langle -\frac{3}{2} \right| + \sin \theta_- \left\langle +\frac{1}{2} \right| \right) \left(S_x \cos \theta_+ \left| +\frac{3}{2} \right\rangle + S_x \sin \theta_+ \left| -\frac{1}{2} \right\rangle \right) \right]^2 \\
& = \left[\left(\cos \theta_- \left\langle -\frac{3}{2} \right| + \sin \theta_- \left\langle +\frac{1}{2} \right| \right) \left(\frac{\sqrt{3}}{2} \cos \theta_+ \left| +\frac{1}{2} \right\rangle + 2 \sin \theta_+ \left| +\frac{1}{2} \right\rangle + \frac{\sqrt{3}}{2} \sin \theta_+ \left| -\frac{3}{2} \right\rangle \right) \right]^2
\end{aligned}$$

$$= \left[2 \sin \theta_+ \sin \theta_- + \frac{\sqrt{3}}{2} \sin \theta_+ \cos \theta_- + \frac{\sqrt{3}}{2} \cos \theta_+ \sin \theta_- \right]^2,$$

where the definition for θ_+ has already been given above and

$$\tan 2\theta_- = \frac{\sqrt{3}E}{D - g_z^{\text{true}}\beta B}$$

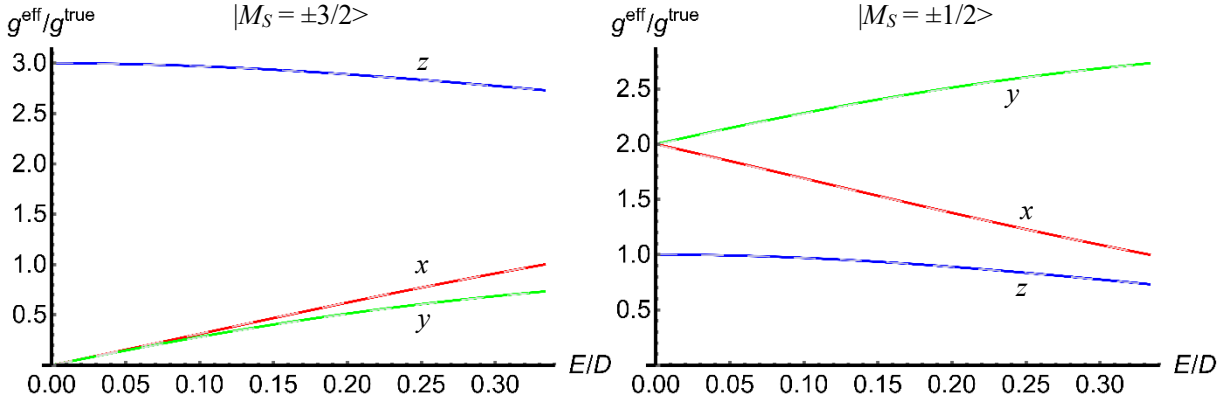


Figure S2 The $g^{\text{eff}}/g^{\text{true}}$ relationships as a function of the ratios of $|E/D|$ for $S = 3/2$. The subscripts, x , y and z denote the principal axes of the \mathbf{g} - and ZFS tensors. The curves of the exact relationships are given in the solid lines. Those derived by the genuine Zeeman perturbation treatment to the second order are depicted in the broken curves. There is no discrepancy between the exact and genuine Zeeman perturbation treatments for $S = 3/2$, as described in the text.

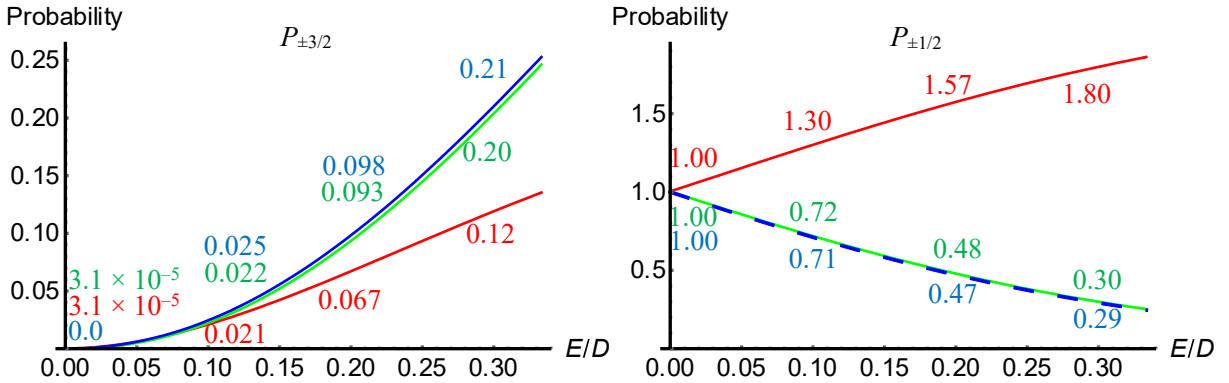


Figure S3 Transition probabilities between the $\pm M_S$ dominant transitions, $|\langle \Psi_{-M_S} | S_x | \Psi_{+M_S} \rangle|^2$ calculated with equations in the text for $g^{\text{true}}\beta B/D = 0.1$. In the right figure, the line for $\mathbf{B} // z$ is broken for clarity.

2.2 The $g^{\text{eff}}-g^{\text{true}}$ relationships by using of the genuine Zeeman perturbation approach in the case of spin-quartet states ($S = 3/2$)

The perturbed energies and wavefunctions for the spin-quartet case were discussed by Pilbrow.^[S5] The matrix representation of the ZFS Hamiltonian in the principal-axis system is

$$H_{\text{ZFS}}^{\text{quartet}} = \begin{pmatrix} \langle +3/2 | & \langle +1/2 | & \langle -1/2 | & \langle -3/2 | \\ D & 0 & \sqrt{3}E & 0 \\ 0 & -D & 0 & \sqrt{3}E \\ \sqrt{3}E & 0 & -D & 0 \\ 0 & \sqrt{3}E & 0 & D \end{pmatrix} \begin{matrix} | +3/2 \rangle \\ | +1/2 \rangle \\ | -1/2 \rangle \\ | -3/2 \rangle \end{matrix}$$

This matrix can be divided into two 2×2 equivalent matrixes of which the basis set is $\{|+3/2\rangle, |-1/2\rangle\}$ and $\{|-3/2\rangle, |+1/2\rangle\}$

$$H_{\text{ZFS}}^{\text{quartet}} = \begin{pmatrix} \langle \pm 3/2 | & \langle \mp 1/2 | \\ D & \sqrt{3}E \\ \sqrt{3}E & -D \end{pmatrix} \begin{matrix} | \pm 3/2 \rangle \\ | \mp 1/2 \rangle \end{matrix}$$

The diagonalized eigenenergies and corresponding eigenfunctions are in the following.

$$\varepsilon_{\pm 3/2}^{(0)} = D^*, \quad \varphi_{\pm 3/2}^{(0)} = \cos \theta \left| \pm \frac{3}{2} \right\rangle + \sin \theta \left| \mp \frac{1}{2} \right\rangle \quad (\text{S12a})$$

$$\varepsilon_{\pm 1/2}^{(0)} = -D^*, \quad \varphi_{\pm 1/2}^{(0)} = \cos \theta \left| \pm \frac{1}{2} \right\rangle - \sin \theta \left| \mp \frac{3}{2} \right\rangle \quad (\text{S12b})$$

where

$$D^* = \sqrt{D^2 + 3E^2}$$

and

$$\tan 2\theta = \frac{\sqrt{3}E}{D}.$$

The electron-Zeeman Hamiltonian is rewritten in terms of the ZFS eigenstates with $\mathbf{B} // z$ as follows;

$$H_{\text{eZ}}^{\text{quartet}} = \begin{pmatrix} \frac{3}{2}g_z^{\text{true}}\beta B & 0 & 0 & 0 \\ 0 & \frac{1}{2}g_z^{\text{true}}\beta B & 0 & 0 \\ 0 & 0 & -\frac{1}{2}g_z^{\text{true}}\beta B & 0 \\ 0 & 0 & 0 & -\frac{3}{2}g_z^{\text{true}}\beta B \end{pmatrix}$$

$$\rightarrow H'_{\text{eZ}} = \frac{g_z^{\text{true}}\beta B}{2} \begin{pmatrix} 3 \cos^2 \theta - \sin^2 \theta & 0 & -4 \sin \theta \cos \theta & 0 \\ 0 & \cos^2 \theta - 3 \sin^2 \theta & 0 & -4 \sin \theta \cos \theta \\ -4 \sin \theta \cos \theta & 0 & -\cos^2 \theta + 3 \sin^2 \theta & 0 \\ 0 & -4 \sin \theta \cos \theta & 0 & -3 \cos^2 \theta + \sin^2 \theta \end{pmatrix}.$$

Thus the second-order energies and the first-order spin functions are

$$E'_{+\frac{3}{2}} = D^* + \frac{1}{2}g_z^{\text{true}}\beta B(3 \cos^2 \theta - \sin^2 \theta) + \frac{2(g_z^{\text{true}}\beta B)^2 \sin^2 \theta \cos^2 \theta}{D^*} \quad (\text{S13a})$$

$$E'_{-\frac{3}{2}} = D^* - \frac{1}{2}g_z^{\text{true}}\beta B(3 \cos^2 \theta - \sin^2 \theta) + \frac{2(g_z^{\text{true}}\beta B)^2 \sin^2 \theta \cos^2 \theta}{D^*} \quad (\text{S13d})$$

$$E'_{+\frac{1}{2}} = -D^* + \frac{1}{2}g_z^{\text{true}}\beta B(\cos^2\theta - 3\sin^2\theta) - \frac{2(g_z^{\text{true}}\beta B)^2\sin^2\theta\cos^2\theta}{D^*} \quad (\text{S13b})$$

$$E'_{-\frac{1}{2}} = -D^* - \frac{1}{2}g_z^{\text{true}}\beta B(\cos^2\theta - 3\sin^2\theta) - \frac{2(g_z^{\text{true}}\beta B)^2\sin^2\theta\cos^2\theta}{D^*} \quad (\text{S13c})$$

$$\Psi'_{+\frac{3}{2}} = \cos\theta \left| +\frac{3}{2} \right\rangle + \left[\frac{g_z^{\text{true}}\beta B \sin\theta \cos\theta}{D^*} + \sin\theta \right] \left| -\frac{1}{2} \right\rangle \quad (\text{S14a})$$

$$\Psi'_{-\frac{3}{2}} = \cos\theta \left| -\frac{3}{2} \right\rangle + \left[\frac{g_z^{\text{true}}\beta B \sin\theta \cos\theta}{D^*} + \sin\theta \right] \left| +\frac{1}{2} \right\rangle \quad (\text{S14b})$$

$$\Psi'_{+\frac{1}{2}} = \cos\theta \left| +\frac{1}{2} \right\rangle - \left[\frac{g_z^{\text{true}}\beta B \sin\theta \cos\theta}{D^*} + \sin\theta \right] \left| -\frac{3}{2} \right\rangle \quad (\text{S14c})$$

$$\Psi'_{-\frac{1}{2}} = \cos\theta \left| -\frac{1}{2} \right\rangle - \left[\frac{g_z^{\text{true}}\beta B \sin\theta \cos\theta}{D^*} + \sin\theta \right] \left| +\frac{3}{2} \right\rangle \quad (\text{S14d})$$

Noticeably, these perturbed energies are equivalent to the set of the exact energies derived in the previous section. Equalizing the energy differences between the conjugate spin sublevels to $g_z^{\text{eff}}\beta B$.

$$E'_{+\frac{3}{2}} - E'_{-\frac{3}{2}} = g_z^{\text{true}}\beta B(3\cos^2\theta - \sin^2\theta) = g_z^{\text{eff}}\beta B$$

$$E'_{+\frac{1}{2}} - E'_{-\frac{1}{2}} = g_z^{\text{true}}\beta B(\cos^2\theta - 3\sin^2\theta) = g_z^{\text{eff}}\beta B$$

Therefore, the $g_z^{\text{eff}}/g_z^{\text{true}}$ as a function of $\lambda = E/D$ (θ is a function of λ) is

$$\frac{g_z^{\text{eff}}}{g_z^{\text{true}}} = 3\cos^2\theta - \sin^2\theta \quad (\text{S15a})$$

for the $|M_S = \pm 3/2\rangle$ -dominant transition and

$$\frac{g_z^{\text{eff}}}{g_z^{\text{true}}} = \cos^2\theta - 3\sin^2\theta \quad (\text{S15b})$$

for the $|M_S = \pm 1/2\rangle$ -dominant transition. Figure S2 depicts the $g_z^{\text{eff}}/g_z^{\text{true}}$ derived from the genuine Zeeman perturbation approach as well as the exact treatment described in the previous section. The cyclic permutation of the subscripts of x , y and z yields the $g_z^{\text{eff}}-g_z^{\text{true}}$ relationship in the case of $\mathbf{B} // x$ and y without difficulty.^[S1-S4]

2.3 Global permutation rules for the ZFS energy in the case of $S = 3/2$

In the case of spin-quartet states ($S = 3/2$), the zeroth-order energy (from the ZFS Hamiltonian) is given by

$$D^* = \sqrt{D^2 + 3E^2}.$$

This value is field independent. Thus, it must hold for the cyclic permutation of the subscripts for the axes $D_z \rightarrow D_x, D_x \rightarrow D_y, D_y \rightarrow D_z$. For the static magnetic field \mathbf{B} parallel to the principal x -axis, the transformation of $D \rightarrow \frac{1}{2}(3E - D)$ and $E \rightarrow -\frac{1}{2}(E + D)$, and for $\mathbf{B} // y$, $D \rightarrow$

$-\frac{1}{2}(3E + D)$ and $E \rightarrow \frac{1}{2}(E - D)$ under the definition of the D - and E -values give the corresponding expressions, respectively.^[S1-S4] Here, we show the preservation of the zeroth-order energy in the case of $\mathbf{B} // x$,

$$D^2 + 3E^2 \xrightarrow{\mathbf{B} // x} \left[\frac{1}{2}(3E - D) \right]^2 + 3 \left[-\frac{1}{2}(E + D) \right]^2 = D^2 + 3E^2,$$

and in the case of $\mathbf{B} // y$,

$$D^2 + 3E^2 \xrightarrow{\mathbf{B} // y} \left[-\frac{1}{2}(3E + D) \right]^2 + 3 \left[\frac{1}{2}(E - D) \right]^2 = D^2 + 3E^2.$$

3. Analytical formula for spin-quintet states

3.1 Derivation of the g_z^{eff} - g_z^{true} relationships as a function of $|E/D|$ in spin-triplet states ($S = 2$)

The ZFS-electronic Zeeman Hamiltonian in the case of quintet states can be divided to two matrixes. The basis set of one of the two is $\{|+1\rangle, |-1\rangle\}$ (referring to $H_{\text{ZFS+eZ},1}^{\text{quintet}}$) and the other is $\{|+2\rangle, |0\rangle, |-2\rangle\}$ ($H_{\text{ZFS+eZ},2}^{\text{quintet}}$). The division scheme arises from the spin symmetry of permutation. The former is related to the odd parity and the latter to the even parity. $H_{\text{ZFS+eZ},1}^{\text{quintet}}$ with \mathbf{B}/z can easily be diagonalized and we obtain the eigenenergies and eigenfunctions in the following.

$$H_{\text{ZFS+eZ},1}^{\text{quintet}} = \begin{pmatrix} \langle +1| & \langle -1| \\ -D + g_z^{\text{true}}\beta B & 3E \\ 3E & -D - g_z^{\text{true}}\beta B \end{pmatrix} \begin{matrix} | +1\rangle \\ | -1\rangle \end{matrix}$$

$$E_{\pm 1} = -D \pm \sqrt{9E^2 + (g_z^{\text{true}}\beta B)^2}, \quad \varphi_{\pm 1} = \cos \theta |\pm 1\rangle \pm \sin \theta |\mp 1\rangle \quad (\text{S16})$$

$$\tan 2\theta = \frac{3E}{g_z^{\text{true}}\beta B}$$

Equalizing the energy difference E_{+1} between E_{-1} to $g_z^{\text{eff}}\beta B$,

$$E_{+1} - E_{-1} = 2\sqrt{9E^2 + (g_z^{\text{true}}\beta B)^2} = g_z^{\text{eff}}\beta B$$

leading to

$$36E^2 + 4(g_z^{\text{true}}\beta B)^2 = (g_z^{\text{eff}}\beta B)^2. \quad (\text{S17})$$

Similar to the case of spin triplet states, comparing the coefficients of B in Equation (S17) provides the specific relation $g_z^{\text{eff}}/g_z^{\text{true}} = 2$ if and only if $E = 0$. Otherwise the general g_z^{eff} - g_z^{true} relationship does not hold.

The matrix representation of $H_{\text{ZFS+eZ},2}^{\text{quintet}}$ in the basis of $\{|+2\rangle, |0\rangle, |-2\rangle\}$ with \mathbf{B}/z is as follows:

$$H_{\text{ZFS+eZ},2}^{\text{quintet}} = \begin{pmatrix} \langle +2| & \langle 0| & \langle -2| \\ 2D + 2g_z^{\text{true}}\beta B & \sqrt{6}E & 0 \\ \sqrt{6}E & -2D & \sqrt{6}E \\ 0 & \sqrt{6}E & 2D - 2g_z^{\text{true}}\beta B \end{pmatrix} \begin{matrix} | +2\rangle \\ | 0\rangle \\ | -2\rangle \end{matrix}$$

The eigenenergies of this matrix are the solutions of the following cubic equation;

$$x^3 - 2Dx^2 - 4[D^2 + 3E^2 + (g_z^{\text{true}}\beta B)^2]x + 8D^3 + 24DE^2 - 8D(g_z^{\text{true}}\beta B)^2 = 0.$$

In order to use Viète's theorem, eliminating the x^2 term by replacing x with $x + 2D/3$ yields

$$x^3 = \frac{4}{3}[4D^2 + 9E^2 + 3(g_z^{\text{true}}\beta B)^2]x - \frac{128D^3}{27} - 16DE^2 + \frac{32D(g_z^{\text{true}}\beta B)^2}{3}.$$

The trigonometric solutions for the above cubic equation are

$$x_n = 2a \cos \left[\frac{1}{3} \arccos \left(\frac{b}{2a} \right) + \frac{2n\pi}{3} \right] \quad (n = 0, 1, 2)$$

where

$$a = \frac{2}{3} \sqrt{4D^2 + 9E^2 + 3(g_z^{\text{true}} \beta B)^2}$$

$$b = -\frac{32D^3 + 108DE^2 - 72D(g_z^{\text{true}} \beta B)^2}{12D^2 + 27E^2 + 9(g_z^{\text{true}} \beta B)^2}$$

and $n = 0, 1$ and 2 correspond to the $|M_S = +2\rangle$, $|0\rangle$ and $|-2\rangle$ -dominant states, respectively. Thus the eigenenergies and corresponding eigenfunctions are in the following.

$$E_n = 2a \cos \left[\frac{1}{3} \arccos \left(\frac{b}{2a} \right) + \frac{2n\pi}{3} \right] + \frac{2D}{3} \quad (\text{S18})$$

$$\Psi_n = \alpha_n | +2 \rangle + \beta_n | 0 \rangle + \gamma_n | -2 \rangle \quad (\text{S19})$$

$$\frac{\alpha_n}{\beta_n} = \frac{-\sqrt{6}E}{2D + 2g_z^{\text{true}} \beta B - E_n},$$

$$\frac{\gamma_n}{\beta_n} = \frac{-\sqrt{6}E}{2D - 2g_z^{\text{true}} \beta B - E_n},$$

$$\beta_n = \sqrt{1 - \alpha_n^2 - \gamma_n^2}$$

The $g_z^{\text{eff}}/g_z^{\text{true}}$ relationship for the $M_S = \pm 2$ transition is obtained with equalizing the energy difference of $E_{+2} - E_{-2}$ to $g_z^{\text{eff}} \beta B$, which is generally field-dependent and the special solution is $g_z^{\text{eff}}/g_z^{\text{true}} = 4$ if and only if $E = 0$.

Transition probabilities are calculated numerically:

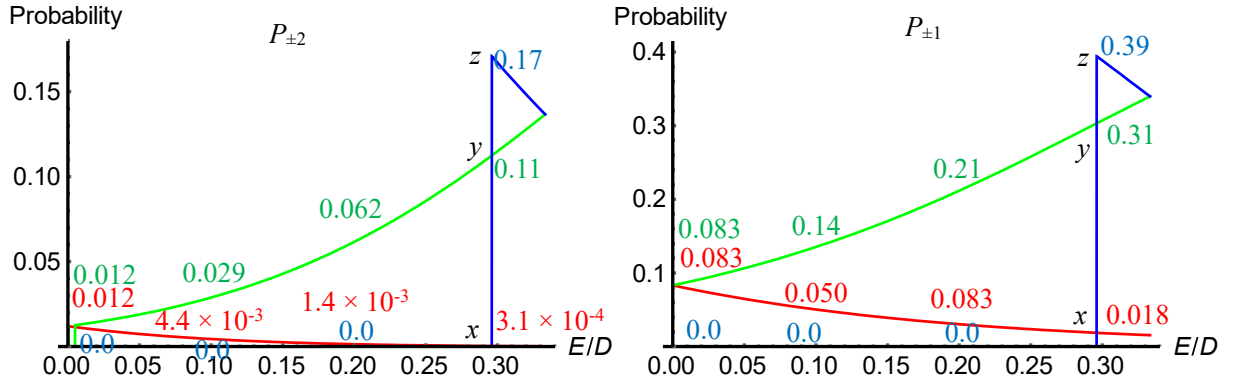


Figure S4 Transition probabilities between the $\pm M_S$ dominant states $P_{M_S} = |\langle \Psi_{-M_S} | S_x | \Psi_{+M_S} \rangle|^2$ for the static magnetic field \mathbf{B} parallel to the x , y and z axis, in the case of $g_z^{\text{true}} \beta B / D = 0.1$.

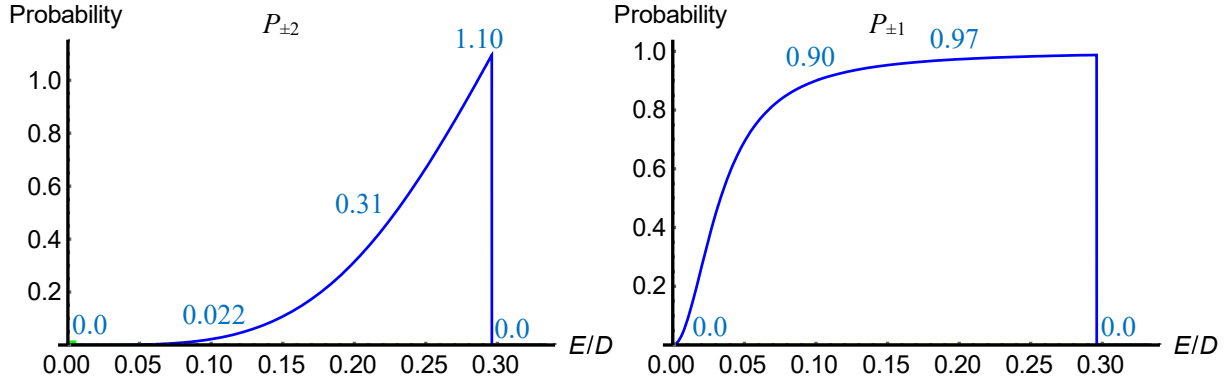


Figure S5 Transition probabilities between the $\pm M_S$ dominant states $P_{\pm M_S} = |\langle \Psi_{-M_S} | S_z | \Psi_{+M_S} \rangle|^2$ for the static magnetic field \mathbf{B} parallel to z axis, in the case of $g^{\text{true}}\beta B/D = 0.1$. In the case of $\mathbf{B} // x$ and y , the transition probabilities are zero in the range of $0 \leq \lambda \leq 1/3$.

3.2 The g^{eff} - g^{true} relationships by using of the genuine Zeeman perturbation approach in the case of spin-quintet states ($S = 2$)

The ZFS Hamiltonian can be divided into two matrices with the size of 2×2 and 3×3 . The 2×2 and 3×3 matrixes correspond to the basis sets of $\{|+1\rangle, |-1\rangle\}$ and $\{|+2\rangle, |0\rangle, |-2\rangle\}$, respectively. The former is

$$H_{\text{ZFS},1}^{\text{quintet}} = \begin{pmatrix} \langle +1| & \langle -1| \\ -D & 3E \\ 3E & -D \end{pmatrix} \begin{matrix} | +1\rangle \\ | -1\rangle \end{matrix}$$

The diagonalized eigenenergies and eigenfunctions are

$$\varepsilon_{+1}^{(0)} = -D + 3E, \quad \varphi_{+1}^{(0)} = (|+1\rangle + |-1\rangle)/\sqrt{2} \quad (\text{S20a})$$

$$\varepsilon_{-1}^{(0)} = -D - 3E, \quad \varphi_{-1}^{(0)} = (|+1\rangle - |-1\rangle)/\sqrt{2}. \quad (\text{S20b})$$

The perturbing electron-Zeeman Hamiltonian in the basis of $\{\varphi_{+1}^{(0)}, \varphi_{-1}^{(0)}\}$ with \mathbf{B}/z is

$$H_{\text{eZ}}^{\text{quintet}} = g_z^{\text{true}} \beta B \begin{pmatrix} 1 & 0 \\ 0 & -1 \end{pmatrix} \rightarrow H'_{\text{eZ}} = g_z^{\text{true}} \beta B \begin{pmatrix} 0 & 1 \\ 1 & 0 \end{pmatrix}.$$

Being different from the quartet case, the electron-Zeeman terms exist in the off-diagonal elements in the perturbing Hamiltonian. Thus the perturbation effects are taken to the second order in the Rayleigh-Schrödinger perturbation theory. This is due to the spin symmetry of the system.

The ZFS Hamiltonian in the basis of $\{|+2\rangle, |0\rangle, |-2\rangle\}$ is given as follows:

$$H_{\text{ZFS},2}^{\text{quintet}} = \begin{pmatrix} \langle +2| & \langle 0| & \langle -2| \\ 2D & \sqrt{6}E & 0 \\ \sqrt{6}E & -2D & \sqrt{6}E \\ 0 & \sqrt{6}E & 2D \end{pmatrix} \begin{matrix} | +2\rangle \\ | 0\rangle \\ | -2\rangle \end{matrix}$$

The diagonalized eigenenergies and eigenfunctions are

$$\varepsilon_{+2}^{(0)} = 2D^*, \quad \varphi_{+2}^{(0)} = \alpha_{+2}|+2\rangle + \beta_{+2}|0\rangle + \gamma_{+2}|-2\rangle \quad (\text{S21a})$$

$$\varepsilon_0^{(0)} = -2D^*, \quad \varphi_0^{(0)} = \alpha_0|+2\rangle + \beta_0|0\rangle + \gamma_0|-2\rangle \quad (\text{S21b})$$

$$\varepsilon_{-2}^{(0)} = 2D, \quad \varphi_{-2}^{(0)} = (|+2\rangle - |-2\rangle)/\sqrt{2} \quad (\text{S21c})$$

where

$$\frac{\alpha_{+2}}{\beta_{+2}} = \frac{\gamma_{+2}}{\beta_{+2}} = \frac{\sqrt{6}E}{2D^* - 2D}, \quad \beta_{+2} = \left[1 + \frac{3E^2}{2(D^* - D)^2} \right]^{-\frac{1}{2}}$$

$$\frac{\alpha_0}{\beta_0} = \frac{\gamma_0}{\beta_0} = \frac{\sqrt{6}E}{-2D^* - 2D}, \quad \beta_0 = \left[1 + \frac{3E^2}{2(D^* + D)^2} \right]^{-\frac{1}{2}}$$

and

$$D^* = \sqrt{D^2 + 3E^2}.$$

The electron-Zeeman Hamiltonian can be transformed in the basis of $\{\varphi_{+2}^{(0)}, \varphi_0^{(0)}, \varphi_{-2}^{(0)}\}$ with $\mathbf{B} // z$,

$$H_{eZ,2}^{\text{quintet}} = 2g_z^{\text{true}}\beta B \begin{pmatrix} 1 & 0 & 0 \\ 0 & 0 & 0 \\ 0 & 0 & -1 \end{pmatrix} \rightarrow H'_{eZ,2} = 2\sqrt{2}g_z^{\text{true}}\beta B \begin{pmatrix} 0 & 0 & \alpha_{+2} \\ 0 & 0 & \alpha_0 \\ \alpha_{+2} & \alpha_0 & 0 \end{pmatrix}.$$

The perturbed energies to the second order and the wavefunctions to the first order are

$$E'_{+2} = 2D^* + \frac{8(g_z^{\text{true}}\beta B)^2\alpha_{+2}^2}{D^* - D} \quad (\text{S22a})$$

$$E'_{+1} = -D + 3E + \frac{(g_z^{\text{true}}\beta B)^2}{6E} \quad (\text{S22b})$$

$$E'_0 = -2D^* - \frac{8(g_z^{\text{true}}\beta B)^2\alpha_0^2}{D^* + D} \quad (\text{S22c})$$

$$E'_{-1} = -D - 3E - \frac{(g_z^{\text{true}}\beta B)^2}{6E} \quad (\text{S22d})$$

$$E'_{-2} = 2D - \frac{8(g_z^{\text{true}}\beta B)^2\alpha_{+2}^2}{D^* - D} + \frac{8(g_z^{\text{true}}\beta B)^2\alpha_0^2}{D^* + D} \quad (\text{S22e})$$

$$\Psi'_{+2} = \alpha_{+2}|+2\rangle + \beta_{+2}|0\rangle + \left(\gamma_{+2} + \frac{4g_z^{\text{true}}\beta B\alpha_{+2}}{D^* - D}\right)|-2\rangle \quad (\text{S23a})$$

$$\Psi'_{+1} = \frac{1}{\sqrt{2}}|+1\rangle + \left(\frac{1}{\sqrt{2}} + \frac{g_z^{\text{true}}\beta B}{6E}\right)|-1\rangle \quad (\text{S23b})$$

$$\Psi'_0 = \alpha_0|+2\rangle + \beta_0|0\rangle + \left(\gamma_0 - \frac{4g_z^{\text{true}}\beta B\alpha_0}{D^* + D}\right)|-2\rangle \quad (\text{S23c})$$

$$\Psi'_{-1} = \left(\frac{1}{\sqrt{2}} - \frac{g_z^{\text{true}}\beta B}{6E}\right)|+1\rangle - \frac{1}{\sqrt{2}}|-1\rangle \quad (\text{S23d})$$

$$\Psi'_{-2} = \left(\frac{1}{\sqrt{2}} - \frac{4g_z^{\text{true}}\beta B\alpha_{+2}}{D^* - D}\right)|+2\rangle + \frac{4g_z^{\text{true}}\beta B\alpha_0}{D^* + D}|0\rangle - \frac{1}{\sqrt{2}}|-2\rangle. \quad (\text{S23e})$$

The $g_z^{\text{eff}}/g_z^{\text{true}}$ relationship for the $|M_S = \pm 1\rangle$ -dominant transition is

$$E'_{+1} - E'_{-1} = 6E + \frac{(g_z^{\text{true}}\beta B)^2}{3E} = g_z^{\text{eff}}\beta B$$

$$3Eg_z^{\text{eff}}\beta B = 18E^2 + (g_z^{\text{true}}\beta B)^2 \quad (\text{S24a})$$

and for the $|M_S = \pm 2\rangle$ -dominant transition,

$$E'_{+2} - E'_{-2} = 2D^* - 2D + \frac{8(g_z^{\text{true}}\beta B)^2\alpha_{+2}^2}{D^* - D} - \frac{8(g_z^{\text{true}}\beta B)^2\alpha_0^2}{D^* + D} = g_z^{\text{eff}}\beta B$$

$$3E^2g_z^{\text{eff}}\beta B = 6(D^* - D)E^2 + 8[(D^* + D)\alpha_{+2}^2 - (D^* - D)\alpha_0^2](g_z^{\text{true}}\beta B)^2. \quad (\text{S24b})$$

Both equations (S24a) and (S24b) do not have the field-independent general and special solutions in the range of $0 \leq \lambda \leq 1/3$, exemplifying a trivial case of $g_z^{\text{true}} = 0$.

The transition probability between the $|M_S = \pm 1\rangle$ -dominant states $P_{\pm 1} = |\langle \Psi_{-1} | S_z | \Psi_{+1} \rangle|^2$ is

$$\begin{aligned} & \left[\langle -1 | - \frac{g_z^{\text{true}} \beta B}{6E} \langle +1 | \right] S_z \left[| +1 \rangle + \frac{g_z^{\text{true}} \beta B}{6E} | -1 \rangle \right] \\ &= \left[\langle -1 | - \frac{g_z^{\text{true}} \beta B}{6E} \langle +1 | \right] \left[| +1 \rangle - \frac{g_z^{\text{true}} \beta B}{6E} | -1 \rangle \right] \\ &= - \frac{g_z^{\text{true}} \beta B}{3E} \end{aligned}$$

$$P_{\pm 1}(B, E) = \frac{(g_z^{\text{true}} \beta B)^2}{9E^2}$$

Obviously, $P > 1$ if $g_z^{\text{true}} \beta B > 3E$.

3.3 Global permutation for the ZFS energies in the case of $S = 2$

As seen in the quartet state, $D^* = \sqrt{D^2 + 3E^2}$ does not change for the permutation of the subscripts in D_{xx} , D_{yy} and D_{zz} in the spin Hamiltonian. Therefore, $\varepsilon_{+2}^{(0)}$ and $\varepsilon_0^{(0)}$ fulfil the global permutation rule. However, for the other ZFS energies, within the set of $\{\varepsilon_{+1}^{(0)}, \varepsilon_{-1}^{(0)}, \varepsilon_{-2}^{(0)}\}$

$$\varepsilon_{+1}^{(0)} = -D + 3E \xrightarrow{\mathbf{B}\parallel x} -\frac{1}{2}(3E - D) + 3\left[-\frac{1}{2}(E + D)\right]$$

$$= -D - 3E = \varepsilon_{-1}^{(0)}$$

$$\varepsilon_{+1}^{(0)} = -D + 3E \xrightarrow{\mathbf{B}\parallel y} -\left[-\frac{1}{2}(3E + D)\right] + 3\left[\frac{1}{2}(E - D)\right]$$

$$= -D + 3E = \varepsilon_{+1}^{(0)}$$

$$\varepsilon_{-1}^{(0)} = -D - 3E \xrightarrow{\mathbf{B}\parallel x} -\frac{1}{2}(3E - D) - 3\left[-\frac{1}{2}(E + D)\right]$$

$$= 2D = \varepsilon_{-2}^{(0)}$$

$$\varepsilon_{-1}^{(0)} = -D - 3E \xrightarrow{\mathbf{B}\parallel y} -\left[-\frac{1}{2}(3E + D)\right] - 3\left[\frac{1}{2}(E - D)\right]$$

$$= 2D = \varepsilon_{-2}^{(0)}$$

$$\varepsilon_{-2}^{(0)} = 2D \xrightarrow{\mathbf{B}\parallel x} 2\left[\frac{1}{2}(3E - D)\right] = -D + 3E = \varepsilon_{+1}^{(0)}$$

$$\varepsilon_{-2}^{(0)} = 2D \xrightarrow{\mathbf{B}\parallel y} 2\left[-\frac{1}{2}(3E + D)\right] = -D - 3E = \varepsilon_{-1}^{(0)}$$

The interchange of the energies belonging to the M_S -dominant sublevels occurs.

4. Analytical formulas for spin-sextet states

4.1 Derivation of the $g^{\text{eff}}-g^{\text{true}}$ relationships as a function of $|E/D|$ in spin-sextet states ($S = 5/2$)

The matrix representation of ZFS and electron-Zeeman Hamiltonian in the case of spin sextet states with \mathbf{B}/z is given as follows:

$$H_{\text{ZFS+eZ}}^{\text{sextet}} = \begin{pmatrix} \frac{10}{3}D + \frac{5}{2}g_z^{\text{true}}\beta B & 0 & \sqrt{10}E & 0 & 0 & 0 \\ 0 & -\frac{2}{3}D + \frac{3}{2}g_z^{\text{true}}\beta B & 0 & 3\sqrt{2}E & 0 & 0 \\ \sqrt{10}E & 0 & -\frac{8}{3}D + \frac{1}{2}g_z^{\text{true}}\beta B & 0 & 3\sqrt{2}E & 0 \\ 0 & 3\sqrt{2}E & 0 & -\frac{8}{3}D - \frac{1}{2}g_z^{\text{true}}\beta B & 0 & \sqrt{10}E \\ 0 & 0 & 3\sqrt{2}E & 0 & -\frac{2}{3}D - \frac{3}{2}g_z^{\text{true}}\beta B & 0 \\ 0 & 0 & 0 & \sqrt{10}E & 0 & \frac{10}{3}D - \frac{5}{2}g_z^{\text{true}}\beta B \end{pmatrix}$$

This matrix can be divided into two conjugate matrixes whose basis sets are $\{|+5/2\rangle, |-3/2\rangle, |+1/2\rangle\}$ and $\{|-5/2\rangle, |+3/2\rangle, |-1/2\rangle\}$, respectively. The former is represented as

$$H_{\text{ZFS+eZ},1}^{\text{sextet}} = \begin{pmatrix} \langle +5/2 | & \langle -3/2 | & \langle +1/2 | \\ \frac{10}{3}D + \frac{5}{2}g_z^{\text{true}}\beta B & 0 & \sqrt{10}E \\ 0 & -\frac{2}{3}D - \frac{3}{2}g_z^{\text{true}}\beta B & 3\sqrt{2}E \\ \sqrt{10}E & 3\sqrt{2}E & -\frac{8}{3}D + \frac{1}{2}g_z^{\text{true}}\beta B \end{pmatrix} \begin{matrix} | +5/2 \rangle \\ | -3/2 \rangle \\ | +1/2 \rangle \end{matrix}$$

In order to obtain the eigenenergies and eigenfunctions, we solve the corresponding secular equation as follows;

$$\begin{aligned} x^3 - \frac{3}{2}g_z^{\text{true}}\beta B x^2 - \left[\frac{28}{3}D^2 + 28E^2 + 8Dg_z^{\text{true}}\beta B + \frac{13}{4}(g_z^{\text{true}}\beta B)^2 \right] x - \frac{160}{27}D^3 \\ + \frac{160}{3}DE^2 - \frac{50}{3}D^2g_z^{\text{true}}\beta B + 30E^2g_z^{\text{true}}\beta B - \frac{20}{3}D(g_z^{\text{true}}\beta B)^2 \\ + \frac{15}{8}(g_z^{\text{true}}\beta B)^3 = 0. \end{aligned}$$

In order to eliminate the x^2 term, replacing x with $x + g_z^{\text{true}}\beta B/2$ yields

$$\begin{aligned} x^3 = \left[\frac{28}{3}D^2 + 28E^2 + 8Dg_z^{\text{true}}\beta B + 4(g_z^{\text{true}}\beta B)^2 \right] x + \frac{160}{27}D^3 - \frac{160}{3}DE^2 \\ + \frac{64}{3}D^2g_z^{\text{true}}\beta B - 16E^2g_z^{\text{true}}\beta B + \frac{32}{3}D(g_z^{\text{true}}\beta B)^2. \end{aligned}$$

According to the Viète's method, the set of the three eigenenergies are given as

$$E_n = 2a \cos \left[\frac{1}{3} \arccos \left(\frac{b}{2a} \right) + \frac{2n\pi}{3} \right] + \frac{1}{2}g_z^{\text{true}}\beta B \quad (\text{S25})$$

$$\Psi_n = \alpha_n \left| +\frac{5}{2} \right\rangle + \beta_n \left| -\frac{3}{2} \right\rangle + \gamma_n \left| +\frac{1}{2} \right\rangle \quad (\text{S26})$$

where

$$a = \frac{2}{3} \sqrt{7D^2 + 21E^2 + 6Dg_z^{\text{true}}\beta B + 3(g_z^{\text{true}}\beta B)^2}$$

$$b = \frac{40(D^3 - 90DE^2) + 36(4D^2 - 3E^2)g_z^{\text{true}}\beta B + 72D(g_z^{\text{true}}\beta B)^2}{7(D^2 + 3E^2) + 18Dg_z^{\text{true}}\beta B + 9(g_z^{\text{true}}\beta B)^2}$$

$$\frac{\alpha_n}{\gamma_n} = \frac{\sqrt{10}E}{E_n - \frac{10}{3}D - \frac{5}{2}g_z^{\text{true}}\beta B}$$

$$\frac{\beta_n}{\gamma_n} = \frac{3\sqrt{2}E}{E_n + \frac{2}{3}D + \frac{3}{2}g_z^{\text{true}}\beta B}$$

$$\gamma_n^2 = \left[\left(\frac{\alpha_n}{\gamma_n} \right)^2 + \left(\frac{\beta_n}{\gamma_n} \right)^2 + 1 \right]^{-1}$$

and $n = 0, 1, 2$ correspond to the $|M_S = +5/2\rangle$, $|+1/2\rangle$ and $|-3/2\rangle$ dominant state, respectively. The counterpart eigenvalues and eigenfunctions in the basis of $\{|-5/2\rangle, |+3/2\rangle, |-1/2\rangle\}$ can be obtained with substituting B to $-B$. The analytical formulas given above are explicitly derived for the first time together with those for $S = 7/2$ as given later in this work. The $g_z^{\text{eff}}-g_z^{\text{true}}$ relationships as a function of $\lambda = E/D$ are only numerically obtained with equalizing $E_{M_S} - E_{-M_S}$ to $g_z^{\text{eff}}\beta B$, as Figure S6 given below.

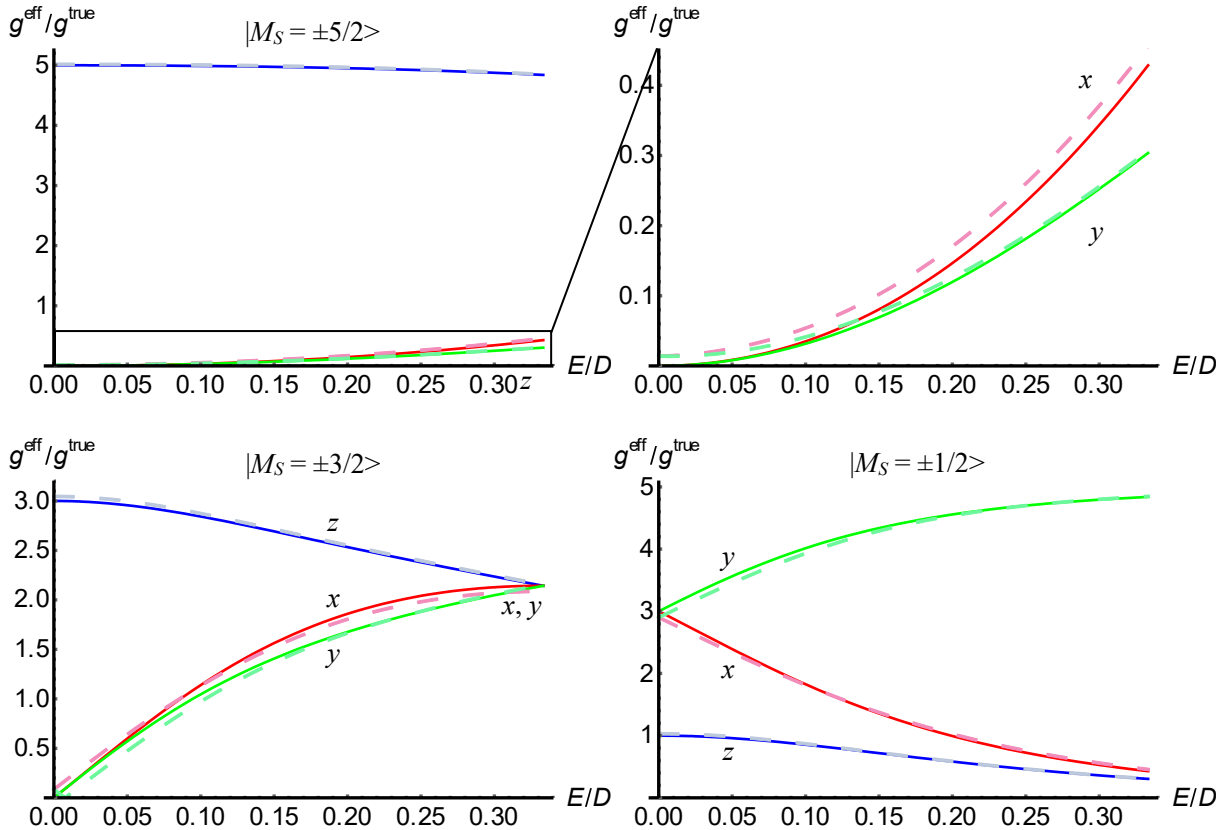


Figure S6 The $g^{\text{eff}}/g^{\text{true}}$ relationships as a function of the ratios of $|E/D|$ for $S = 5/2$. The subscripts, x , y and z denote the principal axes of the \mathbf{g} - and ZFS tensors. The curves of the exact relationships in the broken lines are based on the exact solutions with the spin Hamiltonian parameters as follows: $g^{\text{true}}\beta B/D = 0.3$. Those derived by the genuine Zeeman perturbation treatment to the second order are depicted in the solid curves based on Equations (S31a)–(S31c).

4.2 The $g^{\text{eff}}-g^{\text{true}}$ relationships by using of the genuine Zeeman perturbation approach in the case of spin-sextet states ($S = 5/2$)

The ZFS Hamiltonian in spin-sextet states can be divided to two equivalent 3×3 matrices whose conjugate basis sets are $\{|+5/2\rangle, |-3/2\rangle, |+1/2\rangle\}$ and $\{|-5/2\rangle, |+3/2\rangle, |-1/2\rangle\}$, respectively.

$$H_{\text{ZFS}}^{\text{sextet}} = \begin{pmatrix} \frac{10}{3}D & 0 & \sqrt{10}E \\ 0 & -\frac{2}{3}D & 3\sqrt{2}E \\ \sqrt{10}E & 3\sqrt{2}E & -\frac{8}{3}D \end{pmatrix}$$

In order to obtain the eigenenergies of the ZFS matrix, we solve the secular equation.

$$x^3 = \frac{28}{3}(D^2 + 3E^2)x + \frac{160}{27}(D^3 - 9DE^2)$$

The three eigenenergies and three eigenfunctions are

$$\varepsilon_n^{(0)} = 2a \cos \left[\frac{1}{3} \arccos \left(\frac{b}{2a} \right) + \frac{2n\pi}{3} \right] \quad (\text{S27})$$

$$\varphi_n^{(0)} = \alpha_n \left| +\frac{5}{2} \right\rangle + \beta_n \left| -\frac{3}{2} \right\rangle + \gamma_n \left| +\frac{1}{2} \right\rangle \quad (\text{S28})$$

where

$$a = \frac{2\sqrt{7(D^2 + 3E^2)}}{3} = \frac{2D\sqrt{7(1 + 3\lambda^2)}}{3}$$

$$b = \frac{40(D^3 - 9DE^2)}{21(D^2 + 3E^2)} = \frac{40D(1 - 9\lambda^2)}{21(1 + 3\lambda^2)}$$

$$\frac{\alpha_n}{\gamma_n} = \frac{\sqrt{10}E}{\varepsilon_n^{(0)} - \frac{10}{3}D}$$

$$\frac{\beta_n}{\gamma_n} = \frac{3\sqrt{2}E}{\varepsilon_n^{(0)} + \frac{2}{3}D}$$

$$\gamma_n^2 = \left[\frac{10E^2}{\left(\varepsilon_n^{(0)} - \frac{10}{3}D \right)^2} + \frac{18E^2}{\left(\varepsilon_n^{(0)} + \frac{2}{3}D \right)^2} + 1 \right]^{-1}$$

$$(n = 0, 1, 2).$$

Here, $n = 0, 1$ and 2 corresponds to the $|M_S = \pm 5/2\rangle, |\pm 1/2\rangle$ and $|\pm 3/2\rangle$ -dominant states, respectively. The perturbing Hamiltonian in the basis of $\{|+5/2\rangle, |-3/2\rangle, |+1/2\rangle\}$ with \mathbf{B}/z is

$$H'_{eZ}{}^{\text{sextet}} = g_z^{\text{true}} \beta B \begin{pmatrix} \frac{5}{2}\alpha_0^2 - \frac{3}{2}\beta_0^2 + \frac{1}{2}\gamma_0^2 & \frac{5}{2}\alpha_0\alpha_2 - \frac{3}{2}\beta_0\beta_2 + \frac{1}{2}\gamma_0\gamma_2 & \frac{5}{2}\alpha_0\alpha_1 - \frac{3}{2}\beta_0\beta_1 + \frac{1}{2}\gamma_0\gamma_1 \\ \frac{5}{2}\alpha_0\alpha_2 - \frac{3}{2}\beta_0\beta_2 + \frac{1}{2}\gamma_0\gamma_2 & \frac{5}{2}\alpha_2^2 - \frac{3}{2}\beta_2^2 + \frac{1}{2}\gamma_2^2 & \frac{5}{2}\alpha_1\alpha_2 - \frac{3}{2}\beta_1\beta_2 + \frac{1}{2}\gamma_1\gamma_2 \\ \frac{5}{2}\alpha_0\alpha_1 - \frac{3}{2}\beta_0\beta_1 + \frac{1}{2}\gamma_0\gamma_1 & \frac{5}{2}\alpha_1\alpha_2 - \frac{3}{2}\beta_1\beta_2 + \frac{1}{2}\gamma_1\gamma_2 & \frac{5}{2}\alpha_1^2 - \frac{3}{2}\beta_1^2 + \frac{1}{2}\gamma_1^2 \end{pmatrix}$$

The conjugate Hamiltonian in the corresponding basis of $\{|-5/2\rangle, |+3/2\rangle, |-1/2\rangle\}$ can be obtained by replacing B with $-B$. The perturbed energies to the second order are

$$E'_{+5/2} = \varepsilon_0^{(0)} + \left(\frac{5}{2}\alpha_0^2 - \frac{3}{2}\beta_0^2 + \frac{1}{2}\gamma_0^2\right) g_z^{\text{true}} \beta B + \frac{\left(\frac{5}{2}\alpha_0\alpha_2 - \frac{3}{2}\beta_0\beta_2 + \frac{1}{2}\gamma_0\gamma_2\right)^2 (g_z^{\text{true}} \beta B)^2}{\varepsilon_0^{(0)} - \varepsilon_2^{(0)}} + \frac{\left(\frac{5}{2}\alpha_0\alpha_1 - \frac{3}{2}\beta_0\beta_1 + \frac{1}{2}\gamma_0\gamma_1\right)^2 (g_z^{\text{true}} \beta B)^2}{\varepsilon_0^{(0)} - \varepsilon_1^{(0)}} \quad (\text{S29a})$$

$$E'_{+3/2} = \varepsilon_2^{(0)} + \left(\frac{5}{2}\alpha_2^2 - \frac{3}{2}\beta_2^2 + \frac{1}{2}\gamma_2^2\right) g_z^{\text{true}} \beta B + \frac{\left(\frac{5}{2}\alpha_0\alpha_2 - \frac{3}{2}\beta_0\beta_2 + \frac{1}{2}\gamma_0\gamma_2\right)^2 (g_z^{\text{true}} \beta B)^2}{\varepsilon_2^{(0)} - \varepsilon_0^{(0)}} + \frac{\left(\frac{5}{2}\alpha_1\alpha_2 - \frac{3}{2}\beta_1\beta_2 + \frac{1}{2}\gamma_1\gamma_2\right)^2 (g_z^{\text{true}} \beta B)^2}{\varepsilon_2^{(0)} - \varepsilon_1^{(0)}} \quad (\text{S29b})$$

$$E'_{+1/2} = \varepsilon_1^{(0)} + \left(\frac{5}{2}\alpha_1^2 - \frac{3}{2}\beta_1^2 + \frac{1}{2}\gamma_1^2\right) g_z^{\text{true}} \beta B + \frac{\left(\frac{5}{2}\alpha_0\alpha_1 - \frac{3}{2}\beta_0\beta_1 + \frac{1}{2}\gamma_0\gamma_1\right)^2 (g_z^{\text{true}} \beta B)^2}{\varepsilon_1^{(0)} - \varepsilon_0^{(0)}} + \frac{\left(\frac{5}{2}\alpha_1\alpha_2 - \frac{3}{2}\beta_1\beta_2 + \frac{1}{2}\gamma_1\gamma_2\right)^2 (g_z^{\text{true}} \beta B)^2}{\varepsilon_1^{(0)} - \varepsilon_2^{(0)}} \quad (\text{S29c})$$

and the perturbed spin functions to the first order are

$$\Psi'_{+5/2} = \frac{1}{N_0} \left[\alpha_0 \left| +\frac{5}{2} \right\rangle + \left(\beta_0 + \frac{\frac{5}{2}\alpha_0\alpha_2 - \frac{3}{2}\beta_0\beta_2 + \frac{1}{2}\gamma_0\gamma_2}{\varepsilon_0^{(0)} - \varepsilon_2^{(0)}} g_z^{\text{true}} \beta B \right) \left| -\frac{3}{2} \right\rangle + \left(\gamma_0 + \frac{\frac{5}{2}\alpha_0\alpha_1 - \frac{3}{2}\beta_0\beta_1 + \frac{1}{2}\gamma_0\gamma_1}{\varepsilon_0^{(0)} - \varepsilon_1^{(0)}} g_z^{\text{true}} \beta B \right) \left| +\frac{1}{2} \right\rangle \right] \quad (\text{S30a})$$

$$\Psi'_{+3/2} = \frac{1}{N_2} \left[\left(\alpha_2 + \frac{\frac{5}{2}\alpha_0\alpha_2 - \frac{3}{2}\beta_0\beta_2 + \frac{1}{2}\gamma_0\gamma_2}{\varepsilon_2^{(0)} - \varepsilon_0^{(0)}} g_z^{\text{true}} \beta B \right) \left| +\frac{5}{2} \right\rangle + \beta_2 \left| -\frac{3}{2} \right\rangle + \left(\gamma_2 + \frac{\frac{5}{2}\alpha_1\alpha_2 - \frac{3}{2}\beta_1\beta_2 + \frac{1}{2}\gamma_1\gamma_2}{\varepsilon_2^{(0)} - \varepsilon_1^{(0)}} g_z^{\text{true}} \beta B \right) \left| +\frac{1}{2} \right\rangle \right] \quad (\text{S30b})$$

$$\Psi'_{+1/2} = \frac{1}{N_1} \left[\left(\alpha_1 + \frac{\frac{5}{2}\alpha_0\alpha_1 - \frac{3}{2}\beta_0\beta_1 + \frac{1}{2}\gamma_0\gamma_1}{\varepsilon_1^{(0)} - \varepsilon_0^{(0)}} g_z^{\text{true}} \beta B \right) \left| +\frac{5}{2} \right\rangle + \left(\beta_1 + \frac{\frac{5}{2}\alpha_1\alpha_2 - \frac{3}{2}\beta_1\beta_2 + \frac{1}{2}\gamma_1\gamma_2}{\varepsilon_1^{(0)} - \varepsilon_2^{(0)}} g_z^{\text{true}} \beta B \right) \left| -\frac{3}{2} \right\rangle + \gamma_1 \left| +\frac{1}{2} \right\rangle \right] \quad (\text{S30c})$$

$$\Psi'_{-5/2} = \frac{1}{N_0'} \left[\alpha_0 \left| -\frac{5}{2} \right\rangle + \left(\beta_0 - \frac{\frac{5}{2}\alpha_0\alpha_2 - \frac{3}{2}\beta_0\beta_2 + \frac{1}{2}\gamma_0\gamma_2}{\varepsilon_0^{(0)} - \varepsilon_2^{(0)}} g_z^{\text{true}} \beta B \right) \left| +\frac{3}{2} \right\rangle + \left(\gamma_0 - \frac{\frac{5}{2}\alpha_0\alpha_1 - \frac{3}{2}\beta_0\beta_1 + \frac{1}{2}\gamma_0\gamma_1}{\varepsilon_0^{(0)} - \varepsilon_1^{(0)}} g_z^{\text{true}} \beta B \right) \left| -\frac{1}{2} \right\rangle \right] \quad (\text{S30d})$$

$$\Psi'_{-3/2} = \frac{1}{N_2'} \left[\left(\alpha_2 - \frac{\frac{5}{2}\alpha_0\alpha_2 - \frac{3}{2}\beta_0\beta_2 + \frac{1}{2}\gamma_0\gamma_2}{\varepsilon_2^{(0)} - \varepsilon_0^{(0)}} g_z^{\text{true}} \beta B \right) \left| -\frac{5}{2} \right\rangle + \beta_2 \left| +\frac{3}{2} \right\rangle + \left(\gamma_2 - \frac{\frac{5}{2}\alpha_1\alpha_2 - \frac{3}{2}\beta_1\beta_2 + \frac{1}{2}\gamma_1\gamma_2}{\varepsilon_2^{(0)} - \varepsilon_1^{(0)}} g_z^{\text{true}} \beta B \right) \left| -\frac{1}{2} \right\rangle \right] \quad (\text{S30e})$$

$$\Psi'_{-1/2} = \frac{1}{N_1'} \left[\left(\alpha_1 - \frac{\frac{5}{2}\alpha_0\alpha_1 - \frac{3}{2}\beta_0\beta_1 + \frac{1}{2}\gamma_0\gamma_1}{\varepsilon_1^{(0)} - \varepsilon_0^{(0)}} g_z^{\text{true}} \beta B \right) \left| -\frac{5}{2} \right\rangle + \left(\beta_1 - \frac{\frac{5}{2}\alpha_1\alpha_2 - \frac{3}{2}\beta_1\beta_2 + \frac{1}{2}\gamma_1\gamma_2}{\varepsilon_1^{(0)} - \varepsilon_2^{(0)}} g_z^{\text{true}} \beta B \right) \left| +\frac{3}{2} \right\rangle + \gamma_1 \left| -\frac{1}{2} \right\rangle \right] \quad (\text{S30f})$$

where $N_0, N_0', N_1, N_1', N_2$ and N_2' are the normalization factors. Notice that the zeroth and the contributions of the second-order energies vanish when the energy differences between $\pm M_s$, $E'_{M_s} - E'_{-M_s}$, are taken. Thus, the $g_z^{\text{eff}}-g_z^{\text{true}}$ relationships as a function of $\lambda = E/D$ are;

$$\frac{g_z^{\text{eff}}}{g_z^{\text{true}}} = \frac{\frac{50\lambda^2}{\left(\varepsilon_0'^{(0)} - \frac{10}{3}\right)^2} - \frac{54\lambda^2}{\left(\varepsilon_0'^{(0)} + \frac{2}{3}\right)^2} + 1}{\frac{10\lambda^2}{\left(\varepsilon_0'^{(0)} - \frac{10}{3}\right)^2} + \frac{18\lambda^2}{\left(\varepsilon_0'^{(0)} + \frac{2}{3}\right)^2} + 1} \quad (\text{S31a})$$

for the $|M_S = \pm 5/2\rangle$ dominant transition,

$$\frac{g_z^{\text{eff}}}{g_z^{\text{true}}} = \frac{\frac{50\lambda^2}{\left(\varepsilon_2'^{(0)} - \frac{10}{3}\right)^2} - \frac{54\lambda^2}{\left(\varepsilon_2'^{(0)} + \frac{2}{3}\right)^2} + 1}{\frac{10\lambda^2}{\left(\varepsilon_2'^{(0)} - \frac{10}{3}\right)^2} + \frac{18\lambda^2}{\left(\varepsilon_2'^{(0)} + \frac{2}{3}\right)^2} + 1} \quad (\text{S31b})$$

for the $|M_S = \pm 3/2\rangle$ dominant transition, and

$$\frac{g_z^{\text{eff}}}{g_z^{\text{true}}} = \frac{\frac{50\lambda^2}{\left(\varepsilon_1'^{(0)} - \frac{10}{3}\right)^2} - \frac{54\lambda^2}{\left(\varepsilon_1'^{(0)} + \frac{2}{3}\right)^2} + 1}{\frac{10\lambda^2}{\left(\varepsilon_1'^{(0)} - \frac{10}{3}\right)^2} + \frac{18\lambda^2}{\left(\varepsilon_1'^{(0)} + \frac{2}{3}\right)^2} + 1} \quad (\text{S31c})$$

for the $|M_S = \pm 1/2\rangle$ dominant transition.

The transition probabilities between $\pm M_S$ are functions of $\lambda = E/D$ and B . Similar to the case of the quartet state, here we consider only the group-theoretic quantum transition probabilities described as $|\langle \Psi'_{-M_S} | S_x | \Psi'_{+M_S} \rangle|^2$. For the $|M_S = \pm 5/2\rangle$ -dominant transition,

$$\begin{aligned} \langle \Psi'_{-\frac{5}{2}} | S_x | \Psi'_{+\frac{5}{2}} \rangle &= \frac{1}{N'_0} \frac{1}{N_0} \left[\sqrt{5}\alpha_0\beta_0 + 2\sqrt{2}\beta_0\gamma_0 + \frac{3}{2}\gamma_0^2 \right. \\ &\quad - 2\sqrt{2} \frac{\left(\frac{5}{2}\alpha_0\alpha_1 - \frac{3}{2}\beta_0\beta_1 + \frac{1}{2}\gamma_0\gamma_1\right)\left(\frac{5}{2}\alpha_0\alpha_2 - \frac{3}{2}\beta_0\beta_2 + \frac{1}{2}\gamma_0\gamma_2\right)}{\left(\varepsilon_0^{(0)} - \varepsilon_1^{(0)}\right)\left(\varepsilon_0^{(0)} - \varepsilon_2^{(0)}\right)} (g_z^{\text{true}}\beta B)^2 \\ &\quad \left. - \frac{3}{2} \frac{\left(\frac{5}{2}\alpha_0\alpha_1 - \frac{3}{2}\beta_0\beta_1 + \frac{1}{2}\gamma_0\gamma_1\right)^2}{\left(\varepsilon_0^{(0)} - \varepsilon_1^{(0)}\right)^2} (g_z^{\text{true}}\beta B)^2 \right]. \end{aligned}$$

For the $|M_S = \pm 3/2\rangle$ transition,

$$\langle \Psi'_{+\frac{3}{2}} | S_x | \Psi'_{-\frac{3}{2}} \rangle = \frac{1}{N'_2} \frac{1}{N_2} \left[\sqrt{5}\alpha_2\beta_2 + 2\sqrt{2}\beta_2\gamma_2 + \frac{3}{2}\gamma_2^2 - \frac{3}{2} \frac{\left(\frac{5}{2}\alpha_1\alpha_2 - \frac{3}{2}\beta_1\beta_2 + \frac{1}{2}\gamma_1\gamma_2\right)^2}{\left(\varepsilon_2^{(0)} - \varepsilon_1^{(0)}\right)^2} (g_z^{\text{true}}\beta B)^2 \right]$$

For the $|M_S = \pm 1/2\rangle$ transition,

$$\langle \Psi'_{-\frac{1}{2}} | S_x | \Psi'_{+\frac{1}{2}} \rangle = \frac{1}{N'_1} \frac{1}{N_1} \left[\sqrt{5}\alpha_1\beta_1 + 2\sqrt{2}\beta_1\gamma_1 + \frac{3}{2}\gamma_1^2 - \sqrt{5} \frac{\left(\frac{5}{2}\alpha_0\alpha_1 - \frac{3}{2}\beta_0\beta_1 + \frac{1}{2}\gamma_0\gamma_1\right)\left(\frac{5}{2}\alpha_1\alpha_2 - \frac{3}{2}\beta_1\beta_2 + \frac{1}{2}\gamma_1\gamma_2\right)}{\left(\varepsilon_1^{(0)} - \varepsilon_0^{(0)}\right)\left(\varepsilon_1^{(0)} - \varepsilon_2^{(0)}\right)} (g_z^{\text{true}}\beta B)^2 \right]$$

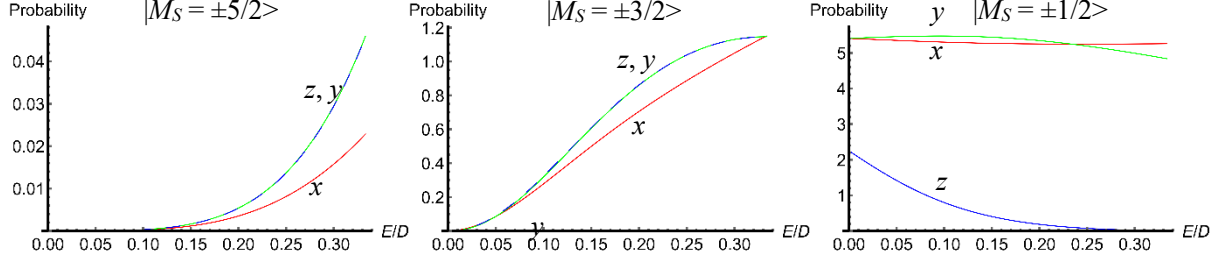


Figure S7 The transition probabilities $|\langle \Psi'_{-M_S} | S_x | \Psi'_{+M_S} \rangle|^2$ for $S = 5/2$. The subscripts x , y and z denote the principal axes of the \mathbf{g} - and ZFS tensors. The curves are based on the exact solutions with the spin Hamiltonian parameters with $g^{\text{true}}\beta B/D = 0.1$. Those derived by the genuine Zeeman perturbation treatment to the third order are depicted in the solid curves.

The energy corrections to the third order, $\varepsilon_n^{(3)}$ ($n = 0, 1, 2$) are given in the following:

For the $|M_S = +5/2\rangle$ dominant state,

$$\begin{aligned}
& \varepsilon_0^{(3)} \\
&= \frac{(5\alpha_0\alpha_1 - 3\beta_0\beta_1 + \gamma_0\gamma_1)^2(5\alpha_1^2 - 5\alpha_0^2 - 3\beta_1^2 + 3\beta_0^2 + \gamma_1^2 - \gamma_0^2)}{8(\varepsilon_0^{(0)} - \varepsilon_1^{(0)})^2} (g_z^{\text{true}}\beta B)^3 \\
&+ \frac{(5\alpha_0\alpha_2 - 3\beta_0\beta_2 + \gamma_0\gamma_2)(5\alpha_1\alpha_2 - 3\beta_1\beta_2 + \gamma_1\gamma_2)(5\alpha_0\alpha_1 - 3\beta_0\beta_1 + \gamma_0\gamma_1)}{4(\varepsilon_0^{(0)} - \varepsilon_2^{(0)})(\varepsilon_0^{(0)} - \varepsilon_1^{(0)})} (g_z^{\text{true}}\beta B)^3 \\
&+ \frac{(5\alpha_0\alpha_2 - 3\beta_0\beta_2 + \gamma_0\gamma_2)^2(5\alpha_2^2 - 5\alpha_0^2 - 3\beta_2^2 + 3\beta_0^2 + \gamma_2^2 - \gamma_0^2)}{8(\varepsilon_0^{(0)} - \varepsilon_2^{(0)})^2} (g_z^{\text{true}}\beta B)^3
\end{aligned}$$

$$\begin{aligned}
&= \frac{\left[\frac{50E^2}{\left(\varepsilon_0^{(0)} - \frac{10}{3}d\right)\left(\varepsilon_1^{(0)} - \frac{10}{3}d\right)} - \frac{54E^2}{\left(\varepsilon_0^{(0)} + \frac{2}{3}d\right)\left(\varepsilon_1^{(0)} + \frac{2}{3}d\right)} + 1 \right]^2}{\left[\frac{10E^2}{\left(\varepsilon_0^{(0)} - \frac{10}{3}d\right)^2} + \frac{18E^2}{\left(\varepsilon_0^{(0)} + \frac{2}{3}d\right)^2} + 1 \right] \left[\frac{10E^2}{\left(\varepsilon_1^{(0)} - \frac{10}{3}d\right)^2} + \frac{18E^2}{\left(\varepsilon_1^{(0)} + \frac{2}{3}d\right)^2} + 1 \right]} \times \frac{\left[\frac{50E^2}{\left(\varepsilon_1^{(0)} - \frac{10}{3}d\right)^2} - \frac{54E^2}{\left(\varepsilon_1^{(0)} + \frac{2}{3}d\right)^2} + 1 \right] \frac{50E^2}{\left(\varepsilon_0^{(0)} - \frac{10}{3}d\right)^2} - \frac{54E^2}{\left(\varepsilon_0^{(0)} + \frac{2}{3}d\right)^2} + 1}{\left[\frac{10E^2}{\left(\varepsilon_1^{(0)} - \frac{10}{3}d\right)^2} + \frac{18E^2}{\left(\varepsilon_1^{(0)} + \frac{2}{3}d\right)^2} + 1 \right] \left[\frac{10E^2}{\left(\varepsilon_0^{(0)} - \frac{10}{3}d\right)^2} + \frac{18E^2}{\left(\varepsilon_0^{(0)} + \frac{2}{3}d\right)^2} + 1 \right]} \\
&\times \frac{(g_z^{\text{true}} \beta B)^3}{8 \left(\varepsilon_0^{(0)} - \varepsilon_1^{(0)}\right)^2} + \frac{\left[\frac{50E^2}{\left(\varepsilon_0^{(0)} - \frac{10}{3}d\right)\left(\varepsilon_2^{(0)} - \frac{10}{3}d\right)} - \frac{54E^2}{\left(\varepsilon_0^{(0)} + \frac{2}{3}d\right)\left(\varepsilon_2^{(0)} + \frac{2}{3}d\right)} + 1 \right]^2}{\left[\frac{10E^2}{\left(\varepsilon_0^{(0)} - \frac{10}{3}d\right)^2} + \frac{18E^2}{\left(\varepsilon_0^{(0)} + \frac{2}{3}d\right)^2} + 1 \right] \left[\frac{10E^2}{\left(\varepsilon_2^{(0)} - \frac{10}{3}d\right)^2} + \frac{18E^2}{\left(\varepsilon_2^{(0)} + \frac{2}{3}d\right)^2} + 1 \right]} \\
&\times \frac{\left[\frac{50E^2}{\left(\varepsilon_2^{(0)} - \frac{10}{3}d\right)^2} - \frac{54E^2}{\left(\varepsilon_2^{(0)} + \frac{2}{3}d\right)^2} + 1 \right] \frac{50E^2}{\left(\varepsilon_0^{(0)} - \frac{10}{3}d\right)^2} - \frac{54E^2}{\left(\varepsilon_0^{(0)} + \frac{2}{3}d\right)^2} + 1}{\left[\frac{10E^2}{\left(\varepsilon_2^{(0)} - \frac{10}{3}d\right)^2} + \frac{18E^2}{\left(\varepsilon_2^{(0)} + \frac{2}{3}d\right)^2} + 1 \right] \left[\frac{10E^2}{\left(\varepsilon_0^{(0)} - \frac{10}{3}d\right)^2} + \frac{18E^2}{\left(\varepsilon_0^{(0)} + \frac{2}{3}d\right)^2} + 1 \right]} \times \frac{(g_z^{\text{true}} \beta B)^3}{8 \left(\varepsilon_0^{(0)} - \varepsilon_2^{(0)}\right)^2} \\
&+ \frac{\left[\frac{50E^2}{\left(\varepsilon_1^{(0)} - \frac{10}{3}d\right)\left(\varepsilon_2^{(0)} - \frac{10}{3}d\right)} - \frac{54E^2}{\left(\varepsilon_1^{(0)} + \frac{2}{3}d\right)\left(\varepsilon_2^{(0)} + \frac{2}{3}d\right)} + 1 \right]}{\left[\frac{10E^2}{\left(\varepsilon_0^{(0)} - \frac{10}{3}d\right)^2} + \frac{18E^2}{\left(\varepsilon_0^{(0)} + \frac{2}{3}d\right)^2} + 1 \right]} \times \frac{\left[\frac{50E^2}{\left(\varepsilon_0^{(0)} - \frac{10}{3}d\right)\left(\varepsilon_2^{(0)} - \frac{10}{3}d\right)} - \frac{54E^2}{\left(\varepsilon_0^{(0)} + \frac{2}{3}d\right)\left(\varepsilon_2^{(0)} + \frac{2}{3}d\right)} + 1 \right]}{\left[\frac{10E^2}{\left(\varepsilon_1^{(0)} - \frac{10}{3}d\right)^2} + \frac{18E^2}{\left(\varepsilon_1^{(0)} + \frac{2}{3}d\right)^2} + 1 \right]} \\
&\times \frac{\left[\frac{50E^2}{\left(\varepsilon_0^{(0)} - \frac{10}{3}d\right)\left(\varepsilon_1^{(0)} - \frac{10}{3}d\right)} - \frac{54E^2}{\left(\varepsilon_0^{(0)} + \frac{2}{3}d\right)\left(\varepsilon_1^{(0)} + \frac{2}{3}d\right)} + 1 \right]}{\left[\frac{10E^2}{\left(\varepsilon_2^{(0)} - \frac{10}{3}d\right)^2} + \frac{18E^2}{\left(\varepsilon_2^{(0)} + \frac{2}{3}d\right)^2} + 1 \right]} \times \frac{(g_z^{\text{true}} \beta B)^3}{4 \left(\varepsilon_0^{(0)} - \varepsilon_2^{(0)}\right) \left(\varepsilon_0^{(0)} - \varepsilon_1^{(0)}\right)}; \tag{S32a}
\end{aligned}$$

For the $|M_S = -3/2\rangle$ dominant state,

$$\begin{aligned}
&\varepsilon_2^{(3)} \\
&= \frac{(5\alpha_0\alpha_2 - 3\beta_0\beta_2 + \gamma_0\gamma_2)^2(5\alpha_0^2 - 5\alpha_2^2 - 3\beta_0^2 + 3\beta_2^2 + \gamma_0^2 - \gamma_2^2)}{8 \left(\varepsilon_2^{(0)} - \varepsilon_0^{(0)}\right)^2} (g_z^{\text{true}} \beta B)^3 \\
&+ \frac{(5\alpha_0\alpha_2 - 3\beta_0\beta_2 + \gamma_0\gamma_2)(5\alpha_1\alpha_2 - 3\beta_1\beta_2 + \gamma_1\gamma_2)(5\alpha_0\alpha_1 - 3\beta_0\beta_1 + \gamma_0\gamma_1)}{4 \left(\varepsilon_2^{(0)} - \varepsilon_0^{(0)}\right) \left(\varepsilon_2^{(0)} - \varepsilon_1^{(0)}\right)} (g_z^{\text{true}} \beta B)^3 \\
&+ \frac{(5\alpha_1\alpha_2 - 3\beta_1\beta_2 + \gamma_1\gamma_2)^2(5\alpha_1^2 - 5\alpha_2^2 - 3\beta_1^2 + 3\beta_2^2 + \gamma_1^2 - \gamma_2^2)}{8 \left(\varepsilon_2^{(0)} - \varepsilon_1^{(0)}\right)^2} (g_z^{\text{true}} \beta B)^3
\end{aligned}$$

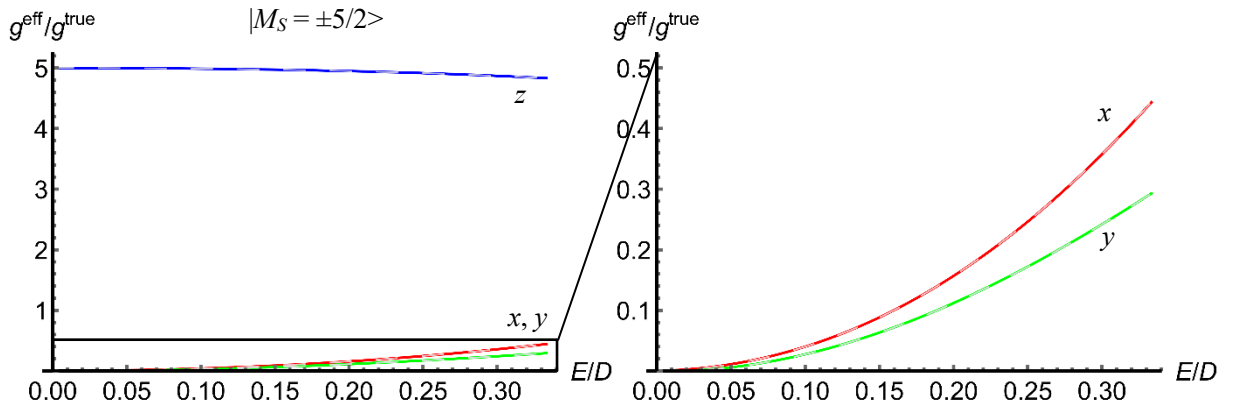
$$\begin{aligned}
&= \frac{\left[\frac{50E^2}{(\varepsilon_2^{(0)} - \frac{10}{3}d)(\varepsilon_0^{(0)} - \frac{10}{3}d)} - \frac{54E^2}{(\varepsilon_2^{(0)} + \frac{2}{3}d)(\varepsilon_0^{(0)} + \frac{2}{3}d)} + 1 \right]^2}{\left[\frac{10E^2}{(\varepsilon_2^{(0)} - \frac{10}{3}d)^2} + \frac{18E^2}{(\varepsilon_2^{(0)} + \frac{2}{3}d)^2} + 1 \right] \left[\frac{10E^2}{(\varepsilon_0^{(0)} - \frac{10}{3}d)^2} + \frac{18E^2}{(\varepsilon_0^{(0)} + \frac{2}{3}d)^2} + 1 \right]} \\
&\times \left[\frac{\frac{50E^2}{(\varepsilon_0^{(0)} - \frac{10}{3}d)^2} - \frac{54E^2}{(\varepsilon_0^{(0)} + \frac{2}{3}d)^2} + 1}{\frac{10E^2}{(\varepsilon_0^{(0)} - \frac{10}{3}d)^2} + \frac{18E^2}{(\varepsilon_0^{(0)} + \frac{2}{3}d)^2} + 1} - \frac{\frac{50E^2}{(\varepsilon_2^{(0)} - \frac{10}{3}d)^2} - \frac{54E^2}{(\varepsilon_2^{(0)} + \frac{2}{3}d)^2} + 1}{\frac{10E^2}{(\varepsilon_2^{(0)} - \frac{10}{3}d)^2} + \frac{18E^2}{(\varepsilon_2^{(0)} + \frac{2}{3}d)^2} + 1} \right] \times \frac{(g_z^{\text{true}} \beta B)^3}{8(\varepsilon_2^{(0)} - \varepsilon_0^{(0)})^2} \\
&+ \frac{\left[\frac{50E^2}{(\varepsilon_2^{(0)} - \frac{10}{3}d)(\varepsilon_1^{(0)} - \frac{10}{3}d)} - \frac{54E^2}{(\varepsilon_2^{(0)} + \frac{2}{3}d)(\varepsilon_1^{(0)} + \frac{2}{3}d)} + 1 \right]^2}{\left[\frac{10E^2}{(\varepsilon_1^{(0)} - \frac{10}{3}d)^2} + \frac{18E^2}{(\varepsilon_1^{(0)} + \frac{2}{3}d)^2} + 1 \right] \left[\frac{10E^2}{(\varepsilon_2^{(0)} - \frac{10}{3}d)^2} + \frac{18E^2}{(\varepsilon_2^{(0)} + \frac{2}{3}d)^2} + 1 \right]} \\
&\times \left[\frac{\frac{50E^2}{(\varepsilon_1^{(0)} - \frac{10}{3}d)^2} - \frac{54E^2}{(\varepsilon_1^{(0)} + \frac{2}{3}d)^2} + 1}{\frac{10E^2}{(\varepsilon_1^{(0)} - \frac{10}{3}d)^2} + \frac{18E^2}{(\varepsilon_1^{(0)} + \frac{2}{3}d)^2} + 1} - \frac{\frac{50E^2}{(\varepsilon_2^{(0)} - \frac{10}{3}d)^2} - \frac{54E^2}{(\varepsilon_2^{(0)} + \frac{2}{3}d)^2} + 1}{\frac{10E^2}{(\varepsilon_2^{(0)} - \frac{10}{3}d)^2} + \frac{18E^2}{(\varepsilon_2^{(0)} + \frac{2}{3}d)^2} + 1} \right] \times \frac{(g_z^{\text{true}} \beta B)^3}{8(\varepsilon_2^{(0)} - \varepsilon_1^{(0)})^2} \\
&+ \frac{\left[\frac{50E^2}{(\varepsilon_1^{(0)} - \frac{10}{3}d)(\varepsilon_2^{(0)} - \frac{10}{3}d)} - \frac{54E^2}{(\varepsilon_1^{(0)} + \frac{2}{3}d)(\varepsilon_2^{(0)} + \frac{2}{3}d)} + 1 \right]}{\left[\frac{10E^2}{(\varepsilon_0^{(0)} - \frac{10}{3}d)^2} + \frac{18E^2}{(\varepsilon_0^{(0)} + \frac{2}{3}d)^2} + 1 \right]} \times \frac{\left[\frac{50E^2}{(\varepsilon_0^{(0)} - \frac{10}{3}d)(\varepsilon_2^{(0)} - \frac{10}{3}d)} - \frac{54E^2}{(\varepsilon_0^{(0)} + \frac{2}{3}d)(\varepsilon_2^{(0)} + \frac{2}{3}d)} + 1 \right]}{\left[\frac{10E^2}{(\varepsilon_1^{(0)} - \frac{10}{3}d)^2} + \frac{18E^2}{(\varepsilon_1^{(0)} + \frac{2}{3}d)^2} + 1 \right]} \\
&\times \frac{\left[\frac{50E^2}{(\varepsilon_0^{(0)} - \frac{10}{3}d)(\varepsilon_1^{(0)} - \frac{10}{3}d)} - \frac{54E^2}{(\varepsilon_0^{(0)} + \frac{2}{3}d)(\varepsilon_1^{(0)} + \frac{2}{3}d)} + 1 \right]}{\left[\frac{10E^2}{(\varepsilon_2^{(0)} - \frac{10}{3}d)^2} + \frac{18E^2}{(\varepsilon_2^{(0)} + \frac{2}{3}d)^2} + 1 \right]} \times \frac{(g_z^{\text{true}} \beta B)^3}{4(\varepsilon_2^{(0)} - \varepsilon_0^{(0)})(\varepsilon_2^{(0)} - \varepsilon_1^{(0)})}; \tag{S32b}
\end{aligned}$$

For the $|M_S = +1/2\rangle$ dominant state,

$$\begin{aligned}
&\varepsilon_1^{(3)} \\
&= \frac{(5\alpha_0\alpha_1 - 3\beta_0\beta_1 + \gamma_0\gamma_1)^2(5\alpha_0^2 - 5\alpha_1^2 - 3\beta_0^2 + 3\beta_1^2 + \gamma_0^2 - \gamma_1^2)}{8(\varepsilon_1^{(0)} - \varepsilon_0^{(0)})^2} (g_z^{\text{true}} \beta B)^3 \\
&+ \frac{(5\alpha_0\alpha_2 - 3\beta_0\beta_2 + \gamma_0\gamma_2)(5\alpha_1\alpha_2 - 3\beta_1\beta_2 + \gamma_1\gamma_2)(5\alpha_0\alpha_1 - 3\beta_0\beta_1 + \gamma_0\gamma_1)}{4(\varepsilon_1^{(0)} - \varepsilon_0^{(0)})(\varepsilon_1^{(0)} - \varepsilon_2^{(0)})} (g_z^{\text{true}} \beta B)^3 \\
&+ \frac{(5\alpha_1\alpha_2 - 3\beta_1\beta_2 + \gamma_1\gamma_2)^2(5\alpha_2^2 - 5\alpha_1^2 - 3\beta_2^2 + 3\beta_1^2 + \gamma_2^2 - \gamma_1^2)}{8(\varepsilon_2^{(0)} - \varepsilon_1^{(0)})^2} (g_z^{\text{true}} \beta B)^3
\end{aligned}$$

$$\begin{aligned}
&= \frac{\left[\frac{50E^2}{(\varepsilon_1^{(0)} - \frac{10}{3}d)(\varepsilon_0^{(0)} - \frac{10}{3}d)} - \frac{54E^2}{(\varepsilon_1^{(0)} + \frac{2}{3}d)(\varepsilon_0^{(0)} + \frac{2}{3}d)} + 1 \right]^2}{\left[\frac{10E^2}{(\varepsilon_1^{(0)} - \frac{10}{3}d)^2} + \frac{18E^2}{(\varepsilon_1^{(0)} + \frac{2}{3}d)^2} + 1 \right] \left[\frac{10E^2}{(\varepsilon_0^{(0)} - \frac{10}{3}d)^2} + \frac{18E^2}{(\varepsilon_0^{(0)} + \frac{2}{3}d)^2} + 1 \right]} \\
&\times \left[\frac{\frac{50E^2}{(\varepsilon_0^{(0)} - \frac{10}{3}d)^2} - \frac{54E^2}{(\varepsilon_0^{(0)} + \frac{2}{3}d)^2} + 1}{\frac{10E^2}{(\varepsilon_0^{(0)} - \frac{10}{3}d)^2} + \frac{18E^2}{(\varepsilon_0^{(0)} + \frac{2}{3}d)^2} + 1} - \frac{\frac{50E^2}{(\varepsilon_1^{(0)} - \frac{10}{3}d)^2} - \frac{54E^2}{(\varepsilon_1^{(0)} + \frac{2}{3}d)^2} + 1}{\frac{10E^2}{(\varepsilon_1^{(0)} - \frac{10}{3}d)^2} + \frac{18E^2}{(\varepsilon_1^{(0)} + \frac{2}{3}d)^2} + 1} \right] \times \frac{(g_z^{\text{true}}\beta B)^3}{8(\varepsilon_1^{(0)} - \varepsilon_0^{(0)})^2} \\
&+ \frac{\left[\frac{50E^2}{(\varepsilon_1^{(0)} - \frac{10}{3}d)(\varepsilon_2^{(0)} - \frac{10}{3}d)} - \frac{54E^2}{(\varepsilon_1^{(0)} + \frac{2}{3}d)(\varepsilon_2^{(0)} + \frac{2}{3}d)} + 1 \right]^2}{\left[\frac{10E^2}{(\varepsilon_2^{(0)} - \frac{10}{3}d)^2} + \frac{18E^2}{(\varepsilon_2^{(0)} + \frac{2}{3}d)^2} + 1 \right] \left[\frac{10E^2}{(\varepsilon_1^{(0)} - \frac{10}{3}d)^2} + \frac{18E^2}{(\varepsilon_1^{(0)} + \frac{2}{3}d)^2} + 1 \right]} \\
&\times \left[\frac{\frac{50E^2}{(\varepsilon_2^{(0)} - \frac{10}{3}d)^2} - \frac{54E^2}{(\varepsilon_2^{(0)} + \frac{2}{3}d)^2} + 1}{\frac{10E^2}{(\varepsilon_2^{(0)} - \frac{10}{3}d)^2} + \frac{18E^2}{(\varepsilon_2^{(0)} + \frac{2}{3}d)^2} + 1} - \frac{\frac{50E^2}{(\varepsilon_1^{(0)} - \frac{10}{3}d)^2} - \frac{54E^2}{(\varepsilon_1^{(0)} + \frac{2}{3}d)^2} + 1}{\frac{10E^2}{(\varepsilon_1^{(0)} - \frac{10}{3}d)^2} + \frac{18E^2}{(\varepsilon_1^{(0)} + \frac{2}{3}d)^2} + 1} \right] \times \frac{(g_z^{\text{true}}\beta B)^3}{8(\varepsilon_1^{(0)} - \varepsilon_2^{(0)})^2} \\
&+ \frac{\left[\frac{50E^2}{(\varepsilon_1^{(0)} - \frac{10}{3}d)(\varepsilon_2^{(0)} - \frac{10}{3}d)} - \frac{54E^2}{(\varepsilon_1^{(0)} + \frac{2}{3}d)(\varepsilon_2^{(0)} + \frac{2}{3}d)} + 1 \right]}{\left[\frac{10E^2}{(\varepsilon_0^{(0)} - \frac{10}{3}d)^2} + \frac{18E^2}{(\varepsilon_0^{(0)} + \frac{2}{3}d)^2} + 1 \right]} \times \frac{\left[\frac{50E^2}{(\varepsilon_0^{(0)} - \frac{10}{3}d)(\varepsilon_2^{(0)} - \frac{10}{3}d)} - \frac{54E^2}{(\varepsilon_0^{(0)} + \frac{2}{3}d)(\varepsilon_2^{(0)} + \frac{2}{3}d)} + 1 \right]}{\left[\frac{10E^2}{(\varepsilon_1^{(0)} - \frac{10}{3}d)^2} + \frac{18E^2}{(\varepsilon_1^{(0)} + \frac{2}{3}d)^2} + 1 \right]} \\
&\times \frac{\left[\frac{50E^2}{(\varepsilon_0^{(0)} - \frac{10}{3}d)(\varepsilon_1^{(0)} - \frac{10}{3}d)} - \frac{54E^2}{(\varepsilon_0^{(0)} + \frac{2}{3}d)(\varepsilon_1^{(0)} + \frac{2}{3}d)} + 1 \right]}{\left[\frac{10E^2}{(\varepsilon_2^{(0)} - \frac{10}{3}d)^2} + \frac{18E^2}{(\varepsilon_2^{(0)} + \frac{2}{3}d)^2} + 1 \right]} \times \frac{(g_z^{\text{true}}\beta B)^3}{4(\varepsilon_1^{(0)} - \varepsilon_0^{(0)})(\varepsilon_1^{(0)} - \varepsilon_2^{(0)})}. \tag{S32c}
\end{aligned}$$

The third order energies corresponding to the $|M_S = -5/2\rangle$, $|+3/2\rangle$ and $|-1/2\rangle$ dominant states are obtained with replacing B with $-B$ in the energy equations for the conjugate $|M_S = +5/2\rangle$, $|-3/2\rangle$ and $|+1/2\rangle$ -dominant states, respectively. The $g^{\text{eff}}-g^{\text{true}}$ relationships are obtained from the equation $E'_{M_S} - E'_{-M_S} = g^{\text{eff}}\beta B$ where $E'_{\pm M_S}$ is the energy to the third order. Figure S8 depicts $g^{\text{eff}}/g^{\text{true}}$ as a function of the ratios of $|E/D|$ for $S = 5/2$, as derived from the genuine Zeeman perturbation treatment to the third order and exact solutions for a particular set of the spin Hamiltonian parameters given in the caption.



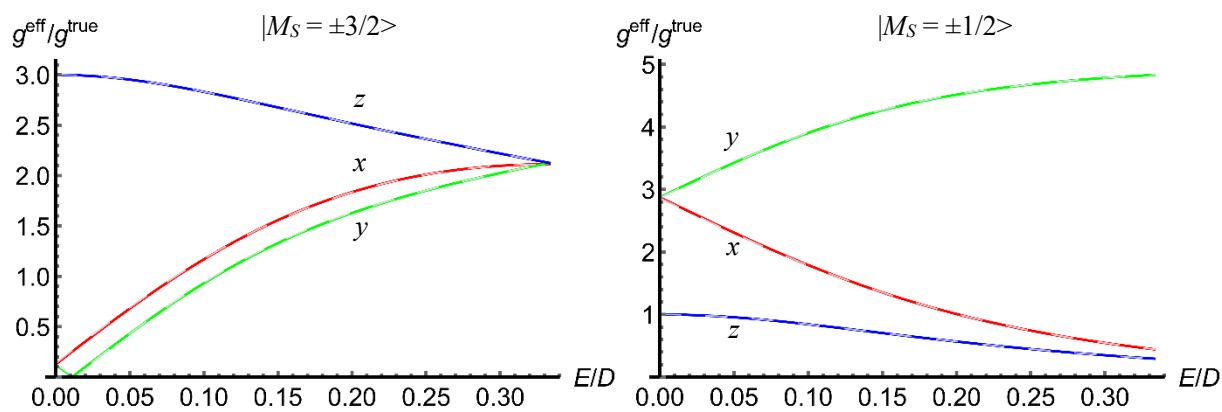


Figure S8 The $g^{\text{eff}}/g^{\text{true}}$ relationships as a function of the ratios of $|E/D|$ for $S = 5/2$. The subscripts x , y and z denote the principal axes of the \mathbf{g} - and ZFS tensors. The curves of the exact relationships in the broken lines are based on the exact solutions of the spin Hamiltonian parameters with $g_z^{\text{true}}\beta B/D = 0.3$. Those derived by the genuine Zeeman perturbation treatment to the third order are depicted in the solid curves.

4.3 Global permutation rules for the ZFS energy in the case of $S = 5/2$

As seen above, the physical quantity of $D^2 + 3E^2$ does not change with the permutation of the subscripts and thus the term a in the expressions for the trigonometric eigenenergy of the ZFS Hamiltonian preserves in the permutation. For the term b ,

$$\begin{aligned} & D^3 - 9DE^2 \\ & \xrightarrow{B_{\parallel x}} \left[\frac{1}{2}(3E - D) \right]^3 - 9 \left[\frac{1}{2}(3E - D) \right] \left[-\frac{1}{2}(E + D) \right]^2 = D^3 - 9DE^2, \\ & D^3 - 9DE^2 \\ & \xrightarrow{B_{\parallel y}} \left[-\frac{1}{2}(3E + D) \right]^3 - 9 \left[-\frac{1}{2}(3E + D) \right] \left[\frac{1}{2}(E - D) \right]^2 = D^3 - 9DE^2. \end{aligned}$$

Therefore, the term b meets the global permutation rules and thus the set of eigenenergy does.

4.4 Derivation of approximate $g^{\text{eff}}-g^{\text{true}}$ relationships in the spin-sextet case ($S = 5/2$)

As mentioned in the text, the diagonalized (exact) eigenenergies of the Hamiltonian with electron-Zeeman and ZFS terms are expressed in terms of trigonometric functions as a function of $\lambda = E/D$ and B . In order to explicitly describe the $g^{\text{eff}}-g^{\text{true}}$ relationships as a function of $\lambda = E/D$, as given in the case of the genuine Zeeman perturbation treatment, we are allowed to exploit a series of the expansion of arccosine and cosine at a desired order of the expansion, exemplifying to the first order in the following.

$$\arccos x \approx \frac{\pi}{2} - x$$

$$\cos \left[\frac{1}{3} \arccos x \right] \approx \cos \left[\frac{1}{3} \left(\frac{\pi}{2} - x \right) \right] \approx \frac{\sqrt{3}}{2} + \frac{1}{6}x - \frac{1}{12\sqrt{3}}x^2$$

$$\cos \left[\frac{1}{3} \arccos x + \frac{2\pi}{3} \right] \approx \cos \left[\frac{1}{3} \left(\frac{\pi}{2} - x \right) + \frac{2\pi}{3} \right] \approx -\frac{\sqrt{3}}{2} + \frac{1}{6}x + \frac{1}{12\sqrt{3}}x^2$$

$$\cos \left[\frac{1}{3} \arccos x + \frac{4\pi}{3} \right] \approx \cos \left[\frac{1}{3} \left(\frac{\pi}{2} - x \right) + \frac{4\pi}{3} \right] \approx -\frac{1}{3}x$$

$$E''_{+\frac{5}{2}} = 2a_1 \cos \left[\frac{1}{3} \arccos \frac{b_1}{2a_1} \right] + \frac{g_z^{\text{true}} \beta B}{2} \approx 2a_1 \left[\frac{\sqrt{3}}{2} + \frac{1}{6} \frac{b_1}{2a_1} - \frac{1}{12\sqrt{3}} \left(\frac{b_1}{2a_1} \right)^2 \right] + \frac{g_z^{\text{true}} \beta B}{2}$$

$$E''_{+\frac{1}{2}} = 2a_1 \cos \left[\frac{1}{3} \arccos \frac{b_1}{2a_1} + \frac{2\pi}{3} \right] + \frac{g_z^{\text{true}} \beta B}{2}$$

$$\approx 2a_1 \left[-\frac{\sqrt{3}}{2} + \frac{1}{6} \frac{b_1}{2a_1} + \frac{1}{12\sqrt{3}} \left(\frac{b_1}{2a_1} \right)^2 \right] + \frac{g_z^{\text{true}} \beta B}{2}$$

$$E''_{-\frac{3}{2}} = 2a_1 \cos \left[\frac{1}{3} \arccos \frac{b_1}{2a_1} + \frac{4\pi}{3} \right] + \frac{g_z^{\text{true}} \beta B}{2} \approx 2a_1 \left[-\frac{1}{3} \frac{b_1}{2a_1} \right] + \frac{g_z^{\text{true}} \beta B}{2}$$

where

$$a_1 = \frac{2}{3} \sqrt{7(D^2 + 3E^2) + 6Dg_z^{\text{true}}\beta B + 3(g_z^{\text{true}}\beta B)^2}$$

$$b_1 = \frac{40(D^3 - 9DE^2) + 144D^2g_z^{\text{true}}\beta B - 108E^2g_z^{\text{true}}\beta B + 72D(g_z^{\text{true}}\beta B)^2}{21(D^2 + 3E^2) + 18Dg_z^{\text{true}}\beta B + 9(g_z^{\text{true}}\beta B)^2}.$$

Notice that the equations above are equivalent to those in the main text (Equations (6a)–(6c)). The other eigenvalues corresponding to the conjugate spin states $\{E_{-5/2}, E_{+3/2}, E_{-1/2}\}$ are derived by replacing B with $-B$. Figure S9 compares the exact and approximate energies. The energy difference between the conjugate spin state is equated to $g_z^{\text{eff}}\beta B$, i.e. $E_{+M_S} - E_{-M_S} = g_z^{\text{eff}}\beta B$, yielding identities with respect to B . In order to explicitly obtain the formula of $g_z^{\text{eff}}/g_z^{\text{true}}$, we exemplify the transition between the $|M_S = \pm 5/2\rangle$ -dominant states. Both sides of the equation are multiplied by a_1^5 and a_2^5 (a_2 is obtained with replacing B with $-B$ in a_1) to eliminate B from the denominators.

$$a_1^5 a_2^5 \left(E''_{+\frac{5}{2}} - E''_{-\frac{5}{2}} \right) = a_1^5 a_2^5 g_z^{\text{eff}} \beta B$$

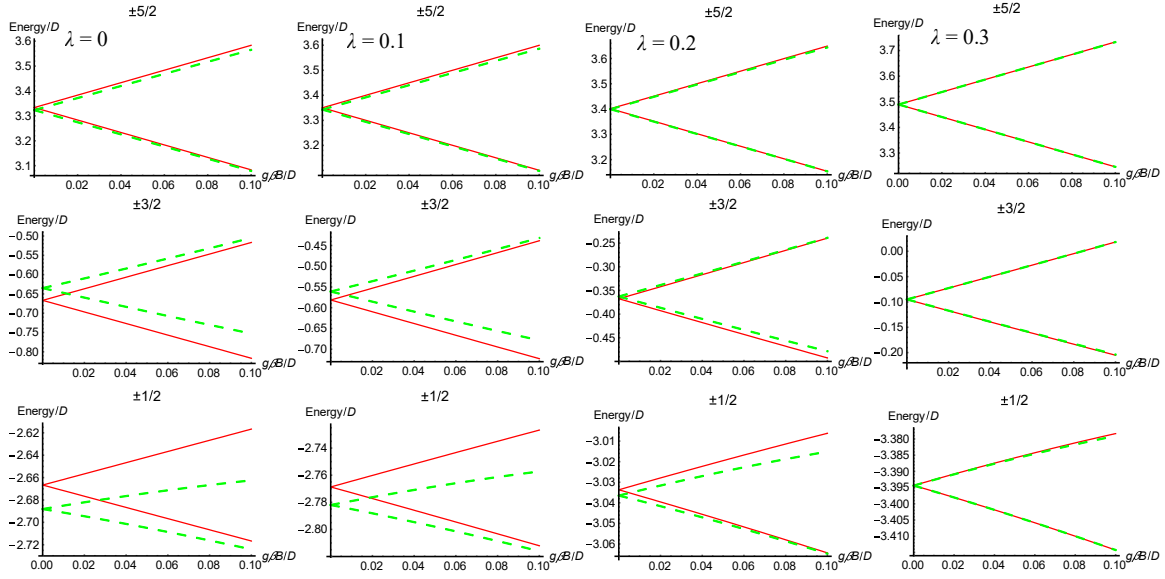


Figure S9 The energy diagrams of the exact (red) and approximate (green) eigenenergies of each M_S -dominant state for $\lambda = 0, 0.1, 0.2$ and 0.3 , respectively. Since $b_1/2a_1$ in arccosine is a monotonically decreasing function of λ , the approximate values become close to the exact ones.

Then, we separate the group of terms with only the even indices from those with only the odd indices of a_1 and a_2 and transpose the former terms to the opposite side of the equation. Squaring the equation yields identities with respect to B . The comparison of the coefficients with respect to the same order of B provides the quadratic or quartic equations, acquiring the $g^{\text{eff}}-g^{\text{true}}$ relationships as a function of $\lambda = E/D$. For example, the coefficient of the B^2 term gives a quadratic equation with respect to g^{eff} (or g^{true});

$$\begin{aligned}
& -\frac{92236816}{6561}(1+3\lambda^2)^8(3037+28683\lambda^2+79299\lambda^4+83349\lambda^6)^2 \\
& \times \left[22235661g_z^{\text{eff}^2}(1+3\lambda^2)^7 \right. \\
& - 3025226g_z^{\text{true}}g_z^{\text{eff}}(1+3\lambda^2)^5(403+2358\lambda^2+567\lambda^4) \\
& + g_z^{\text{eff}^2}(67358717+1146273129\lambda^2+5104268649\lambda^4-3003959115\lambda^6 \\
& - 56486583225\lambda^8-15603560469\lambda^{10}+12809086227\lambda^{12} \\
& \left. + 8931928887\lambda^{14}) \right] = 0. \tag{S33}
\end{aligned}$$

One of the solutions, which is too long and complicated to write, gives the $g^{\text{eff}}-g^{\text{true}}$ relationships as a function of $\lambda = E/D$. An expansion procedure similar to the above is applicable to eigenfield solutions, and the analytical expressions for $g^{\text{eff}}-g^{\text{true}}$ relationships are all lengthy. There is no significant advantage to exploit expansion approaches compared with the genuine Zeeman perturbation treatment.

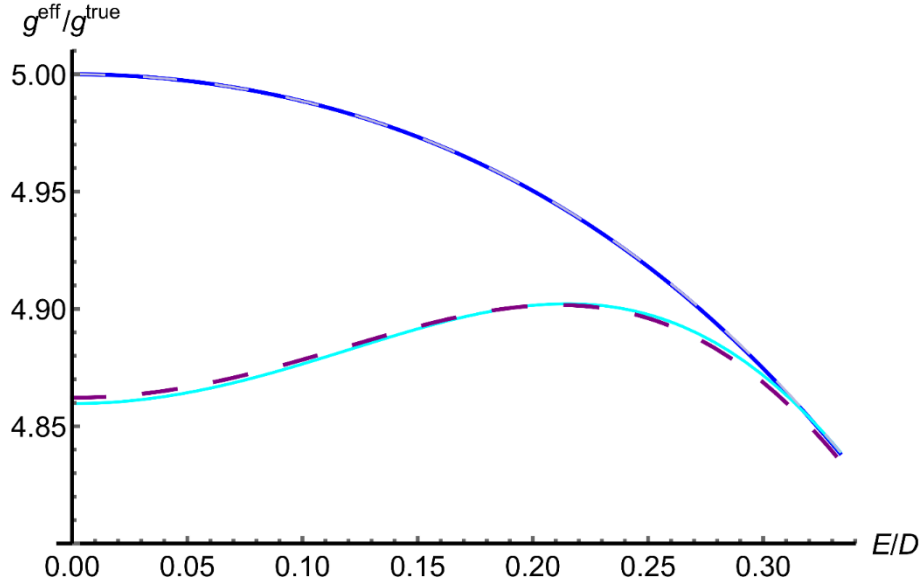


Figure S10 The $g_z^{\text{eff}}/g_z^{\text{true}}$ relationships as a function of the ratios of $|E/D|$ between the $|M_S = \pm 5/2\rangle$ -dominant sublevels in terms of the three different derivations. The blue solid line was from the genuine Zeeman perturbation approach, blue broken line denotes the numerical calculation using exact eigenenergies (Equation (S25) and its counterpart) with $g_z^{\text{true}}\beta B = 0.1$, purple broken line denotes the numerical calculation using $E''_{+5/2} - E''_{-5/2} = g_z^{\text{true}}\beta B$ with $g_z^{\text{true}}\beta B = 0.1$, and the curve denoted by the cyan solid line was obtained by solving the quadratic equation (S33). The discrepancy between the cyan and purple lines is due to the ignorance of the higher-order of series expansion of arccosine and cosine.

The resolvent cubic equation of this quartic equation is

$$s^3 + 2ps^2 + (p^2 - 4r)s - q^2 = 0.$$

where

$$p = -32D^2 - 66E^2 - 10(g_z^{\text{true}}\beta B)^2$$

$$q = 288DE^2 - 64D(g_z^{\text{true}}\beta B)^2$$

$$r = 256D^4 - 96D^2E^2 - 160D^2(g_z^{\text{true}}\beta B)^2 + 225E^4 + 234E^2(g_z^{\text{true}}\beta B)^2 + 9(g_z^{\text{true}}\beta B)^4.$$

Replacing s with $s - 2p/3$, we obtain the following simplified cubic equation;

$$s^3 = \frac{1}{3}(p^2 + 12r)s + \frac{1}{27}(27q^2 + 2p^3 - 72pr).$$

According to the Viète's method, all the analytical solutions are obtained, and one of the solutions is

$$s_0 = 2a_0 \cos \left[\frac{1}{3} \arccos \left(\frac{b_0}{2a_0} \right) \right] - \frac{2p}{3}$$

where

$$a_0 = \frac{\sqrt{p^2 + 12r}}{3}$$

$$b_0 = \frac{27q^2 + 2p^3 - 72pr}{3p^2 + 36r}.$$

Then, the quartic equation can be rewritten as the product of two quadratic equations with s_0

$$\left\{ \left(x^2 + \frac{p + s_0}{2} \right) + \sqrt{s_0} \left(x - \frac{q}{2s_0} \right) \right\} \left\{ \left(x^2 + \frac{p + s_0}{2} \right) - \sqrt{s_0} \left(x - \frac{q}{2s_0} \right) \right\} = 0$$

$$\Leftrightarrow \begin{cases} x = \frac{1}{2} \left[-\sqrt{s_0} \pm \sqrt{-2p - s_0 - \frac{2q}{\sqrt{s_0}}} \right] \\ x = \frac{1}{2} \left[\sqrt{s_0} \pm \sqrt{-2p - s_0 + \frac{2q}{\sqrt{s_0}}} \right]. \end{cases}$$

Therefore, the exact eigenenergies of the $|M_S = \pm 3\rangle, |\pm 1\rangle$ -dominant states are

$$E_{+3} = \frac{1}{2} \left[2D + \sqrt{s_0} + \sqrt{-2p - s_0 - \frac{2q}{\sqrt{s_0}}} \right] \quad (\text{S34a})$$

$$E_{-3} = \frac{1}{2} \left[2D + \sqrt{s_0} - \sqrt{-2p - s_0 - \frac{2q}{\sqrt{s_0}}} \right] \quad (\text{S34b})$$

$$E_{+1} = \frac{1}{2} \left[2D - \sqrt{s_0} + \sqrt{-2p - s_0 + \frac{2q}{\sqrt{s_0}}} \right] \quad (\text{S34c})$$

$$E_{-1} = \frac{1}{2} \left[2D - \sqrt{s_0} - \sqrt{-2p - s_0 + \frac{2q}{\sqrt{s_0}}} \right]. \quad (\text{S34d})$$

Next, we focus on the eigenenergies of $H_{\text{ZFS}+\text{eZ},2}^{\text{septet}}$. The corresponding secular equation is cubic as follows;

$$y^3 + 4Dy^2 - [60E^2 + 4(g_z^{\text{true}}\beta B)^2]y - 16DB^2 = 0.$$

In order to use the Viète's solution, replacing y with $y - 4D/3$ yields

$$y^3 = \left[\frac{16}{3}D^2 + 60E^2 + 4(g_z^{\text{true}}\beta B)^2 \right] y - \frac{128}{27}D^3 - 80DE^2 + \frac{32}{3}D(g_z^{\text{true}}\beta B)^2.$$

Thus the eigenenergies in the trigonometric form are

$$E_n = 2a \cos \left[\frac{1}{3} \arccos \frac{b}{2a} + \frac{2n\pi}{3} \right] - \frac{4D}{3} \quad (n = 0, 1, 2) \quad (\text{S35})$$

where

$$a = \frac{2}{3} \sqrt{2D^2 + 15E^2 + (g_z^{\text{true}}\beta B)^2}$$

$$b = - \frac{32D^3 + 540DE^2 - 72D(g_z^{\text{true}}\beta B)^2}{6D^2 + 45E^2 + 3(g_z^{\text{true}}\beta B)^2}$$

and $n = 0, 1$ and 2 correspond to the $|M_S = +2\rangle$, $|-2\rangle$ and $|0\rangle$ dominant states, respectively. The $g^{\text{eff}}-g^{\text{true}}$ relationships as a function of $\lambda = E/D$ between the $\pm M_S$ -dominant states can be obtained from the equation $E_{M_S} - E_{-M_S} = g^{\text{eff}}\beta B$. Considering this equation as identities with respect to B , we obtained the specific solutions $g_z^{\text{eff}}/g_z^{\text{true}} = 6, 4$ and 2 , for the $|M_S = \pm 3\rangle$, $|\pm 2\rangle$ and $|\pm 1\rangle$ -dominant transition, respectively, if and only if $E/D = 0$.

5.2 The $g^{\text{eff}}-g^{\text{true}}$ relationships by using of a genuine Zeeman perturbation approach in the case of spin-septet states ($S = 3$)

The ZFS Hamiltonian in the spin-septet case can be prepared with $B = 0$ in the $H_{\text{ZFS}+eZ}^{\text{septet}}$ in the previous section. This Hamiltonian can be also divided into two matrixes, and the matrix representation of the ZFS Hamiltonian on the basis of $\{|+3\rangle, |+1\rangle, |-1\rangle, |-3\rangle\}$ is

$$H_{\text{ZFS},1}^{\text{septet}} = \begin{pmatrix} \langle +3| & \langle +1| & \langle -1| & \langle -3| \\ 5D & \sqrt{15}E & 0 & 0 \\ \sqrt{15}E & -3D & 6E & 0 \\ 0 & 6E & -3D & \sqrt{15}E \\ 0 & 0 & \sqrt{15}E & 5D \end{pmatrix} \begin{matrix} |+3\rangle \\ |+1\rangle \\ |-1\rangle \\ |-3\rangle \end{matrix}$$

The eigenenergies and corresponding eigenfunctions of $H_{\text{ZFS},1}^{\text{septet}}$ are

$$\varepsilon_{+3}^{(0)} = D + 3E + 2\sqrt{2}\sqrt{2D^2 - 3DE + 3E^2} \quad (\text{S36a})$$

$$\varepsilon_{+1}^{(0)} = D + 3E - 2\sqrt{2}\sqrt{2D^2 - 3DE + 3E^2} \quad (\text{S36b})$$

$$\varepsilon_{-1}^{(0)} = D - 3E - 2\sqrt{2}\sqrt{2D^2 + 3DE + 3E^2} \quad (\text{S36c})$$

$$\varepsilon_{-3}^{(0)} = D - 3E + 2\sqrt{2}\sqrt{2D^2 + 3DE + 3E^2} \quad (\text{S36d})$$

$$\varphi_{+3}^{(0)} = \alpha_{+3}|+3\rangle + \beta_{+3}|+1\rangle + \gamma_{+3}|-1\rangle + \delta_{+3}|-3\rangle \quad (\text{S37a})$$

$$\varphi_{+1}^{(0)} = \alpha_{+1}|+3\rangle + \beta_{+1}|+1\rangle + \gamma_{+1}|-1\rangle + \delta_{+1}|-3\rangle \quad (\text{S37b})$$

$$\varphi_{-1}^{(0)} = \alpha_{-1}|+3\rangle + \beta_{-1}|+1\rangle + \gamma_{-1}|-1\rangle + \delta_{-1}|-3\rangle \quad (\text{S37c})$$

$$\varphi_{-3}^{(0)} = \alpha_{-3}|+3\rangle + \beta_{-3}|+1\rangle + \gamma_{-3}|-1\rangle + \delta_{-3}|-3\rangle \quad (\text{S37d})$$

where

$$\begin{aligned} \frac{\gamma_n}{\delta_n} &= \frac{\beta_n}{\alpha_n} = \frac{\varepsilon_n^{(0)} - 5D}{\sqrt{15}E}, \\ \frac{\alpha_n}{\delta_n} &= \begin{cases} 1 & (\text{if } n = +3, +1) \\ -1 & (\text{if } n = -3, -1) \end{cases}, \\ \frac{\beta_n}{\delta_n} &= \frac{\alpha_n \beta_n}{\delta_n \alpha_n} = \begin{cases} \frac{\varepsilon_n^{(0)} - 5D}{\sqrt{15}E} & (\text{if } n = +3, +1) \\ -\frac{\varepsilon_n^{(0)} - 5D}{\sqrt{15}E} & (\text{if } n = -3, -1) \end{cases}, \\ \delta_n^2 &= \left[2 + \frac{2(\varepsilon_n^{(0)} - 5D)^2}{15E^2} \right]^{-1} \\ &(n = \pm 1, \pm 3). \end{aligned}$$

The matrix elements of the perturbing electron-Zeeman Hamiltonian can be represented as

$$(H_{eZ,1}^{\text{septet}})_{l,m} = g_z^{\text{true}} \beta B (S_z)_{l,m}$$

$$\begin{aligned}
&\rightarrow (H'_{eZ,1})_{l,m} = g_z^{\text{true}} \beta B (3\alpha_l \alpha_m + \beta_l \beta_m - \gamma_l \gamma_m - 3\delta_l \delta_m) \\
&= g_z^{\text{true}} \beta B \left(3 \frac{\alpha_l \alpha_m}{\delta_l \delta_m} + \frac{\beta_l \beta_m}{\delta_l \delta_m} - \frac{\gamma_l \gamma_m}{\delta_l \delta_m} - 3 \right) \delta_l \delta_m \\
&= \begin{cases} 0 & (\text{if } lm > 0) \\ \frac{g_z^{\text{true}} \beta B \left[(E_l^{(0)} - 5D)(E_m^{(0)} - 5D) - 45E^2 \right]}{\sqrt{(E_l^{(0)} - 5D)^2 + 15E^2} \sqrt{(E_m^{(0)} - 5D)^2 + 15E^2}} & (\text{if } lm < 0) \end{cases}
\end{aligned}$$

where $l, m = \pm 1, \pm 3$. For example, $(H'_{eZ,1})_{+3,-1}$ represents $\langle \varphi_{+3}^{(0)} | H'_{eZ,1} | \varphi_{-1}^{(0)} \rangle$. The perturbed energies will be obtained with the Hamiltonian $H'_{eZ,1}$.

The matrix representation of the ZFS Hamiltonian counterpart $H_{\text{ZFS},2}^{\text{septet}}$ is

$$H_{\text{ZFS},2}^{\text{septet}} = \begin{pmatrix} \langle +2 | & \langle 0 | & \langle -2 | \\ 0 & \sqrt{30}E & 0 \\ \sqrt{30}E & -4D & \sqrt{30}E \\ 0 & \sqrt{30}E & 0 \end{pmatrix} \begin{matrix} | +2 \rangle \\ | 0 \rangle \\ | -2 \rangle \end{matrix}$$

The eigenenergies and eigenfunctions are

$$\varepsilon_{+2}^{(0)} = -2D + 2\sqrt{D^2 + 15E^2}, \quad \varphi_{+2}^{(0)} = \alpha_{+2}|+2\rangle + \beta_{+2}|0\rangle + \gamma_{+2}|-2\rangle \quad (\text{S38a})$$

$$\varepsilon_{-2}^{(0)} = 0, \quad \varphi_{-2}^{(0)} = (|+2\rangle - |-2\rangle)/\sqrt{2} \quad (\text{S38b})$$

$$\varepsilon_0^{(0)} = -2D - 2\sqrt{D^2 + 15E^2}, \quad \varphi_0^{(0)} = \alpha_0|+2\rangle + \beta_0|0\rangle + \gamma_0|-2\rangle \quad (\text{S38c})$$

where

$$\frac{\alpha_{+2}}{\beta_{+2}} = \frac{\gamma_{+2}}{\beta_{+2}} = \frac{\sqrt{30}E}{-2D + 2\sqrt{D^2 + 15E^2}}, \quad \beta_{+2} = \left[1 + \frac{30E^2}{2D^2 + 15E^2 - 2D\sqrt{D^2 + 15E^2}} \right]^{-\frac{1}{2}}$$

$$\frac{\alpha_0}{\beta_0} = \frac{\gamma_0}{\beta_0} = \frac{\sqrt{30}E}{-2D - 2\sqrt{D^2 + 15E^2}}, \quad \beta_0 = \left[1 + \frac{30E^2}{2D^2 + 15E^2 + 2D\sqrt{D^2 + 15E^2}} \right]^{-\frac{1}{2}}.$$

Thus the perturbing electron-Zeeman Hamiltonian can be rewritten as follows.

$$H_{eZ,2}^{\text{septet}} = \begin{pmatrix} 2g_z^{\text{true}} \beta B & 0 & 0 \\ 0 & 0 & 0 \\ 0 & 0 & -2g_z^{\text{true}} \beta B \end{pmatrix} \rightarrow H'_{eZ,2} = 2g_z^{\text{true}} \beta B \begin{pmatrix} 0 & 0 & \alpha_{+2} \\ 0 & 0 & \alpha_0 \\ \alpha_{+2} & \alpha_0 & 0 \end{pmatrix}$$

Summarizing the perturbed energies to the second order;

$$E'_{+3} = \varepsilon_{+3}^{(0)} + \frac{(g_z^{\text{true}} \beta B)^2 \left[(\varepsilon_{+3}^{(0)} - 5D)(\varepsilon_{-1}^{(0)} - 5D) - 45E^2 \right]^2}{\left[\varepsilon_{+3}^{(0)} - \varepsilon_{-1}^{(0)} \right] \left[(\varepsilon_{+3}^{(0)} - 5D)^2 + 15E^2 \right] \left[(\varepsilon_{-1}^{(0)} - 5D)^2 + 15E^2 \right]} + \frac{(g_z^{\text{true}} \beta B)^2 \left[(\varepsilon_{+3}^{(0)} - 5D)(\varepsilon_{-3}^{(0)} - 5D) - 45E^2 \right]^2}{\left[\varepsilon_{+3}^{(0)} - \varepsilon_{-3}^{(0)} \right] \left[(\varepsilon_{+3}^{(0)} - 5D)^2 + 15E^2 \right] \left[(\varepsilon_{-3}^{(0)} - 5D)^2 + 15E^2 \right]} \quad (\text{S39a})$$

$$E'_{+2} = -2D + 2\sqrt{D^2 + 15E^2} - \frac{2(g_z^{\text{true}} \beta B)^2 \alpha_{+2}^2}{D - \sqrt{D^2 + 15E^2}} \quad (\text{S39b})$$

$$E'_{+1} = \varepsilon_{+1}^{(0)} + \frac{(g_z^{\text{true}} \beta B)^2 \left[(\varepsilon_{+1}^{(0)} - 5D)(\varepsilon_{-1}^{(0)} - 5D) - 45E^2 \right]^2}{\left[\varepsilon_{+1}^{(0)} - \varepsilon_{-1}^{(0)} \right] \left[(\varepsilon_{+1}^{(0)} - 5D)^2 + 15E^2 \right] \left[(\varepsilon_{-1}^{(0)} - 5D)^2 + 15E^2 \right]} + \frac{(g_z^{\text{true}} \beta B)^2 \left[(\varepsilon_{+1}^{(0)} - 5D)(\varepsilon_{-3}^{(0)} - 5D) - 45E^2 \right]^2}{\left[\varepsilon_{+1}^{(0)} - \varepsilon_{-3}^{(0)} \right] \left[(\varepsilon_{+1}^{(0)} - 5D)^2 + 15E^2 \right] \left[(\varepsilon_{-3}^{(0)} - 5D)^2 + 15E^2 \right]} \quad (\text{S39c})$$

$$E'_0 = -2D - 2\sqrt{D^2 + 15E^2} - \frac{2(g_z^{\text{true}} \beta B)^2 \alpha_0^2}{D + \sqrt{D^2 + 15E^2}} \quad (\text{S39d})$$

$$E'_{-1} = \varepsilon_{-1}^{(0)} + \frac{(g_z^{\text{true}} \beta B)^2 \left[(\varepsilon_{-1}^{(0)} - 5D)(\varepsilon_{+3}^{(0)} - 5D) - 45E^2 \right]^2}{\left[\varepsilon_{-1}^{(0)} - \varepsilon_{+3}^{(0)} \right] \left[(\varepsilon_{-1}^{(0)} - 5D)^2 + 15E^2 \right] \left[(\varepsilon_{+3}^{(0)} - 5D)^2 + 15E^2 \right]} + \frac{(g_z^{\text{true}} \beta B)^2 \left[(\varepsilon_{-1}^{(0)} - 5D)(\varepsilon_{+1}^{(0)} - 5D) - 45E^2 \right]^2}{\left[\varepsilon_{-1}^{(0)} - \varepsilon_{+1}^{(0)} \right] \left[(\varepsilon_{-1}^{(0)} - 5D)^2 + 15E^2 \right] \left[(\varepsilon_{+1}^{(0)} - 5D)^2 + 15E^2 \right]} \quad (\text{S39e})$$

$$E'_{-2} = \frac{2(g_z^{\text{true}} \beta B)^2 \alpha_{+2}^2}{D - \sqrt{D^2 + 15E^2}} + \frac{2(g_z^{\text{true}} \beta B)^2 \alpha_0^2}{D + \sqrt{D^2 + 15E^2}} \quad (\text{S39f})$$

$$E'_{-3} = \varepsilon_{-3}^{(0)} + \frac{(g_z^{\text{true}} \beta B)^2 \left[(\varepsilon_{-3}^{(0)} - 5D)(\varepsilon_{+3}^{(0)} - 5D) - 45E^2 \right]^2}{\left[\varepsilon_{-3}^{(0)} - \varepsilon_{+3}^{(0)} \right] \left[(\varepsilon_{-3}^{(0)} - 5D)^2 + 15E^2 \right] \left[(\varepsilon_{+3}^{(0)} - 5D)^2 + 15E^2 \right]} + \frac{(g_z^{\text{true}} \beta B)^2 \left[(\varepsilon_{-3}^{(0)} - 5D)(\varepsilon_{+1}^{(0)} - 5D) - 45E^2 \right]^2}{\left[\varepsilon_{-3}^{(0)} - \varepsilon_{+1}^{(0)} \right] \left[(\varepsilon_{-3}^{(0)} - 5D)^2 + 15E^2 \right] \left[(\varepsilon_{+1}^{(0)} - 5D)^2 + 15E^2 \right]} \quad (\text{S39g})$$

The $g_z^{\text{eff}}/g_z^{\text{true}}$ relationship as a function of $\lambda = E/D$ for the $|M_S = \pm 3\rangle$ dominant transition is calculated from the equation.

$$E'_{+3} - E'_{-3} = g_z^{\text{eff}} \beta B$$

$$\begin{aligned}
\varepsilon_{+3}^{(0)} - \varepsilon_{-3}^{(0)} + & \frac{(g_z^{\text{true}}\beta B)^2 \left[(\varepsilon_{+3}^{(0)} - 5D)(\varepsilon_{-1}^{(0)} - 5D) - 45E^2 \right]^2}{\left[\varepsilon_{+3}^{(0)} - \varepsilon_{-1}^{(0)} \right] \left[(\varepsilon_{+3}^{(0)} - 5D)^2 + 15E^2 \right] \left[(\varepsilon_{-1}^{(0)} - 5D)^2 + 15E^2 \right]} \\
& + \frac{2(g_z^{\text{true}}\beta B)^2 \left[(\varepsilon_{+3}^{(0)} - 5D)(\varepsilon_{-3}^{(0)} - 5D) - 45E^2 \right]^2}{\left[\varepsilon_{+3}^{(0)} - \varepsilon_{-3}^{(0)} \right] \left[(\varepsilon_{+3}^{(0)} - 5D)^2 + 15E^2 \right] \left[(\varepsilon_{-3}^{(0)} - 5D)^2 + 15E^2 \right]} \\
& - \frac{(g_z^{\text{true}}\beta B)^2 \left[(\varepsilon_{-3}^{(0)} - 5D)(\varepsilon_{+1}^{(0)} - 5D) - 45E^2 \right]^2}{\left[\varepsilon_{-3}^{(0)} - \varepsilon_{+1}^{(0)} \right] \left[(\varepsilon_{-3}^{(0)} - 5D)^2 + 15E^2 \right] \left[(\varepsilon_{+1}^{(0)} - 5D)^2 + 15E^2 \right]} = g_z^{\text{eff}}\beta B;
\end{aligned} \tag{S40a}$$

for the $|\pm 2\rangle$ dominant transition,

$$E'_{+2} - E'_{-2} = -2D + 2\sqrt{D^2 + 15E^2} - \frac{4(g_z^{\text{true}}\beta B)^2\alpha_{+2}^2}{D - \sqrt{D^2 + 15E^2}} - \frac{2(g_z^{\text{true}}\beta B)^2\alpha_0^2}{D + \sqrt{D^2 + 15E^2}} = g_z^{\text{eff}}\beta B$$

$$15g_z^{\text{eff}}\beta BE^2 = 4(g_z^{\text{true}}\beta B)^2 \left(D + \sqrt{D^2 + 15E^2} \right) \alpha_{+2}^2$$

$$+ [2(g_z^{\text{true}}\beta B)^2 - 30E^2] \left(D - \sqrt{D^2 + 15E^2} \right) \alpha_0^2$$

$$15g_z^{\text{eff}}\beta BE^2 = (g_z^{\text{true}}\beta B)^2 \left[4 \left(D + \sqrt{D^2 + 15E^2} \right) \alpha_{+2}^2 + 2 \left(D - \sqrt{D^2 + 15E^2} \right) \alpha_0^2 \right]$$

$$- 30E^2 \left(D - \sqrt{D^2 + 15E^2} \right) \alpha_0^2; \tag{S40b}$$

and for the $|\pm 1\rangle$ dominant transition,

$$E'_{+1} - E'_{-1} = g_z^{\text{eff}}\beta B. \tag{S40c}$$

Considering equations (S40a)–(S40c) as identities with respect to B , we obtain the special solution $g_z^{\text{eff}}/g_z^{\text{true}} = 0$ for the $|M_S = \pm 2\rangle$ dominant transition if and only if $E/D = 0$, while no special solutions for the $|M_S = \pm 3\rangle, |\pm 1\rangle$ dominant transitions.

Exploiting the approximate formulas in the following, a simplified expression for E'_{+3} can be obtained.

$$\sqrt{2D^2 - 3DE + 3E^2} \approx \sqrt{2D^2} - \frac{3\sqrt{D^2}E}{2\sqrt{2}D} + \frac{15E^2}{16\sqrt{2}D^2}$$

$$\sqrt{2D^2 + 3DE + 3E^2} \approx \sqrt{2D^2} + \frac{3\sqrt{D^2}E}{2\sqrt{2}D} + \frac{15E^2}{16\sqrt{2}D^2}$$

$$\begin{aligned}
& E'_{+3} \\
&= D + 3E + 2\sqrt{2} \left(\sqrt{2D^2} - \frac{3\sqrt{D^2}E}{2\sqrt{2}D} + \frac{15E^2}{16\sqrt{2D^2}} \right) \\
&\quad + \frac{(g_z^{\text{true}}\beta B)^2 \left[(\varepsilon_{+3}^{(0)} - 5D)(\varepsilon_{-1}^{(0)} - 5D) - 45E^2 \right]^2}{\left[(\varepsilon_{+3}^{(0)} - 5D)^2 + 15E^2 \right] \left[(\varepsilon_{-1}^{(0)} - 5D)^2 + 15E^2 \right]} \\
&+ \frac{6E + 2\sqrt{2} \left(\sqrt{2D^2} - \frac{3\sqrt{D^2}E}{2\sqrt{2}D} + \frac{15E^2}{16\sqrt{2D^2}} \right) + 2\sqrt{2} \left(\sqrt{2D^2} + \frac{3\sqrt{D^2}E}{2\sqrt{2}D} + \frac{15E^2}{16\sqrt{2D^2}} \right)}{6E + 2\sqrt{2} \left(\sqrt{2D^2} - \frac{3\sqrt{D^2}E}{2\sqrt{2}D} + \frac{15E^2}{16\sqrt{2D^2}} \right) - 2\sqrt{2} \left(\sqrt{2D^2} + \frac{3\sqrt{D^2}E}{2\sqrt{2}D} + \frac{15E^2}{16\sqrt{2D^2}} \right)} \\
&\quad + \frac{(g_z^{\text{true}}\beta B)^2 \left[(\varepsilon_{+3}^{(0)} - 5D)(\varepsilon_{-3}^{(0)} - 5D) - 45E^2 \right]^2}{\left[(\varepsilon_{+3}^{(0)} - 5D)^2 + 15E^2 \right] \left[(\varepsilon_{-3}^{(0)} - 5D)^2 + 15E^2 \right]} \\
&= D + 3E + 4\sqrt{D^2} - \frac{3\sqrt{D^2}E}{D} + \frac{15E^2}{8\sqrt{D^2}} \\
&\quad + \frac{4\sqrt{D^2}(g_z^{\text{true}}\beta B)^2 \left[(\varepsilon_{+3}^{(0)} - 5D)(\varepsilon_{-1}^{(0)} - 5D) - 45E^2 \right]^2}{(32D^2 + 24\sqrt{D^2}E + 15E^2) \left[(\varepsilon_{+3}^{(0)} - 5D)^2 + 15E^2 \right] \left[(\varepsilon_{-1}^{(0)} - 5D)^2 + 15E^2 \right]} \\
&\quad + \frac{D(g_z^{\text{true}}\beta B)^2 \left[(\varepsilon_{+3}^{(0)} - 5D)(\varepsilon_{-3}^{(0)} - 5D) - 45E^2 \right]^2}{(6DE - 6\sqrt{D^2}E) \left[(\varepsilon_{+3}^{(0)} - 5D)^2 + 15E^2 \right] \left[(\varepsilon_{-3}^{(0)} - 5D)^2 + 15E^2 \right]}
\end{aligned}$$

Note that this formula is valid if $D < 0$, otherwise $D - \sqrt{D^2}$ is zero.

5.3 Global permutation for ZFS energies in the case of $S = 3$

Let us consider the permutation of the axes in the ZFS energies of the spin septet state. The calculation for the terms $D + 3E$, $D - 3E$ and $-2D$ was mentioned in the quintet state. We demonstrate here the permutation rules of only the square root terms.

$$2\sqrt{2D^2 - 3DE + 3E^2} \xrightarrow{\mathbf{B}\parallel x} \sqrt{2}\sqrt{D^2 + 15E^2}$$

$$2\sqrt{2D^2 - 3DE + 3E^2} \xrightarrow{\mathbf{B}\parallel y} \sqrt{2}\sqrt{D^2 + 15E^2}$$

$$2\sqrt{2D^2 + 3DE + 3E^2} \xrightarrow{\mathbf{B}\parallel x} 2\sqrt{2D^2 - 3ED + 3E^2}$$

$$2\sqrt{2D^2 + 3DE + 3E^2} \xrightarrow{\mathbf{B}\parallel y} 2\sqrt{2D^2 + 3ED + 3E^2}$$

$$2\sqrt{D^2 + 15E^2} \xrightarrow{\mathbf{B}\parallel x} 2\sqrt{2}\sqrt{2D^2 + 3DE + 3E^2}$$

$$2\sqrt{D^2 + 15E^2} \xrightarrow{\mathbf{B}\parallel y} 2\sqrt{2}\sqrt{2D^2 - 3DE + 3E^2}$$

By using of the relationships above, the permutation relationships are obtained.

$$\varepsilon_{+3}^{(0)} = D + 3E + 2\sqrt{2}\sqrt{2D^2 - 3DE + 3E^2} \xrightarrow{\mathbf{B}\parallel x} -2D + 2\sqrt{D^2 + 15E^2} = \varepsilon_{+2}^{(0)}$$

$$\varepsilon_{+3}^{(0)} \xrightarrow{\mathbf{B}\parallel y} -2D + 2\sqrt{D^2 + 15E^2} = \varepsilon_{+2}^{(0)}$$

$$\varepsilon_{+2}^{(0)} = -2D + 2\sqrt{D^2 + 15E^2} \xrightarrow{\mathbf{B}\parallel x} D - 3E + 2\sqrt{2}\sqrt{2D^2 + 3DE + 3E^2} = \varepsilon_{-3}^{(0)}$$

$$\varepsilon_{+2}^{(0)} \xrightarrow{\mathbf{B}\parallel y} D + 3E + 2\sqrt{2}\sqrt{2D^2 - 3DE + 3E^2} = \varepsilon_{+3}^{(0)}$$

$$\varepsilon_{+1}^{(0)} = D + 3E - 2\sqrt{2}\sqrt{2D^2 - 3DE + 3E^2} \xrightarrow{\mathbf{B}\parallel x} -2D - 2\sqrt{D^2 + 15E^2} = \varepsilon_0^{(0)}$$

$$\varepsilon_{+1}^{(0)} \xrightarrow{\mathbf{B}\parallel y} -2D - 2\sqrt{D^2 + 15E^2} = \varepsilon_0^{(0)}$$

$$\varepsilon_0^{(0)} = -2D - 2\sqrt{D^2 + 15E^2} \xrightarrow{\mathbf{B}\parallel x} D - 3E - 2\sqrt{2}\sqrt{2D^2 + 3DE + 3E^2} = \varepsilon_{-1}^{(0)}$$

$$\varepsilon_0^{(0)} \xrightarrow{\mathbf{B}\parallel y} D + 3E - 2\sqrt{2}\sqrt{2D^2 - 3DE + 3E^2} = \varepsilon_{+1}^{(0)}$$

$$\varepsilon_{-1}^{(0)} = D - 3E - 2\sqrt{2}\sqrt{2D^2 + 3DE + 3E^2} \xrightarrow{\mathbf{B}\parallel x} D + 3E - 2\sqrt{2}\sqrt{2D^2 - 3DE + 3E^2} = \varepsilon_{+3}^{(0)}$$

$$\varepsilon_{-1}^{(0)} \xrightarrow{\mathbf{B}\parallel y} D - 3E - 2\sqrt{2}\sqrt{2D^2 + 3DE + 3E^2} = \varepsilon_{-1}^{(0)}$$

$$\varepsilon_{-3}^{(0)} = D - 3E + 2\sqrt{2}\sqrt{2D^2 + 3DE + 3E^2} \xrightarrow{\mathbf{B}\parallel x} D + 3E + 2\sqrt{2}\sqrt{2D^2 - 3DE + 3E^2} = \varepsilon_{+3}^{(0)}$$

$$\varepsilon_{-3}^{(0)} \xrightarrow{\mathbf{B}||y} D - 3E + 2\sqrt{2}\sqrt{2D^2 + 3DE + 3E^2} = \varepsilon_{-3}^{(0)}$$

Table S1 Summarized the permutation relationships in the spin-septet state

B//z	B//x	B//y
+3	+2	+2
+2	-3	+3
+1	0	0
0	-1	+1
-1	+1	-1
-2	-2	-2
-3	+3	-3

*The numbers (0, ±1, ±2, ±3) correspond to the M_S of the ZFS energies (e.g. +3 represents $\varepsilon_{+3}^{(0)}$).

6. Analytical formulas for spin-octet states

6.1 Derivation of the $g^{\text{eff}}-g^{\text{true}}$ relationships as a function of $|E/D|$ in spin-octet states ($S = 7/2$)

The spin Hamiltonian considering the ZFS and electron-Zeeman terms (\mathbf{B}/z) for spin-octet states can be divided into two matrixes whose basis sets are $\{|+7/2\rangle, |-5/2\rangle, |+3/2\rangle, |-1/2\rangle\}$ and $\{|-7/2\rangle, |+5/2\rangle, |-3/2\rangle, |+1/2\rangle\}$, respectively. The matrix representation of the former is

$$H_{\text{ZFS+eZ}}^{\text{octet}} = \begin{pmatrix} \langle +7/2 | & \langle -5/2 | & \langle +3/2 | & \langle -1/2 | \\ 7D + \frac{7}{2}g_z^{\text{true}}\beta B & 0 & \sqrt{21}E & 0 \\ 0 & D - \frac{5}{2}g_z^{\text{true}}\beta B & 0 & 3\sqrt{5}E \\ \sqrt{21}E & 0 & -3D + \frac{3}{2}g_z^{\text{true}}\beta B & 2\sqrt{15}E \\ 0 & 3\sqrt{5}E & 2\sqrt{15}E & -5D - \frac{1}{2}g_z^{\text{true}}\beta B \end{pmatrix} \begin{matrix} |+7/2\rangle \\ |-5/2\rangle \\ |+3/2\rangle \\ |-1/2\rangle \end{matrix}$$

The exact eigenenergies are the solutions of the following quartic equation.

$$\begin{aligned} x^4 - 2g_z^{\text{true}}\beta B x^3 - \left[42(D^2 + 3E^2) + 20Dg_z^{\text{true}}\beta B + \frac{17}{2}(g_z^{\text{true}}\beta B)^2 \right] x^2 \\ - \left[64(D^3 - 9DE^2) + (86D^2 - 222E^2)(g_z^{\text{true}}\beta B) + 44D(g_z^{\text{true}}\beta B)^2 - \frac{19}{2}(g_z^{\text{true}}\beta B)^3 \right] x \\ + 105(D^2 + 3E^2)^2 - 84(3D^3 - 7DE^2)(g_z^{\text{true}}\beta B) - \frac{105}{2}(D^2 - 5E^2)(g_z^{\text{true}}\beta B)^2 \\ + 63D(g_z^{\text{true}}\beta B)^3 + \frac{105}{16}(g_z^{\text{true}}\beta B)^4 = 0 \end{aligned}$$

In order to eliminate the x^3 term, replacing x with $x + g_z^{\text{true}}\beta B/2$.

$$\begin{aligned} x^4 - [42(D^2 + 3E^2) + 20Dg_z^{\text{true}}\beta B + 10(g_z^{\text{true}}\beta B)^2] x^2 \\ - [64(D^3 - 9DE^2) + (128D^2 - 96E^2)(g_z^{\text{true}}\beta B) + 64D(g_z^{\text{true}}\beta B)^2] x \\ + 105(D^2 + 3E^2)^2 - (284D^3 - 876DE^2)(g_z^{\text{true}}\beta B) - (106D^2 - 342E^2)(g_z^{\text{true}}\beta B)^2 \\ + 36D(g_z^{\text{true}}\beta B)^3 + 9(g_z^{\text{true}}\beta B)^4 = 0 \end{aligned}$$

The resolvent cubic equation for the quartic equation above is

$$u^3 + 2pu^2 + (p^2 - 4r)u - q^2 = 0$$

where

$$\begin{aligned} p &= -42(D^2 + 3E^2) - 20Dg_z^{\text{true}}\beta B - 10(g_z^{\text{true}}\beta B)^2 \\ q &= -64(D^3 - 9DE^2) - (128D^2 - 96E^2)(g_z^{\text{true}}\beta B) - 64D(g_z^{\text{true}}\beta B)^2 \\ r &= 105(D^2 + 3E^2)^2 - (284D^3 - 876DE^2)(g_z^{\text{true}}\beta B) - (106D^2 - 342E^2)(g_z^{\text{true}}\beta B)^2 \\ &\quad + 36D(g_z^{\text{true}}\beta B)^3 + 9(g_z^{\text{true}}\beta B)^4. \end{aligned}$$

Replacing u with $u - 2p/3$ gives us the following equation;

$$u^3 = \frac{1}{3}(p^2 + 12r)u + \frac{1}{27}(2p^3 - 72pr + 27q^2).$$

One of the solutions of the cubic equation is

$$u_0 = 2a \cos \left[\frac{1}{3} \arccos \left(\frac{b_0}{2a_0} \right) \right] - \frac{2p}{3}$$

where

$$a_0 = \frac{\sqrt{p^2 + 12r}}{3}$$

$$b_0 = \frac{2p^3 - 72pr + 27q^2}{3p^2 + 36r}.$$

Therefore, the exact energies of the Hamiltonian are

$$E = \frac{g_z^{\text{true}} \beta B}{2} - \frac{1}{2} \left[\sqrt{u_0} \pm \sqrt{-2p - u_0 + \frac{2q}{\sqrt{u_0}}} \right] \quad (\text{S41a})$$

and

$$E = \frac{g_z^{\text{true}} \beta B}{2} + \frac{1}{2} \left[\sqrt{u_0} \pm \sqrt{-2p - u_0 - \frac{2q}{\sqrt{u_0}}} \right] \quad (\text{S41b})$$

The eigenenergies of the conjugate Hamiltonian are obtained with replacing B with $-B$ in the solutions above. The $g^{\text{eff}}-g^{\text{true}}$ relationships between the $|\pm M_S\rangle$ -dominant states assuming $E_{M_S}(B, E/D) - E_{-M_S}(B, E/D) = h\nu = g_z^{\text{eff}} \beta B$. Figure S11 depicts $g^{\text{eff}}/g^{\text{true}}$ as a function of $|E/D|$ together with the counterpart from the genuine Zeeman perturbation treatment.

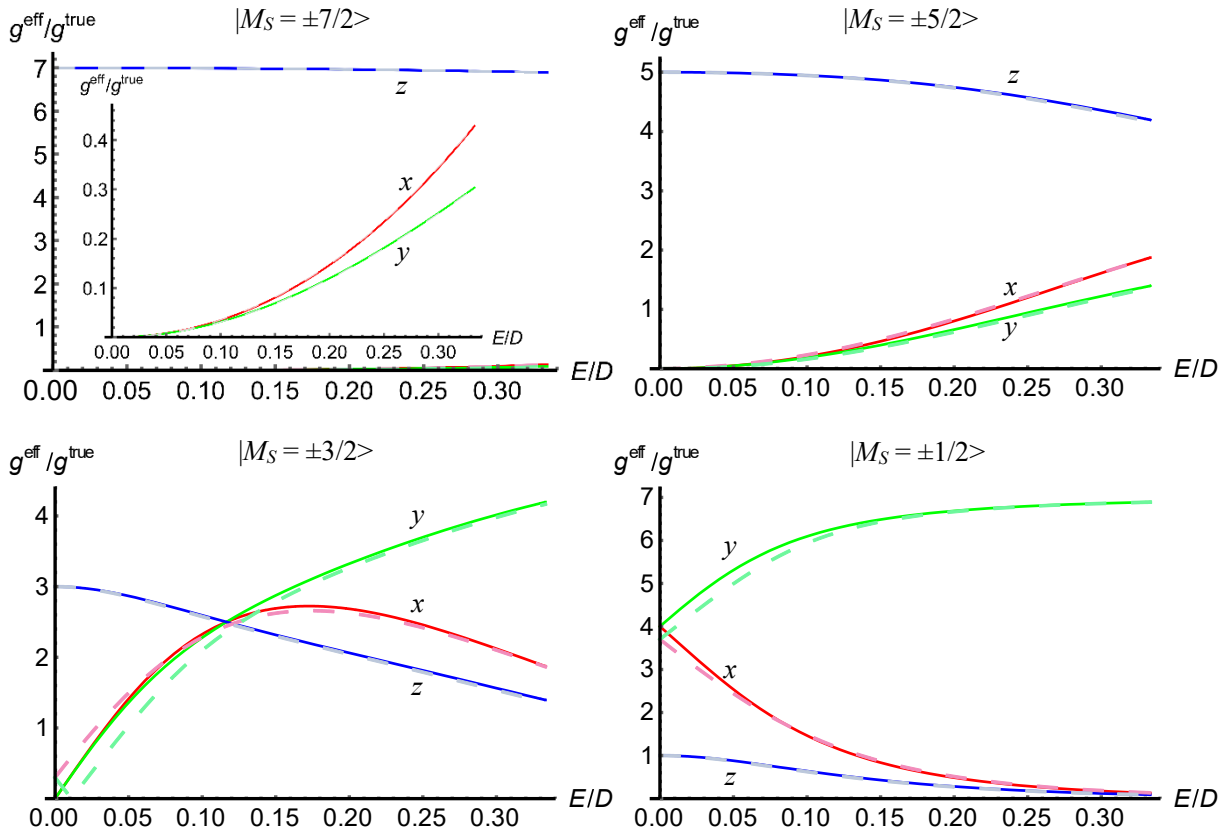


Figure S11 The $g^{\text{eff}}/g^{\text{true}}$ relationships as a function of the ratios of $|E/D|$ for $S = 5/2$. The subscripts x, y and z denote the principal axes of the \mathbf{g} - and ZFS tensors. The curves of the exact relationships in the broken lines

are based on the exact solutions with the spin Hamiltonian parameters with $g_z^{\text{true}}\beta B/D = 0.1$. Those derived by the genuine Zeeman perturbation treatment to the third order are depicted in the solid curves.

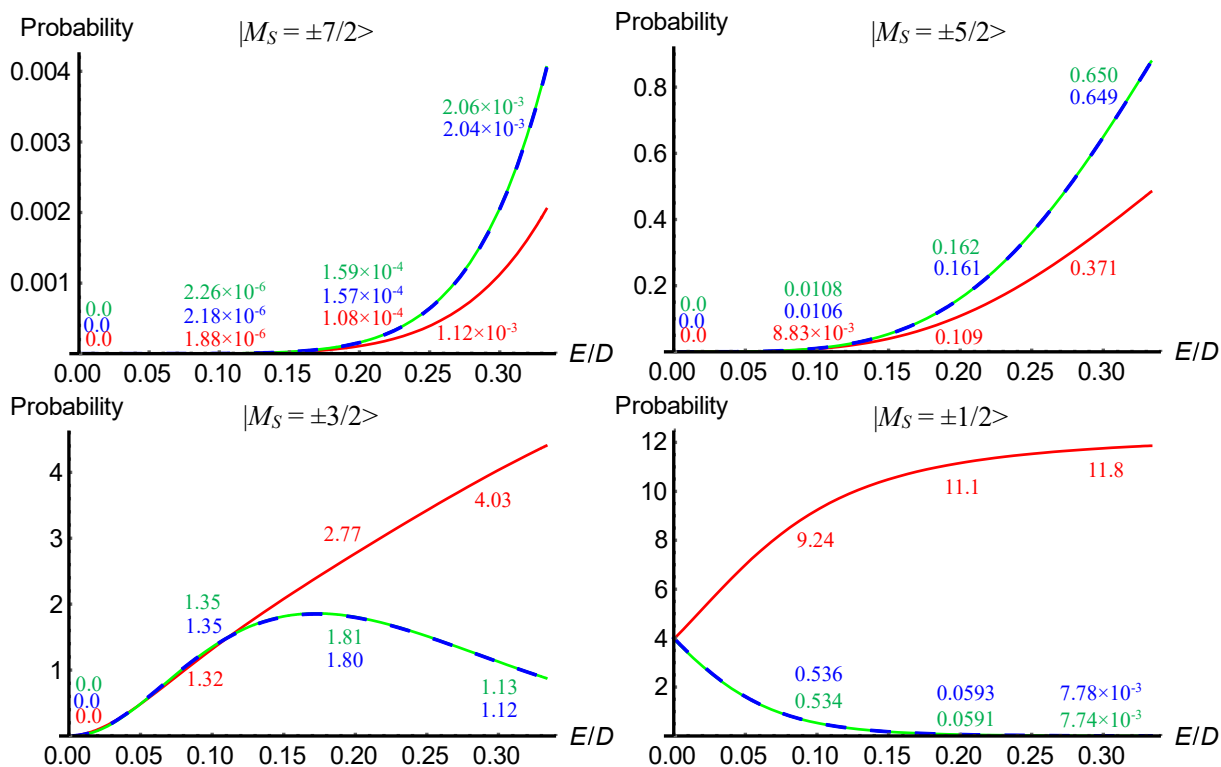


Figure S12 The transition probabilities for $|M_S = \pm 7/2\rangle$, $|\pm 5/2\rangle$, $|\pm 3/2\rangle$, $|\pm 1/2\rangle$ -dominant states ($g_z^{\text{true}}\beta B/D = 0.1$). \mathbf{B}/x (red), y (green), z (blue). Because of the overlapping in the case of \mathbf{B}/y and z , the blue broken line was used.

6.2 The $g^{\text{eff}}-g^{\text{true}}$ relationships by using of a Zeeman perturbation approach in the case of spin-octet states ($S = 7/2$)

The ZFS Hamiltonian ($E \neq 0$) in spin-octet states can be divided to two equivalent 4×4 matrices whose basis sets are $\{|+7/2\rangle, |-5/2\rangle, |+3/2\rangle, |-1/2\rangle\}$ and $\{|-7/2\rangle, |+5/2\rangle, |-3/2\rangle, |+1/2\rangle\}$. The basis sets are conjugate.

$$H_{\text{ZFS}}^{\text{octet}} = \begin{pmatrix} \langle +7/2 | & \langle -5/2 | & \langle +3/2 | & \langle -1/2 | \\ 7D & 0 & \sqrt{21}E & 0 \\ 0 & D & 0 & 3\sqrt{5}E \\ \sqrt{21}E & 0 & -3D & 2\sqrt{15}E \\ 0 & 3\sqrt{5}E & 2\sqrt{15}E & -5D \end{pmatrix} \begin{matrix} | +7/2 \rangle \\ | -5/2 \rangle \\ | +3/2 \rangle \\ | -1/2 \rangle \end{matrix}$$

The eigenenergies are the solutions of the following quartic equation:

$$x^4 - 42(D^2 + 3E^2)x^2 - 64D(D^2 - 9E^2)x + 105(D^2 + 3E^2)^2 = 0.$$

The resolvent cubic equation of this quartic equation is

$$u^3 + 2pu^2 + (p^2 - 4r)u - q^2 = 0$$

where

$$\begin{aligned} p &= -42(D^2 + 3E^2) \\ q &= -64D(D^2 - 9E^2) \\ r &= 105(D^2 + 3E^2)^2. \end{aligned}$$

Replacing u with $u - 2p/3$.

$$u^3 = \frac{1}{3}(p^2 + 12r)u + \frac{1}{27}(27q^2 + 2p^3 - 72pr)$$

According to the Viète's method, one of the solutions is obtained as

$$u_0 = 2a_0 \cos \left[\frac{1}{3} \arccos \left(\frac{b_0}{2a_0} \right) \right] - \frac{2p}{3}$$

where

$$\begin{aligned} a_0 &= \frac{\sqrt{p^2 + 12r}}{3} \\ b_0 &= \frac{27q^2 + 2p^3 - 72pr}{3p^2 + 36r}. \end{aligned}$$

The quartic equation can be rewritten as the product of the two quadratic equation with u_0

$$\begin{aligned} &\left\{ \left(x^2 + \frac{p + u_0}{2} \right) + \sqrt{u_0} \left(x - \frac{q}{2u_0} \right) \right\} \left\{ \left(x^2 + \frac{p + u_0}{2} \right) - \sqrt{u_0} \left(x - \frac{q}{2u_0} \right) \right\} = 0 \\ \Leftrightarrow &\begin{cases} x = \frac{1}{2} \left[-\sqrt{u_0} \pm \sqrt{-2p - u_0 - \frac{2q}{\sqrt{u_0}}} \right] \\ x = \frac{1}{2} \left[\sqrt{u_0} \pm \sqrt{-2p - u_0 + \frac{2q}{\sqrt{u_0}}} \right]. \end{cases} \end{aligned}$$

The eigenenergies $\varepsilon_{M_S}^{(0)}$ and eigenfunctions $\varphi_{M_S}^{(0)}$ are given as

$$\varepsilon_{+\frac{7}{2}}^{(0)} = x_1 = \frac{1}{2} \left[\sqrt{u_0} + \sqrt{-2p - u_0 - \frac{2q}{\sqrt{u_0}}} \right] \quad (\text{S42a})$$

$$\varepsilon_{-\frac{5}{2}}^{(0)} = x_2 = \frac{1}{2} \left[\sqrt{u_0} - \sqrt{-2p - u_0 - \frac{2q}{\sqrt{u_0}}} \right] \quad (\text{S42b})$$

$$\varepsilon_{+\frac{3}{2}}^{(0)} = x_3 = \frac{1}{2} \left[-\sqrt{u_0} + \sqrt{-2p - u_0 + \frac{2q}{\sqrt{u_0}}} \right] \quad (\text{S42c})$$

$$\varepsilon_{-\frac{1}{2}}^{(0)} = x_4 = \frac{1}{2} \left[-\sqrt{u_0} - \sqrt{-2p - u_0 + \frac{2q}{\sqrt{u_0}}} \right] \quad (\text{S42d})$$

$$\varphi_{+\frac{7}{2}}^{(0)} = \varphi_1 = \alpha_1 \left| +\frac{7}{2} \right\rangle + \beta_1 \left| -\frac{5}{2} \right\rangle + \gamma_1 \left| +\frac{3}{2} \right\rangle + \delta_1 \left| -\frac{1}{2} \right\rangle \quad (\text{S43a})$$

$$\varphi_{-\frac{5}{2}}^{(0)} = \varphi_2 = \alpha_2 \left| +\frac{7}{2} \right\rangle + \beta_2 \left| -\frac{5}{2} \right\rangle + \gamma_2 \left| +\frac{3}{2} \right\rangle + \delta_2 \left| -\frac{1}{2} \right\rangle \quad (\text{S43b})$$

$$\varphi_{+\frac{3}{2}}^{(0)} = \varphi_3 = \alpha_3 \left| +\frac{7}{2} \right\rangle + \beta_3 \left| -\frac{5}{2} \right\rangle + \gamma_3 \left| +\frac{3}{2} \right\rangle + \delta_3 \left| -\frac{1}{2} \right\rangle \quad (\text{S43c})$$

$$\varphi_{-\frac{1}{2}}^{(0)} = \varphi_4 = \alpha_4 \left| +\frac{7}{2} \right\rangle + \beta_4 \left| -\frac{5}{2} \right\rangle + \gamma_4 \left| +\frac{3}{2} \right\rangle + \delta_4 \left| -\frac{1}{2} \right\rangle \quad (\text{S43d})$$

where

$$\frac{\alpha_n}{\gamma_n} = \frac{\sqrt{21E}}{x_n - 7D}$$

$$\frac{\delta_n}{\gamma_n} = \frac{1}{2\sqrt{15E}} \left(x_n + 3D - \frac{21E^2}{x_n - 7D} \right)$$

$$\frac{\beta_n}{\gamma_n} = \frac{\sqrt{3}}{2(x_n - D)} \left(x_n + 3D - \frac{21E^2}{x_n - 7D} \right)$$

$$\gamma_n^2 = \left[\frac{21E^2}{(x_n - 7D)^2} + \frac{3E}{4(x_n - D)^2} \left(x_n + 3D - \frac{21E^2}{x_n - 7D} \right)^2 + \frac{1}{60E^2} \left(x_n + 3D - \frac{21E^2}{x_n - 7D} \right)^2 + 1 \right]^{-1}$$

($n = 1, 2, 3, 4$).

The elements of the perturbing Hamiltonian (H'_{eZ}) are given as

$$(H'_{eZ})_{ij} = \left(+\frac{7}{2} \alpha_i \alpha_j - \frac{5}{2} \beta_i \beta_j + \frac{3}{2} \gamma_i \gamma_j - \frac{1}{2} \delta_i \delta_j \right) g_Z^{\text{true}} \beta B$$

where $i, j = 1-4$. For example, $(H'_{eZ})_{12}$ corresponds to $\left\langle \varphi_{+\frac{7}{2}}^{(0)} \left| H'_{eZ} \right| \varphi_{-\frac{5}{2}}^{(0)} \right\rangle$. Since the zeroth and the second-order terms vanish when the energy differences $(E_i - E_j)$ are taken, $g_z^{\text{eff}}/g_z^{\text{true}}$ can be represented as

$$\frac{g_z^{\text{eff}}}{g_z^{\text{true}}} = \frac{\frac{147\lambda^2}{(x'_n - 7)^2} - \frac{15}{4(x'_n - 1)^2} \left(x'_n + 3 - \frac{21\lambda^2}{x'_n - 7}\right)^2 - \frac{1}{60\lambda^2} \left(x'_n + 3 - \frac{21\lambda^2}{x'_n - 7}\right)^2 + 3}{\frac{21\lambda^2}{(x'_n - 7)^2} + \frac{3}{4(x'_n - 1)^2} \left(x'_n + 3 - \frac{21\lambda^2}{x'_n - 7}\right)^2 + \frac{1}{60\lambda^2} \left(x'_n + 3 - \frac{21\lambda^2}{x'_n - 7}\right)^2 + 1} \quad (S44)$$

$(n = 1-4)$

where

$$x'_n = \frac{x_n}{D}$$

$$\lambda = \frac{E}{D}$$

The perturbed wavefunctions to the first order are

$$\Psi'_{+\frac{7}{2}} = \frac{1}{N_1} \left[\varphi_1 + \frac{(H')_{12}}{x_1 - x_2} \left| -\frac{5}{2} \right\rangle + \frac{(H')_{13}}{x_1 - x_3} \left| +\frac{3}{2} \right\rangle + \frac{(H')_{14}}{x_1 - x_4} \left| -\frac{1}{2} \right\rangle \right] \quad (S45a)$$

$$\Psi'_{-\frac{5}{2}} = \frac{1}{N_2} \left[\frac{(H')_{21}}{x_2 - x_1} \left| +\frac{7}{2} \right\rangle + \varphi_2 + \frac{(H')_{23}}{x_2 - x_3} \left| +\frac{3}{2} \right\rangle + \frac{(H')_{24}}{x_2 - x_4} \left| -\frac{1}{2} \right\rangle \right] \quad (S45b)$$

$$\Psi'_{+\frac{3}{2}} = \frac{1}{N_3} \left[\frac{(H')_{31}}{x_3 - x_1} \left| +\frac{7}{2} \right\rangle + \frac{(H')_{32}}{x_3 - x_2} \left| -\frac{5}{2} \right\rangle + \varphi_3 + \frac{(H')_{34}}{x_3 - x_4} \left| -\frac{1}{2} \right\rangle \right] \quad (S45c)$$

$$\Psi'_{-\frac{1}{2}} = \frac{1}{N_4} \left[\frac{(H')_{41}}{x_4 - x_1} \left| +\frac{7}{2} \right\rangle + \frac{(H')_{42}}{x_4 - x_2} \left| -\frac{5}{2} \right\rangle + \frac{(H')_{43}}{x_4 - x_3} \left| +\frac{3}{2} \right\rangle + \varphi_4 \right] \quad (S45d)$$

where N is the normalization factor. The other sets $\{\Psi'_{-7/2}, \Psi'_{+5/2}, \Psi'_{-3/2}, \Psi'_{+1/2}\}$ are obtained with replacing B with $-B$ and the normalization factor is represented as N' .

The transition probabilities $P_{\pm Ms} = |\langle \Psi'_{-Ms} | S_x | \Psi'_{+Ms} \rangle|^2$:

For the $|M_S = \pm 7/2\rangle$ -dominant transition,

$$\begin{aligned} & \frac{1}{N'_1} \frac{1}{N_1} \left[\alpha_1 \left\langle -\frac{7}{2} \right| + \left(\beta_1 - \frac{(H')_{12}}{x_1 - x_2} \right) \left\langle +\frac{5}{2} \right| + \left(\gamma_1 - \frac{(H')_{13}}{x_1 - x_3} \right) \left\langle -\frac{3}{2} \right| \right. \\ & \quad \left. + \left(\delta_1 - \frac{(H')_{14}}{x_1 - x_4} \right) \left\langle +\frac{1}{2} \right| \right] S_x \left[\alpha_1 \left| +\frac{7}{2} \right\rangle + \left(\beta_1 + \frac{(H')_{12}}{x_1 - x_2} \right) \left| -\frac{5}{2} \right\rangle \right. \\ & \quad \left. + \left(\gamma_1 + \frac{(H')_{13}}{x_1 - x_3} \right) \left| +\frac{3}{2} \right\rangle + \left(\delta_1 + \frac{(H')_{14}}{x_1 - x_4} \right) \left| -\frac{1}{2} \right\rangle \right]; \\ & = \frac{1}{N'_1} \frac{1}{N_1} \left[\sqrt{7} \alpha_1 \beta_1 + 2\sqrt{3} \beta_1 \gamma_1 + \sqrt{15} \gamma_1 \delta_1 + 2\delta_1^2 - \frac{2\sqrt{3}(H')_{12}(H')_{13}}{(x_1 - x_2)(x_1 - x_3)} \right. \\ & \quad \left. - \frac{\sqrt{15}(H')_{13}(H')_{14}}{(x_1 - x_3)(x_1 - x_4)} - \frac{2(H')_{14}^2}{(x_1 - x_4)^2} \right]; \end{aligned}$$

for the $|\pm 5/2\rangle$ dominant transition,

$$\begin{aligned}
& \frac{1}{N'_2} \frac{1}{N_2} \left[\left(\alpha_2 + \frac{(H')_{21}}{x_2 - x_1} \right) \left\langle +\frac{7}{2} \right\rangle + \beta_2 \left\langle -\frac{5}{2} \right\rangle + \left(\gamma_2 + \frac{(H')_{23}}{x_2 - x_3} \right) \left\langle +\frac{3}{2} \right\rangle \right. \\
& \quad + \left(\delta_2 + \frac{(H')_{24}}{x_2 - x_4} \right) \left\langle -\frac{1}{2} \right\rangle \left. \right] S_x \left[\left(\alpha_2 - \frac{(H')_{21}}{x_2 - x_1} \right) \left\langle -\frac{7}{2} \right\rangle + \beta_2 \left\langle +\frac{5}{2} \right\rangle \right. \\
& \quad + \left. \left(\gamma_2 - \frac{(H')_{23}}{x_2 - x_3} \right) \left\langle -\frac{3}{2} \right\rangle + \left(\delta_2 - \frac{(H')_{24}}{x_2 - x_4} \right) \left\langle +\frac{1}{2} \right\rangle \right] \\
& = \frac{1}{N'_2} \frac{1}{N_2} \left[\sqrt{7} \alpha_2 \beta_2 + 2\sqrt{3} \beta_2 \gamma_2 + \sqrt{15} \gamma_2 \delta_2 + 2\delta_2^2 - \frac{\sqrt{15} (H')_{23} (H')_{24}}{(x_2 - x_3)(x_2 - x_4)} - \frac{2(H')_{24}^2}{(x_2 - x_4)^2} \right];
\end{aligned}$$

for the $|\pm 3/2\rangle$ dominant transition,

$$\begin{aligned}
& \frac{1}{N'_3} \frac{1}{N_3} \left[\left(\alpha_3 - \frac{(H')_{31}}{x_3 - x_1} \right) \left\langle -\frac{7}{2} \right\rangle + \left(\beta_3 - \frac{(H')_{32}}{x_3 - x_2} \right) \left\langle +\frac{5}{2} \right\rangle + \gamma_3 \left\langle -\frac{3}{2} \right\rangle \right. \\
& \quad + \left(\delta_3 - \frac{(H')_{34}}{x_3 - x_4} \right) \left\langle +\frac{1}{2} \right\rangle \left. \right] S_x \left[\left(\alpha_3 + \frac{(H')_{31}}{x_3 - x_1} \right) \left\langle +\frac{7}{2} \right\rangle + \left(\beta_3 + \frac{(H')_{32}}{x_3 - x_2} \right) \left\langle -\frac{5}{2} \right\rangle \right. \\
& \quad + \left. \gamma_3 \left\langle +\frac{3}{2} \right\rangle + \left(\delta_3 + \frac{(H')_{34}}{x_3 - x_4} \right) \left\langle -\frac{1}{2} \right\rangle \right] \\
& = \frac{1}{N'_3} \frac{1}{N_3} \left[\sqrt{7} \alpha_3 \beta_3 + 2\sqrt{3} \beta_3 \gamma_3 + \sqrt{15} \gamma_3 \delta_3 + 2\delta_3^2 - \frac{\sqrt{7} (H')_{31} (H')_{32}}{(x_3 - x_1)(x_3 - x_2)} - \frac{2(H')_{34}^2}{(x_3 - x_4)^2} \right];
\end{aligned}$$

for the $|\pm 1/2\rangle$ dominant transition,

$$\begin{aligned}
& \frac{1}{N'_4} \frac{1}{N_4} \left[\left(\alpha_4 + \frac{(H')_{41}}{x_4 - x_1} \right) \left\langle +\frac{7}{2} \right\rangle + \left(\beta_4 + \frac{(H')_{42}}{x_4 - x_2} \right) \left\langle -\frac{5}{2} \right\rangle + \left(\gamma_4 + \frac{(H')_{43}}{x_4 - x_3} \right) \left\langle +\frac{3}{2} \right\rangle \right. \\
& \quad + \delta_4 \left\langle -\frac{1}{2} \right\rangle \left. \right] S_x \left[\left(\alpha_4 - \frac{(H')_{41}}{x_4 - x_1} \right) \left\langle -\frac{7}{2} \right\rangle + \left(\beta_4 - \frac{(H')_{42}}{x_4 - x_2} \right) \left\langle +\frac{5}{2} \right\rangle \right. \\
& \quad + \left. \left(\gamma_4 - \frac{(H')_{43}}{x_4 - x_3} \right) \left\langle -\frac{3}{2} \right\rangle + \delta_4 \left\langle +\frac{1}{2} \right\rangle \right] \\
& = \frac{1}{N'_4} \frac{1}{N_4} \left[\sqrt{7} \alpha_4 \beta_4 + 2\sqrt{3} \beta_4 \gamma_4 + \sqrt{15} \gamma_4 \delta_4 + 2\delta_4^2 - \frac{\sqrt{7} (H')_{41} (H')_{42}}{(x_4 - x_1)(x_4 - x_2)} \right. \\
& \quad \left. - \frac{2\sqrt{3} (H')_{42} (H')_{43}}{(x_4 - x_2)(x_4 - x_3)} \right].
\end{aligned}$$

7. Single-crystal cw ESR/ENDOR and pulsed ESR spectroscopy of Fe^{III}(Cl)OEP

7.1 Angular dependence of cw ESR spectra of Fe^{III}(Cl)OEP diluted in Ni^{II}OEP single-crystals in the crystallographic *abc* axis system

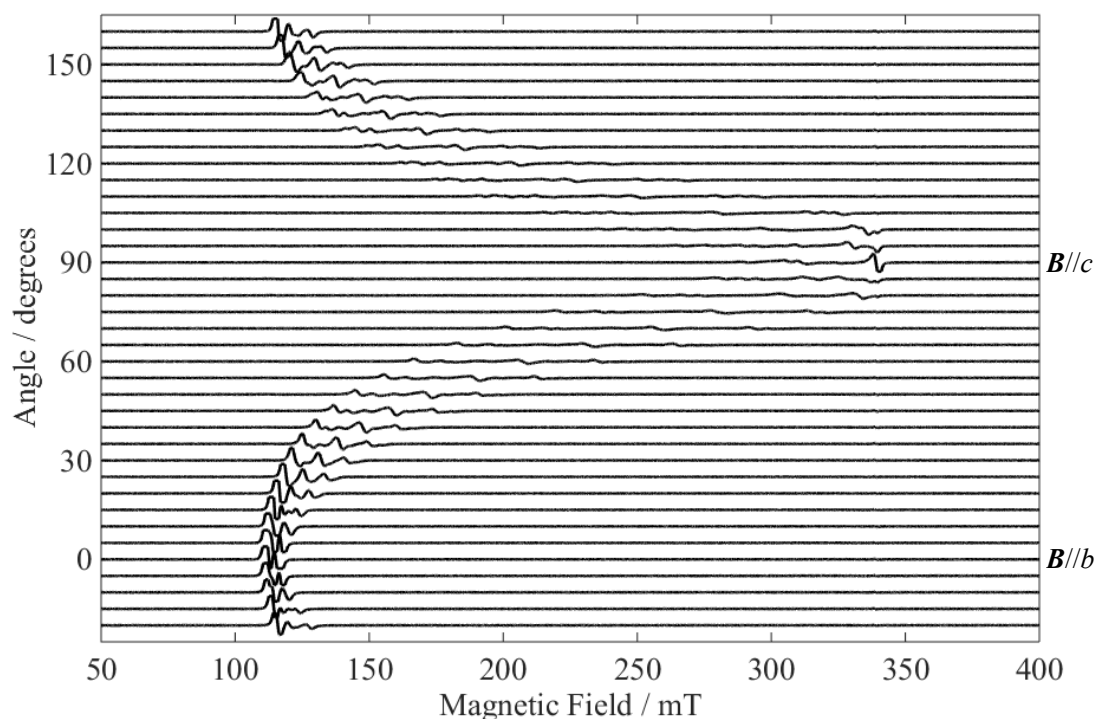


Figure S13 Angular dependence of cw ESR spectra of Fe^{III}(Cl)OEP diluted in a Ni^{II}OEP single-crystal in the *bc*-plane. Four magnetically nonequivalent species were observed due to the distortion originating in a pseudo Jahn-Teller interaction. The experimental angular dependence indicated that the crystal was misaligned on a wedge: the departure from the *c*-axis was estimated around 5 degrees. Microwave frequency: 9.51420 GHz, temperature: 5.0 K.

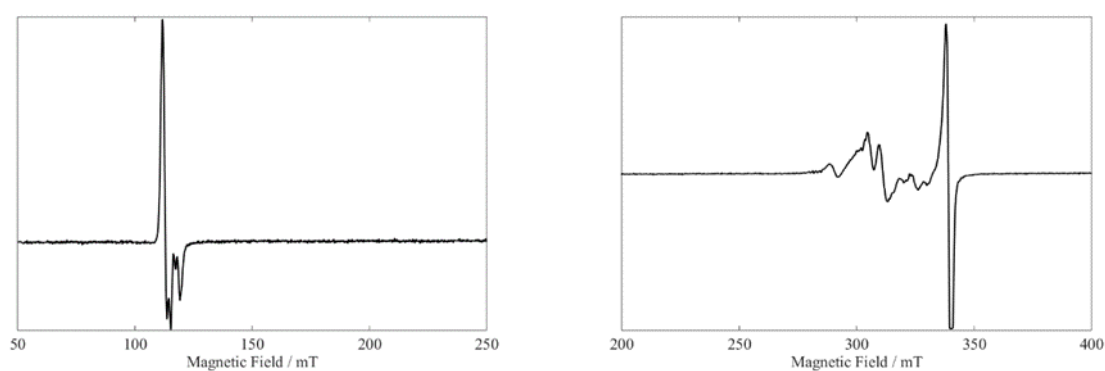


Figure S14 The ESR spectra of Fe^{III}(Cl)OEP observed with **B//b** and nearly *//c*: Microwave frequency used: 9.51420 GHz and temperature: 5.0 K.

7.2 Typical ESR spectra of Fe^{III}(Cl)OEP observed at liquid helium temperature

Typical ESR spectra of Fe^{III}(Cl) diluted in the Ni^{II}OEP single-crystal are shown below with the two coordinate axis systems, the crystallographic *abc* and laboratory (principal) *xyz* systems.

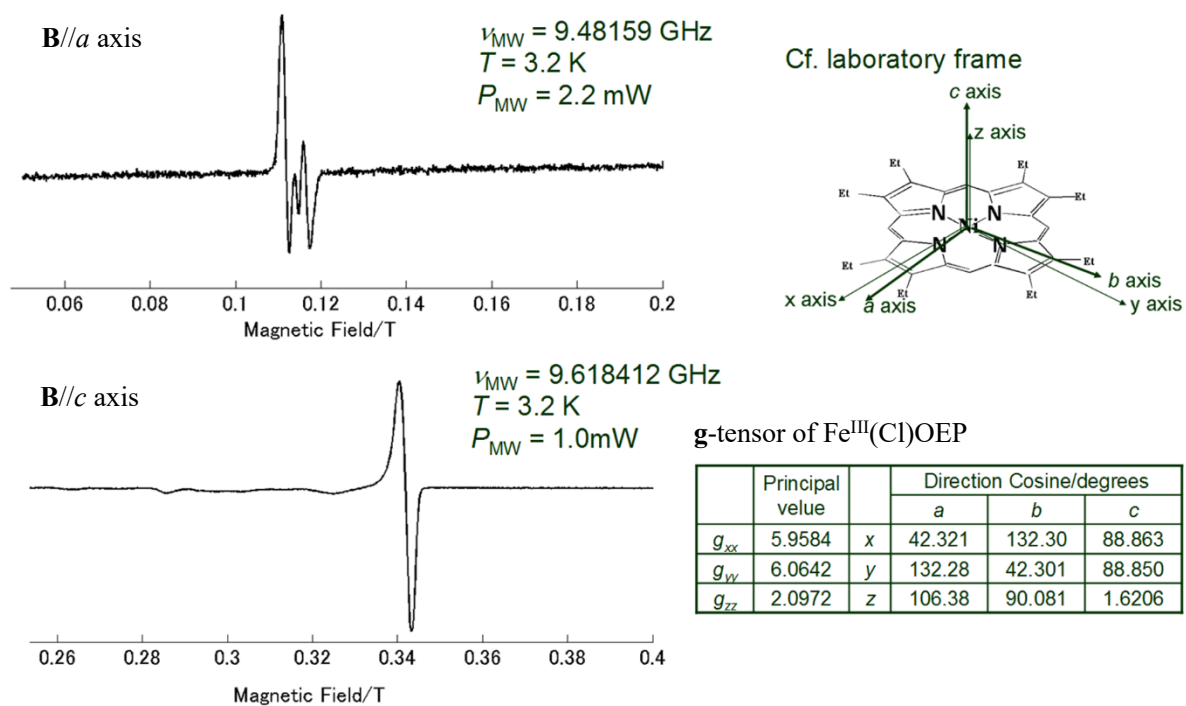


Figure S15 Typical ESR spectra of Fe^{III}(Cl)OEP diluted in the Ni^{II}OEP single-crystal are shown with the two coordinate axis systems, the crystallographic *abc* and laboratory (principal) *xyz* systems. The *c* axis is parallel to the *z* axis and the *a* axis deviates 2.3 degrees from the *x* axis. The experimentally determined principal values and direction cosines of the **g**-tensor in terms of the effective spin Hamiltonian are given. The values are the averaged ones over the four energetically non-equivalent species.

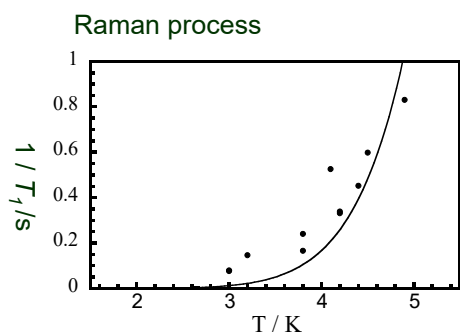
7.3 Temperature dependence of the spin-lattice relaxation time T_1 of $\text{Fe}^{\text{III}}(\text{Cl})\text{OEP}$ determined by an inversion recovery method based on pulsed ESR spectroscopy

We measured the temperature dependence of T_1 of $\text{Fe}^{\text{III}}(\text{Cl})\text{OEP}$ determined by an inversion recovery method based on pulsed ESR spectroscopy. Temperature was the range of 3 to 5 K. We applied the pulse sequence of the π - $\pi/2$ - π -echo scheme. The measurements were carried out with $\mathbf{B} // c$ and $// b$. T_1 with $\mathbf{B} // c$ was shorter, which is ascribable to the occurrence of a sizable spin-orbit interaction.

$$2D^* = \Delta = 14.1 \text{ cm}^{-1}$$

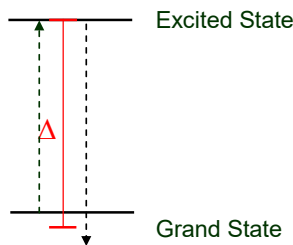
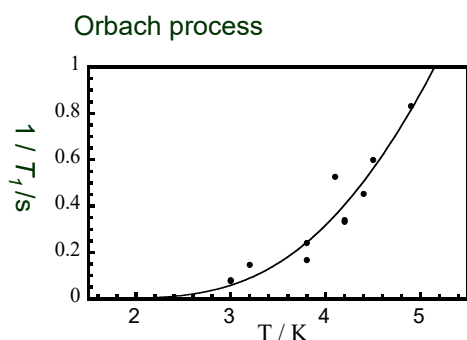
Thus,

$$D^* = +7.05 \text{ cm}^{-1}$$



Temperature dependence of T_1 is governed by three relaxation processes. ($B // c$)

1. Direct process (one-phonon process)
 $1/T_1 \propto T$
2. Raman process (two-phonon process)
 $1/T_1 \propto T^9$
3. Orbach process (two-phonon process)
 $1/T_1 \propto \{\exp(\Delta / kT) - 1\}^{-1}$



$$2D = \Delta = 14.1 \text{ cm}^{-1}$$

$$D = +7 \text{ cm}^{-1}$$

Figure S16 Temperature dependence of T_1 of $\text{Fe}^{\text{III}}(\text{Cl})\text{OEP}$ with $\mathbf{B} // c$ as determined by an inversion recovery method. The Orbach process gave the better fitting, enabling us to derive the energy difference Δ .

7.4 Angular dependences of both the spin-lattice relaxation time T_1 and spin-spin relaxation time T_2 of $\text{Fe}^{\text{III}}(\text{Cl})\text{OEP}$

The T_2 measurements were carried out with the conventional 2-pulse echo method: $\pi/2$ - π -echo. Both relaxation times were observed in $\mathbf{B} // c$ (perpendicular to the porphyrin plane) and a -axes (in the porphyrin plane). It was confirmed that both the spin-lattice and spin-spin relaxation times become short with the magnetic field B in the porphyrin plane (a axis). This phenomenon can be interpreted in terms of the spin sub-level mixing by the spin-orbit interaction.

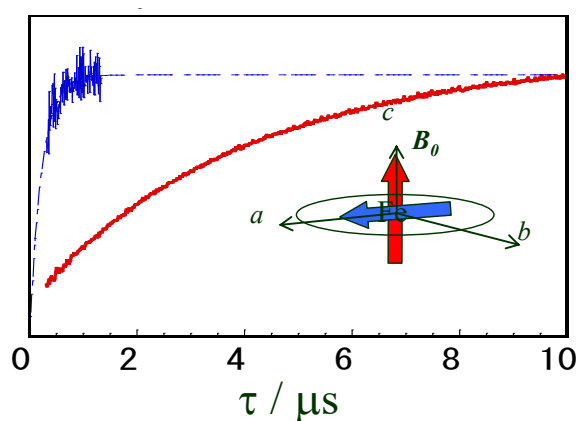


Figure S17 Echo intensity for the pulse interval τ of the first and second pulse in the different external magnetic field orientation. Red: $\mathbf{B} // c$, blue: $\mathbf{B} // a$.

Table S2 Spin-lattice relaxation time (T_1) and spin-spin relaxation time (T_2) in the different crystallographic (principal) axes: $c // z$ and $a // x$.

$\mathbf{B} //$	$T_1 / \mu\text{s}$	$T_2 / \mu\text{s}$
c axis	4.15	0.27
a axis	0.23	0.025

7.5 ^{14}N -ENDOR spectroscopy of $\text{Fe}^{\text{III}}(\text{Cl})\text{OEP}$ diluted in $\text{Ni}^{\text{II}}\text{OEP}$ single-crystals

We simulated the ENDOR spectra of $\text{Fe}^{\text{III}}(\text{Cl})\text{OEP}$ diluted in the $\text{Ni}^{\text{II}}\text{OEP}$ single crystal in terms of a coupled basis set for the effective spin-1/2 state ($S = 1/2$) and the nuclear spin states arising from the four nitrogen nuclei ($I = 1$).

$$H^{\text{eff}} = \beta \tilde{\mathbf{S}} \cdot \mathbf{g}^{\text{eff}} \cdot \mathbf{B} + \sum_{i=1}^4 (\tilde{\mathbf{S}} \cdot \mathbf{A}_i^{\text{eff}} \cdot \mathbf{I}_i + \tilde{\mathbf{I}}_i \cdot \mathbf{Q}_i^{\text{eff}} \cdot \mathbf{I}_i - g_n \beta_n \tilde{\mathbf{I}}_i \cdot \mathbf{B})$$

where $g_x^{\text{eff}} = 5.9584$, $g_y^{\text{eff}} = 6.0642$, $g_z^{\text{eff}} = 2.0972$, $A_x^{\text{eff}} = 9.0$ MHz, $A_y^{\text{eff}} = 7.60$ MHz, $A_z^{\text{eff}} = 7.80$ MHz, $Q_x^{\text{eff}} = -0.80$ MHz, $Q_y^{\text{eff}} = 1.05$ MHz, $Q_z^{\text{eff}} = -0.25$ MHz were determined by the best fitting procedure.

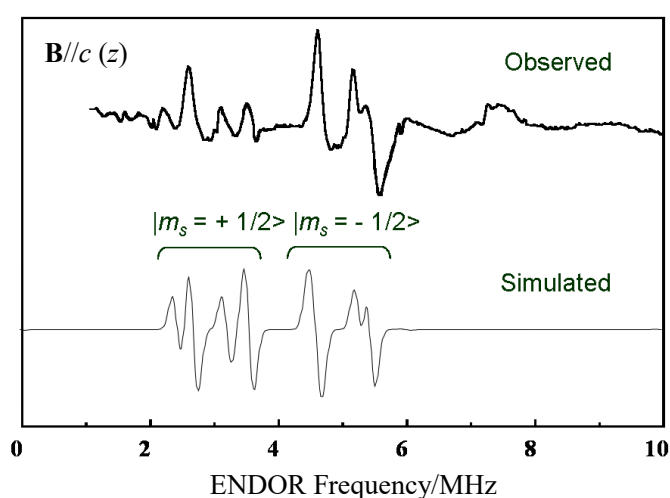
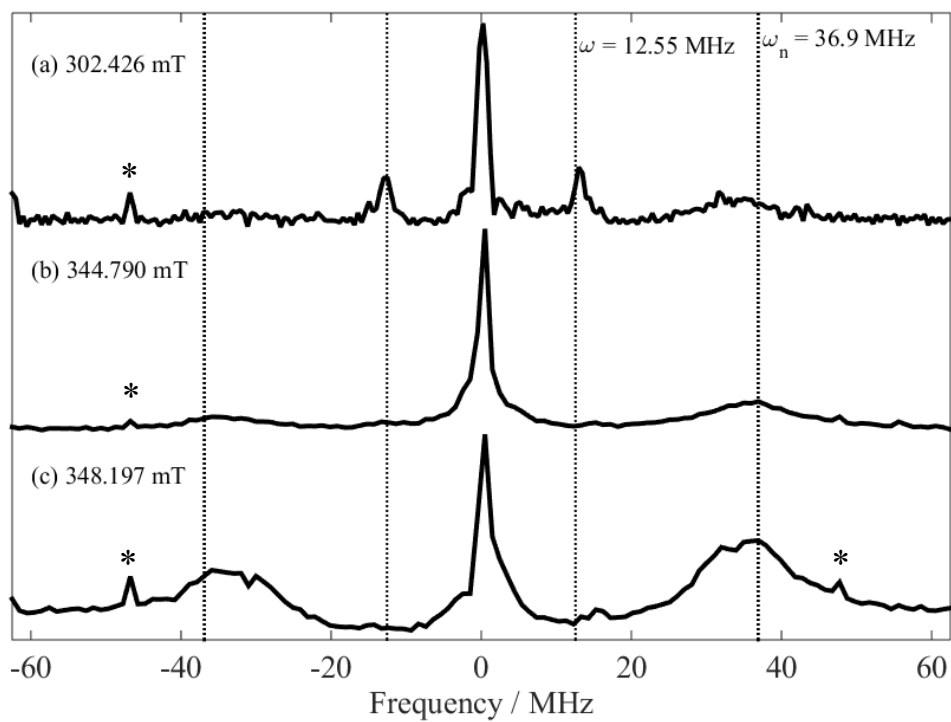
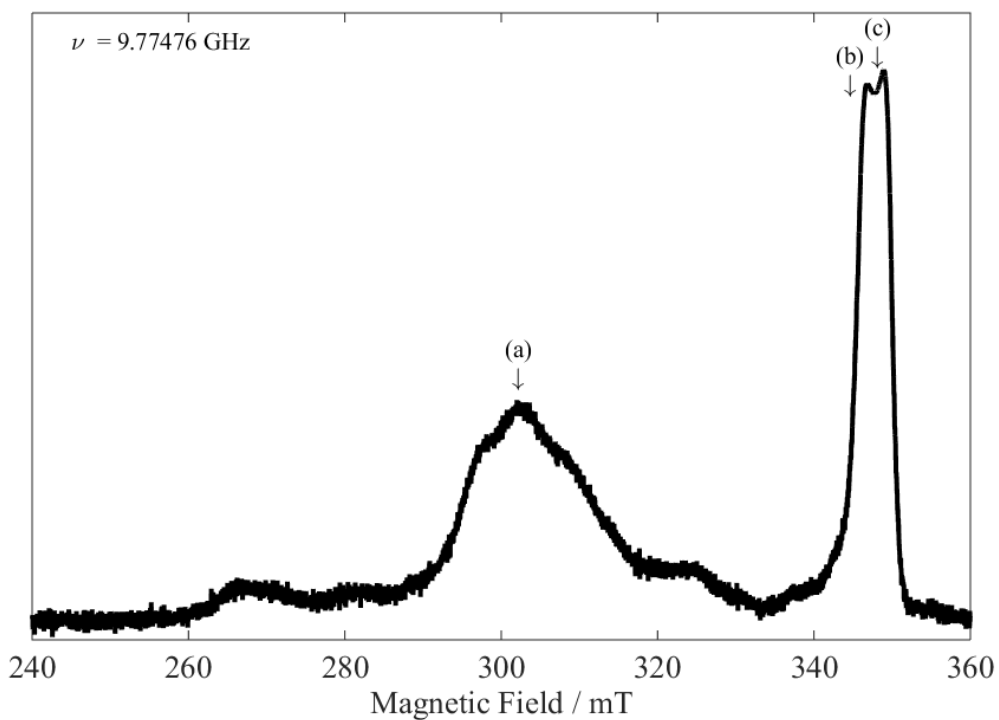


Figure S18 Observed and simulated single-crystal ^{14}N -ENDOR spectra of $\text{Fe}^{\text{III}}(\text{Cl})\text{OEP}$ in $\mathbf{B} // c$ axis.

7.6 Pulse-based electron spin nutation spectroscopy of Fe^{III}(Cl)OEP diluted in Ni^{II}OEP single-crystal



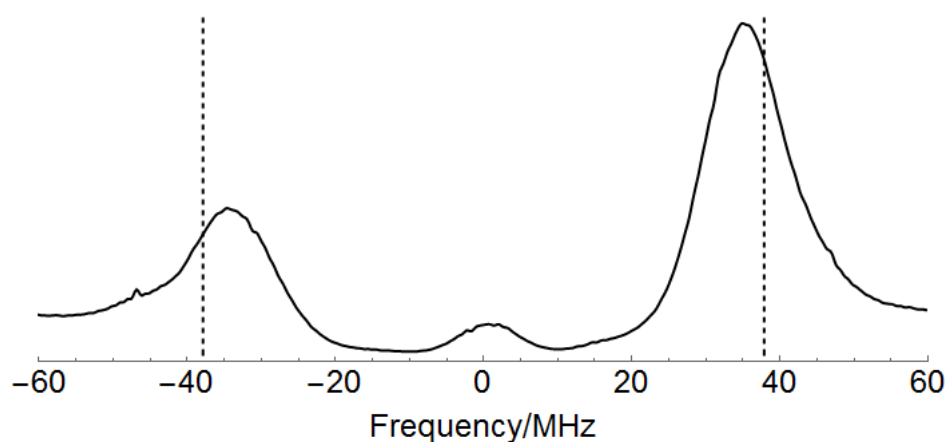


Figure S19 (Top) Echo-detected ESR spectrum at X-band applied to $\text{Fe}^{\text{III}}(\text{Cl})\text{OEP}$ ($S = 5/2$) magnetically diluted in the diamagnetic $\text{Ni}^{\text{II}}\text{OEP}$ single-crystal with the static magnetic field along the principal z -axis at 4 K. The positions marked by (a)-(c) correspond to the external magnetic field at which the one-dimensional electron spin transient nutation (1D-ESTN) experiments were carried out at 3 K (middle). All the signals arise from the $\text{Fe}^{\text{III}}(\text{Cl})\text{OEP}$ molecules with different molecular orientations with respect to the static magnetic field. The peaks assigned with asterisks were analytical artifacts. (Bottom) The nutation spectrum calculated by the set of the full spin Hamiltonian parameters experimentally determined. The calculated nutation frequency is 3.03 times greater than the nutation frequency, 12.2 MHz of DPPH ($S = 1/2$) used as an external reference for the frequency calibration, indicating that the signal denoted by (c) (in the top figure) is assigned to be the transition between the $|\pm 1/2\rangle$ -dominant spin sub-levels of the spin-sextet state. The nutation spectroscopy for the reference signal was detected by using a different scheme of the detection from that for $\text{Fe}^{\text{III}}(\text{Cl})\text{OEP}$, enabling us to experimentally discriminate the nutation frequency of the reference from that of $\text{Fe}^{\text{III}}(\text{Cl})\text{OEP}$.

8. Single-crystal and powder-pattern ESR spectroscopy of Co^{II}OEP diluted in diamagnetic Ni^{II}OEP single-crystals

8.1 Principal values and direction cosine of the magnetic tensors of Co^{II}OEP experimentally determined by the fictitious spin-1/2 spin Hamiltonian approach

Table S3 Principal values and direction cosines of their axes of the spin Hamiltonian parameters of Co^{II}OEP at helium temperature. The direction cosines are given in the crystallographic axis system. The analyses were based on the fully numerical diagonalization with least-square fitting.

Molecule 1	Principal values	Direction cosines		
		<i>a</i>	<i>b</i>	<i>c</i>
g_x	3.4485±0.001	0.66210	-0.74936	0.00252
g_y	3.3287±0.002	-0.74941	-0.6621	0.00173
g_z	1.5421±0.001	-0.00297	0.00074	1.00000
$A_x(^{59}\text{Co})/\text{MHz}$	1391.5±0.74	0.67021	-0.74216	0.00398
$A_y(^{59}\text{Co})/\text{MHz}$	1347.3±1.06	-0.74216	-0.67022	-0.00168
$A_z(^{59}\text{Co})/\text{MHz}$	597.5±0.82	0.00398	0.00183	0.99999
$Q_x(^{59}\text{Co})/\text{MHz}$	-0.10±0.76	0.74703	0.58062	0.32376
$Q_y(^{59}\text{Co})/\text{MHz}$	-2.20±0.72	0.46618	-0.80473	0.36754
$Q_z(^{59}\text{Co})/\text{MHz}$	2.29±0.76	-0.47395	0.12364	0.87183

Molecule 2	Principal values	Direction cosines		
		<i>a</i>	<i>b</i>	<i>c</i>
g_x	3.3296±0.001	0.67729	0.73571	0.00131
g_y	3.4445±0.002	0.73569	-0.67729	-0.00603
g_z	1.5372±0.0004	-0.00535	0.00312	0.99998
$A_x(^{59}\text{Co})/\text{MHz}$	1345.2±0.71	0.69058	0.72325	0.00211
$A_y(^{59}\text{Co})/\text{MHz}$	1390.6±1.04	0.72325	-0.69058	-0.00236
$A_z(^{59}\text{Co})/\text{MHz}$	605.0±0.83	0.00211	-0.00121	1.00000
$Q_x(^{59}\text{Co})/\text{MHz}$	-2.92±0.66	-0.23227	-0.03435	0.97024
$Q_y(^{59}\text{Co})/\text{MHz}$	-3.34±0.63	0.71330	-0.68543	0.14622
$Q_z(^{59}\text{Co})/\text{MHz}$	6.25±0.66	-0.66125	0.72732	-0.18372

8.2 Principal values and direction cosine of the magnetic tensors of ^{14}N nuclei of $\text{Co}^{\text{II}}\text{OEP}$ experimentally determined by the fictitious spin-1/2 Hamiltonian approach

Table S4 Principal values and axes of the magnetic tensors of nitrogen nuclei in molecule 1 (component 1) at helium temperature.

Tensors for N1 and N3	Principal values	Direction cosines		
		<i>a</i>	<i>b</i>	<i>c</i>
$A_x(^{14}\text{N})/\text{MHz}$	2.2155	∓ 0.6694	∓ 0.2994	0.6799
$A_y(^{14}\text{N})/\text{MHz}$	2.7476	± 0.7364	∓ 0.1465	0.6625
$A_z(^{14}\text{N})/\text{MHz}$	5.4474	∓ 0.0982	± 0.9428	0.3185
$Q_x(^{14}\text{N})/\text{MHz}$	-0.7852	0.1308	-0.9913	∓ 0.0982
$Q_y(^{14}\text{N})/\text{MHz}$	0.2326	∓ 0.0119	∓ 0.0165	0.9998
$Q_z(^{14}\text{N})/\text{MHz}$	0.5526	-0.9913	-0.1306	-0.0140

Tensors for N2 and N4	Principal values	Direction cosines		
		<i>a</i>	<i>b</i>	<i>c</i>
$A_x(^{14}\text{N})/\text{MHz}$	2.4151	± 0.3109	∓ 0.7526	0.5789
$A_y(^{14}\text{N})/\text{MHz}$	2.5614	± 0.1557	± 0.6422	0.7505
$A_z(^{14}\text{N})/\text{MHz}$	5.4811	∓ 0.9366	∓ 0.1455	0.3188
$Q_x(^{14}\text{N})/\text{MHz}$	0.2452	∓ 0.9900	∓ 0.1391	∓ 0.0236
$Q_y(^{14}\text{N})/\text{MHz}$	-0.7899	-0.0135	-0.0729	∓ 0.9972
$Q_z(^{14}\text{N})/\text{MHz}$	0.5446	-0.1404	0.9876	∓ 0.0703

* Both the upper and lower signs should be chosen in the double signs.

Table S5 Principal values and axes of the magnetic tensors of nitrogen nuclei in molecule 2 (component 2) at helium temperature.

Tensors for N1 and N3	Principal values	Direction cosines		
		<i>a</i>	<i>b</i>	<i>c</i>
$A_x(^{14}\text{N})/\text{MHz}$	2.6876	± 0.3025	∓ 0.8368	0.4564
$A_y(^{14}\text{N})/\text{MHz}$	1.9565	± 0.1721	± 0.5189	0.8373
$A_z(^{14}\text{N})/\text{MHz}$	5.4859	∓ 0.9375	± 0.1747	0.3010
$Q_x(^{14}\text{N})/\text{MHz}$	0.2412	-0.9968	-0.0772	± 0.0236
$Q_y(^{14}\text{N})/\text{MHz}$	-0.7811	± 0.0222	± 0.0012	0.9998
$Q_z(^{14}\text{N})/\text{MHz}$	0.5369	-0.0772	0.9970	± 0.0005

Tensors for N2 and N4	Principal values	Direction cosines		
		<i>a</i>	<i>b</i>	<i>c</i>
$A_x(^{14}\text{N})/\text{MHz}$	2.2819	∓ 0.6223	∓ 0.3041	-0.7213
$A_y(^{14}\text{N})/\text{MHz}$	2.6443	∓ 0.7784	± 0.1421	0.6115
$A_z(^{14}\text{N})/\text{MHz}$	5.4322	± 0.0834	∓ 0.9420	0.3251
$Q_x(^{14}\text{N})/\text{MHz}$	-0.7798	-0.1249	0.9922	∓ 0.0041
$Q_y(^{14}\text{N})/\text{MHz}$	0.2377	∓ 0.0665	∓ 0.0042	0.9978
$Q_z(^{14}\text{N})/\text{MHz}$	0.5421	0.9899	0.1249	± 0.0665

* Both the upper and lower signs should be chosen in the double signs.

8.3 Angular dependence of the ESR spectra of Co^{II}OEP with the static magnetic field in the principal zx plane; Simulated in terms of the fictitious spin and ZFS/e-Zeeman spin Hamiltonian parameters

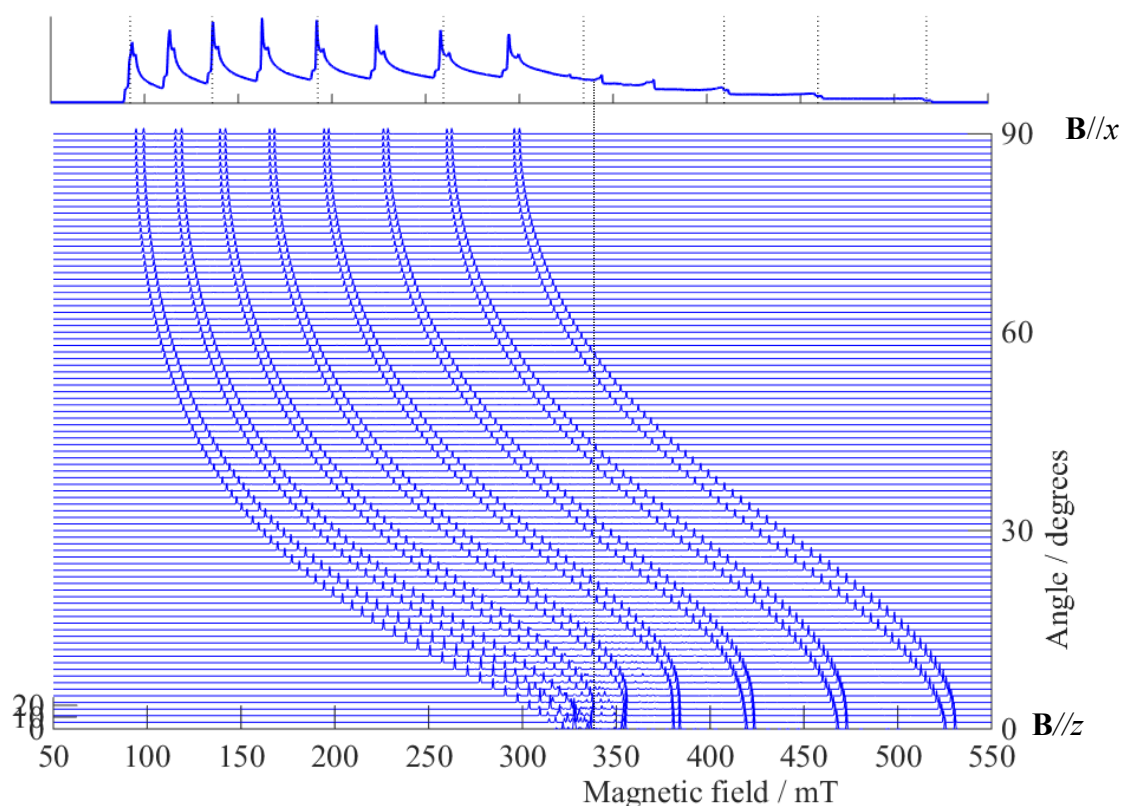


Figure S20 The calculated angular dependence from the principal z - to x -axis in the spectral simulation by using of the **fictitious spin-1/2 Hamiltonian**. Microwave frequency: 9.62541 GHz, peak-to-peak line width: 0.5 mT. Magnetic tensors used: (component 1) $\mathbf{g}^{\text{eff}} = [3.3915, 3.4036, 1.5470]$, $\mathbf{A}^{\text{eff}} = [1349.6, 1372.2, 624.9]$ MHz, $\mathbf{Q} = [-0.10, -2.20, 2.29]$ MHz, (component2) $\mathbf{g}^{\text{eff}} = [3.3232, 3.4532, 1.5570]$, $\mathbf{A}^{\text{eff}} = [1347.7, 1382.3, 614.9]$ MHz, $\mathbf{Q} = [-2.92, -3.34, 6.25]$ MHz. the \mathbf{g}^{eff} -, \mathbf{A}^{eff} - and \mathbf{Q} -tensors of the component 1 were assumed to be collinear. The relative orientations of each tensor of the component 2 were based on the direction cosines shown in Table S3. The top the spectrum is the absorption line corresponding to the summation for the all magnetic field orientations for comparison. Any strain effect of the line width is not included. The simulated spectra were obtained using EasySpin (ver. 5.1.10) with varying the angle of the magnetic field one-degree stepwise. The peak denoted by the dotted line is assigned to the occurrence of the off-principal-axis peak. Noticeably, the zx -plane angular dependence of the fine-structure/hyperfine spectra due to Co^{II}OEP reveals marked difference of the behavior of the transitions appearing in the range of 30 to 60 degrees between the fictitious spin and ZFS/e-Zeeman spin Hamiltonian approaches (see Fig. 21).

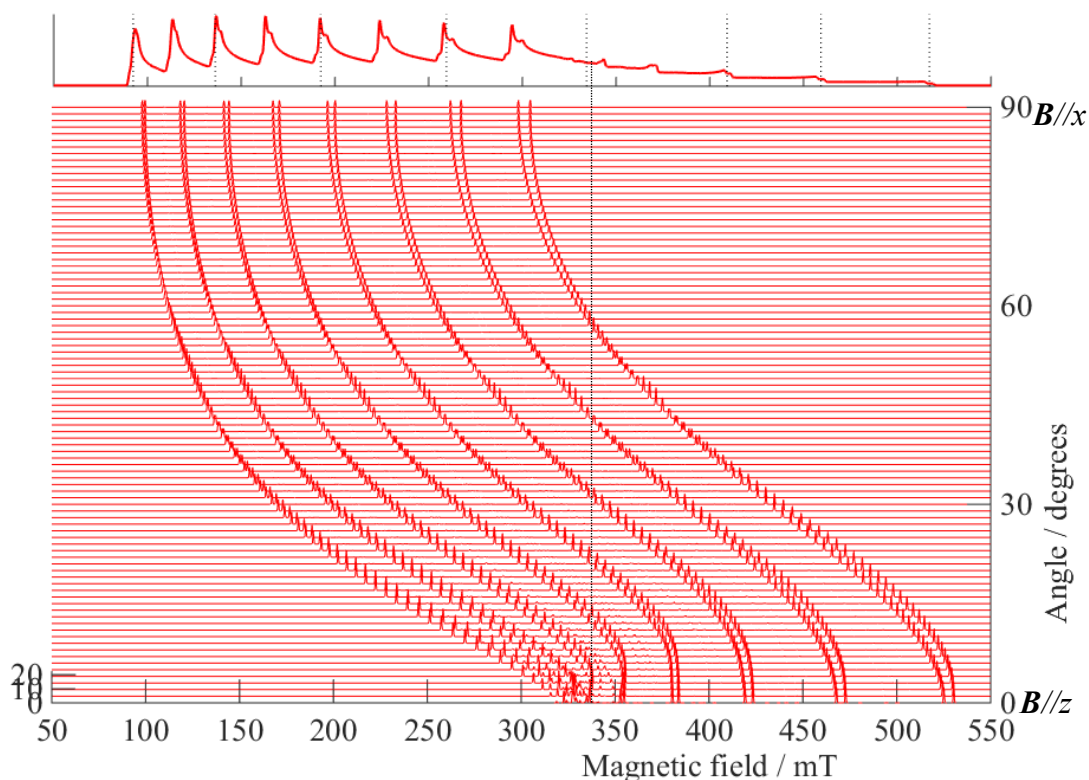


Figure S21 The calculated angular dependence from the principal z - to x -axis in the spectral simulation by using of the **ZFS/e-Zeeman spin Hamiltonian**. Microwave frequency: 9.62541 GHz, peak-to-peak line width: 0.5 mT. Magnetic tensors used: (component 1) $\mathbf{g}^{\text{true}} = [1.7138, 1.6842, 1.5472]$, $\mathbf{A}^{\text{true}} = [682.0, 679.0, 625.0]$ MHz, $D = +10 \text{ cm}^{-1}$, $E/D = 0.007$, $\mathbf{Q} = [-0.99, -1.01, 2.0]$ MHz, (component2) $\mathbf{g}^{\text{true}} = [1.7087, 1.6793, 1.5572]$, $\mathbf{A}^{\text{true}} = [681.0, 684.0, 615.0]$ MHz, $D = +10 \text{ cm}^{-1}$, $E/D = 0.007$, $\mathbf{Q} = [-1.01, -0.99, 2.0]$ MHz. The \mathbf{g}^{true} -, \mathbf{A}^{true} -, \mathbf{D} - and \mathbf{Q} -tensors of the component 1 were collinear. The relative orientations of each tensor of the component 2 were based on the direction cosines shown in Table S3. Any strain effect of the line width is not included. The simulated spectra were obtained using EasySpin (ver. 5.1.10) with varying the angle of the magnetic field one-degree stepwise. The peak denoted by the dotted line is assigned to the occurrence of the off-principal-axis peak. Noticeably, the zx -plane angular dependence of the fine-structure/hyperfine spectra due to Co^{II} OEP reveals marked difference of the behavior of the transitions appearing in the range of 30 to 60 degrees between the fictitious spin and ZFS/e-Zeeman spin Hamiltonian approaches (see Fig. S20).

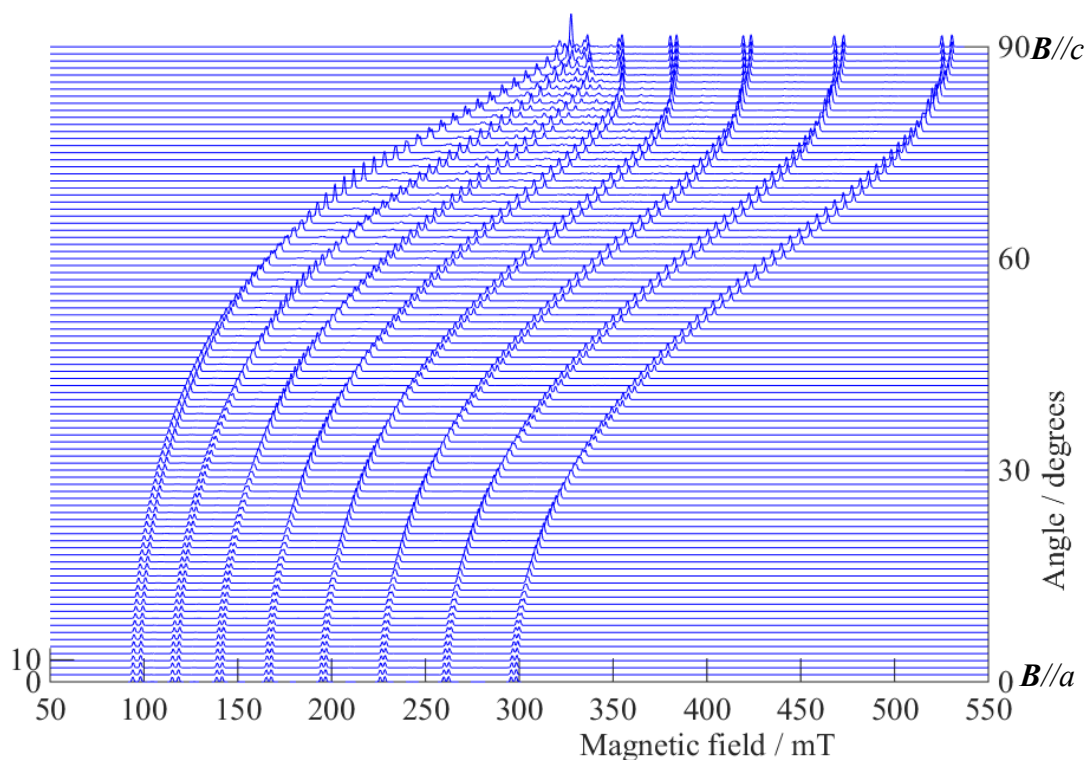


Figure S22 The calculated angular dependence from the crystal *a*- to *c*-axis in the spectral simulation by using of the **fictitious spin-1/2 Hamiltonian**. Microwave frequency: 9.62541 GHz, peak-to-peak line width: 0.5 mT. Magnetic tensors used: (component 1) $\mathbf{g}^{\text{eff}} = [3.3915, 3.4036, 1.5470]$, $\mathbf{A}^{\text{eff}} = [1349.6, 1372.2, 624.9]$ MHz, $\mathbf{Q} = [-0.10, -2.20, 2.29]$ MHz, (component2) $\mathbf{g}^{\text{eff}} = [3.3232, 3.4532, 1.5570]$, $\mathbf{A}^{\text{eff}} = [1347.7, 1382.3, 614.9]$ MHz, $\mathbf{Q} = [-2.92, -3.34, 6.25]$ MHz. the \mathbf{g}^{eff} -, \mathbf{A}^{eff} - and \mathbf{Q} -tensors of the component 1 were assumed to be collinear. The relative orientations of each tensor of the component 2 were based on the direction cosines shown in Table S32. The top the spectrum is the absorption line corresponding to the summation for the all magnetic field orientations for comparison. Any strain effect of the line width is not included. The simulated spectra were obtained using EasySpin (ver. 5.1.10) with varying the angle of the magnetic field one-degree stepwise.

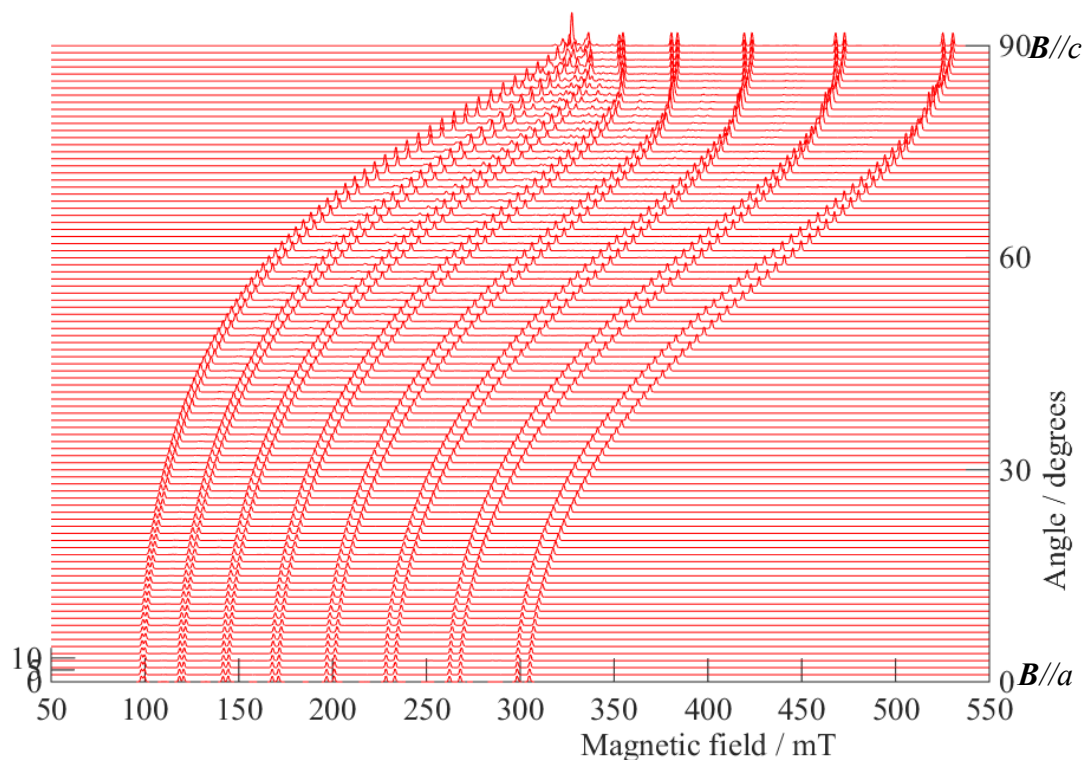


Figure S23 The calculated angular dependence from the crystal a - to c -axis in the spectral simulation by using of the **ZFS/e-Zeeman spin Hamiltonian**. Microwave frequency: 9.62541 GHz, peak-to-peak line width: 0.5 mT. Magnetic tensors used: (component 1) $\mathbf{g}^{\text{true}} = [1.7138, 1.6842, 1.5472]$, $\mathbf{A}^{\text{true}} = [682.0, 679.0, 625.0]$ MHz, $D = +10 \text{ cm}^{-1}$, $E/D = 0.007$, $\mathbf{Q} = [-0.99, -1.01, 2.0]$ MHz, (component2) $\mathbf{g}^{\text{true}} = [1.7087, 1.6793, 1.5572]$, $\mathbf{A}^{\text{true}} = [681.0, 684.0, 615.0]$ MHz, $D = +10 \text{ cm}^{-1}$, $E/D = 0.007$, $\mathbf{Q} = [-1.01, -0.99, 2.0]$ MHz. The \mathbf{g}^{true} -, \mathbf{A}^{true} -, \mathbf{D} - and \mathbf{Q} -tensors of the component 1 were collinear. The relative orientations of each tensor of the component 2 were based on the direction cosines shown in Table S2. Any strain effect of the line width is not included. The simulated spectra were obtained using EasySpin (ver. 5.1.10) with varying the angle of the magnetic field one-degree stepwise.

8.4 Simulation of the powder-pattern fine-structure/hyperfine ESR spectra of Co^{II}OEP/Ni^{II}OEP

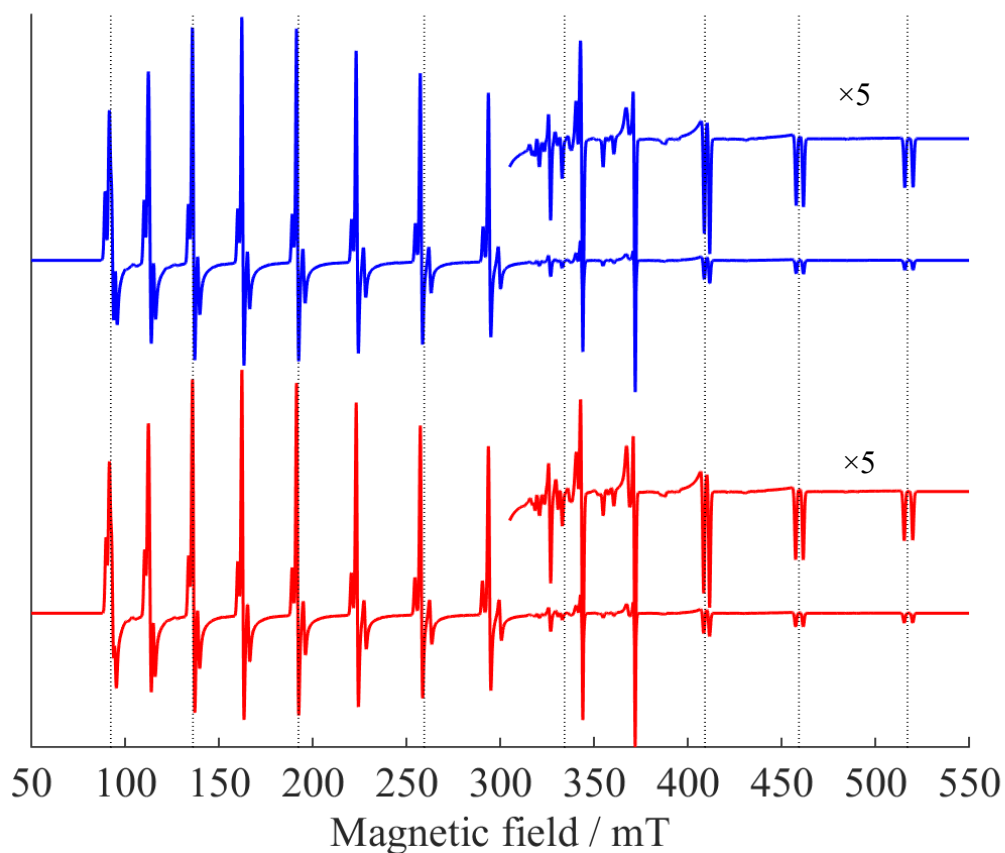


Figure S24 Spectral simulation of the power-pattern ESR spectra of Co^{II}OEP. The spectra in blue and red are based on the fictitious spin-1/2 and ZFS/e-Zeeman spin Hamiltonian approach, respectively. Microwave frequency used: 9.40914 GHz, peak-to-peak line width: 1.0 mT. Magnetic tensors: (component 1) $\mathbf{g}^{\text{true}} = [1.7138, 1.6842, 1.5472]$, $\mathbf{A}^{\text{true}} = [682.0, 679.0, 625.0]$ MHz, $D = +10 \text{ cm}^{-1}$, $E/D = 0.007$, $\mathbf{Q} = [-0.10, -2.20, 2.29]$ MHz, and (component2) $\mathbf{g}^{\text{true}} = [1.7087, 1.6793, 1.5572]$, $\mathbf{A}^{\text{true}} = [681.0, 684.0, 615.0]$ MHz, $D = +10 \text{ cm}^{-1}$, $E/D = 0.007$, $\mathbf{Q} = [-2.92, -3.34, 6.25]$ MHz. The \mathbf{g} -, \mathbf{A} -, \mathbf{D} - and \mathbf{Q} -tensors of the component 1 were collinear. The relative orientations of each tensor of the component 2 were based on the direction cosines shown in Table S3. Any strain effect of the line width is not included. The simulated spectra were obtained by using EasySpin (ver. 5.1.10).

8.5 Simulation of the powder-pattern ESR spectra composed of the forbidden transitions of Co^{II}OEP/Ni^{II}OEP

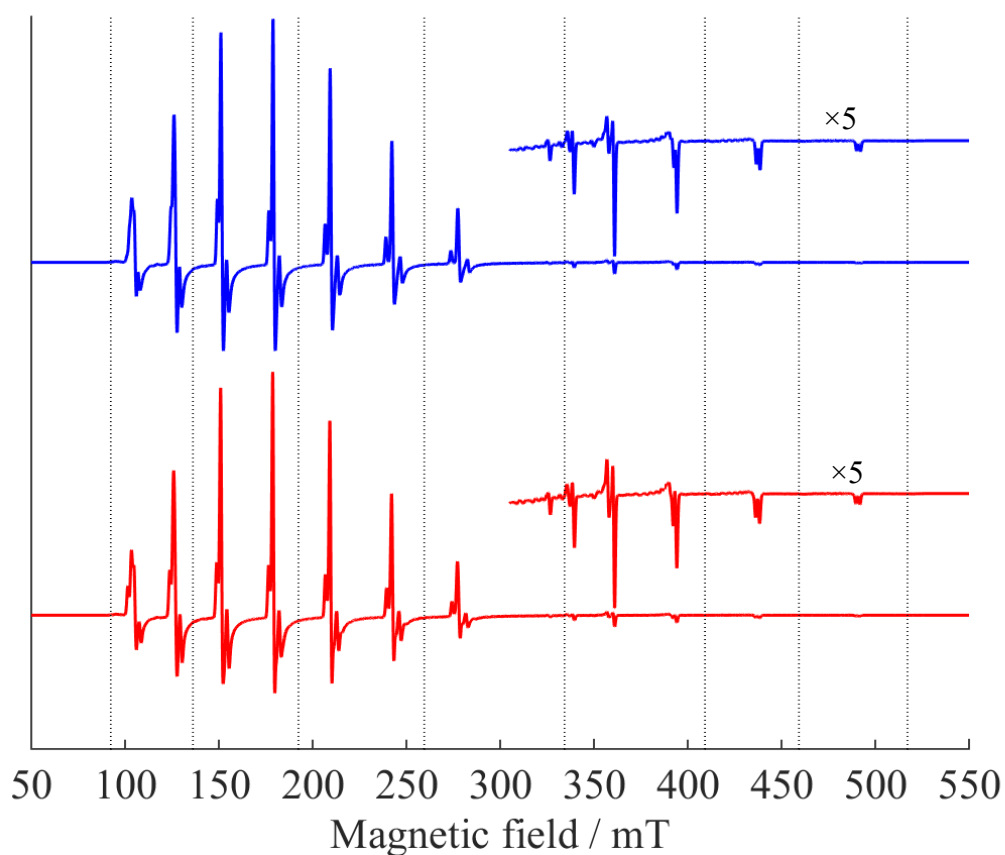


Figure S25 Spectral simulation of the powder-pattern spectra of Co^{II}OEP with the parallel excitation mode. The spectral simulations based on the fictitious spin-1/2 and ZFS/e-Zeeman spin Hamiltonian are given in blue) and red, respectively. Microwave frequency used: 9.62541, peak-to-peak line width: 1.0 mT. Magnetic tensors: (component 1) $\mathbf{g}^{\text{true}} = [1.7138, 1.6842, 1.5472]$, $\mathbf{A}^{\text{true}} = [682.0, 679.0, 625.0]$ MHz, $D = +10 \text{ cm}^{-1}$, $E/D = 0.007$, $\mathbf{Q} = [-0.10, -2.20, 2.29]$ MHz, (component2) $\mathbf{g}^{\text{true}} = [1.7087, 1.6793, 1.5572]$, $\mathbf{A}^{\text{true}} = [681.0, 684.0, 615.0]$ MHz, $D = +10 \text{ cm}^{-1}$, $E/D = 0.007$, $\mathbf{Q} = [-2.92, -3.34, 6.25]$ MHz. The \mathbf{g} -, \mathbf{A} -, \mathbf{D} - and \mathbf{Q} -tensors of the component 1 were collinear. The relative orientations of each tensor of the component 2 were based on the direction cosines shown in Table S3. Any strain of the line width is not included. The simulated spectra were obtained using EasySpin (ver. 5.1.10).

8.6 The powder-pattern ESR spectra observed at a liquid nitrogen temperature showing the dynamic Jahn-Teller distortion

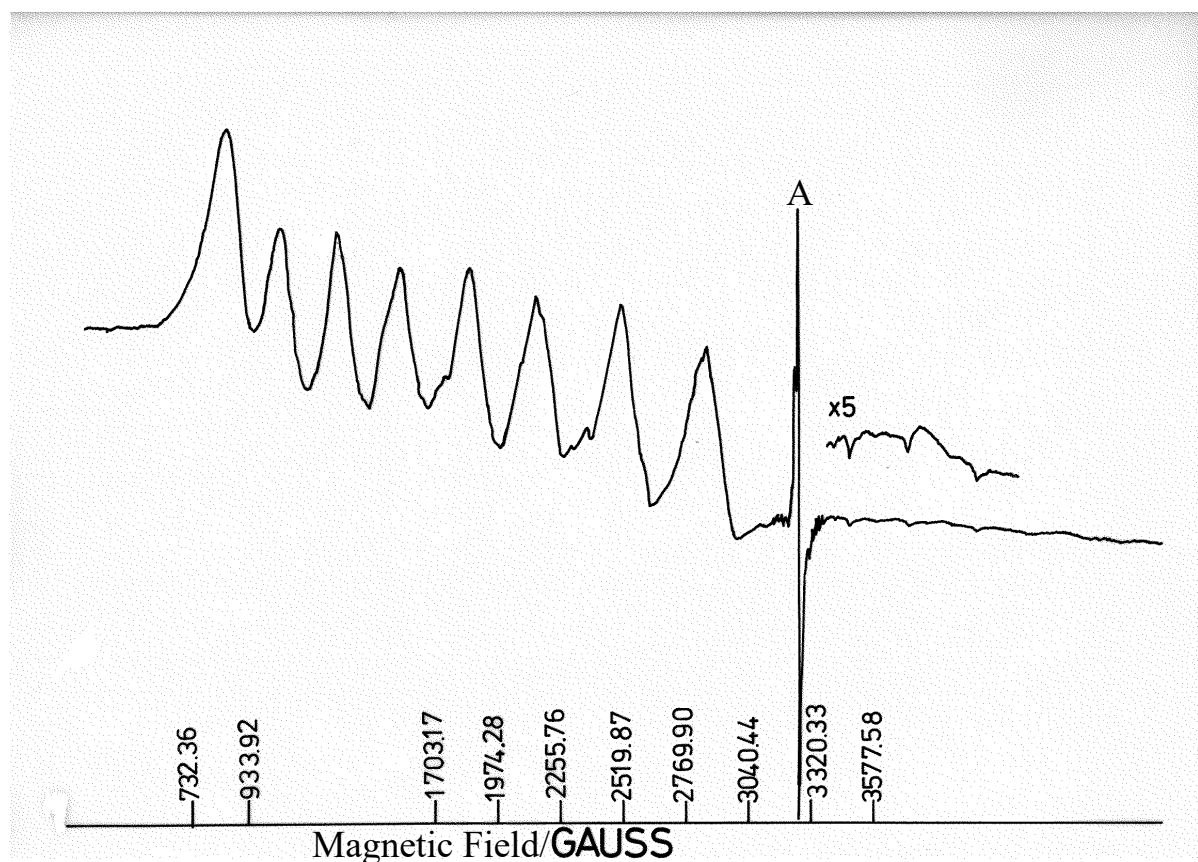


Figure S26 The randomly-oriented ESR spectrum of $\text{Co}^{\text{II}}\text{OEP}$ diluted in the $\text{Ni}^{\text{II}}\text{OEP}$ single crystal observed at 77 K. A denotes the contribution of the appearance of the off-principal-axis extra line. The dominant contribution was due to a small amount of organic radical species. The spectrum was broadened in a dynamical regime, which originates in the dynamic Jahn-Teller effect.

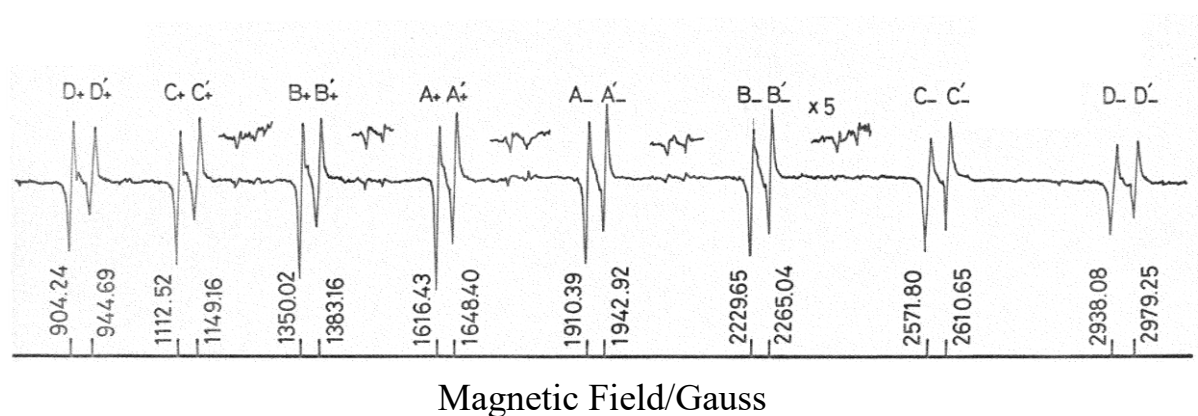


Figure S27 The single-crystal ESR spectrum of $\text{Co}^{\text{II}}\text{OEP}$ observed at 4.2 K. Two sets of the hyperfine splitting patterns are due to the orientations of the energetically distinguishable molecules in the unit cell of the crystal lattice are observed for both the allowed and the forbidden transitions. The spectrum was observed with the static magnetic field oriented by 45 degrees from the a axis in the ab plane. The appearance of the difference in the intensity is due to non-equivalence of the weight of the two molecules. The experimental peak-to-peak line widths are in the range of 8 to 14 G.

8.7 2D electron spin transient nutation spectroscopy of Co^{II}OEP diluted in the Ni^{II}OEP single-crystal

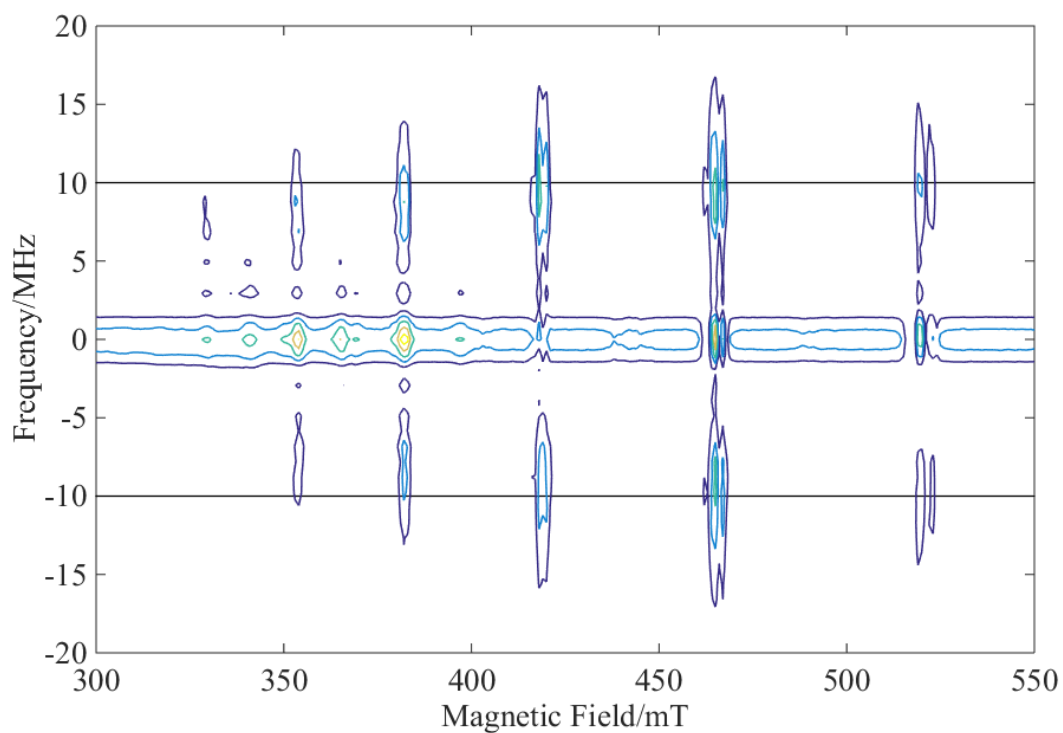


Figure S28 2D contour plot of the electron spin transient nutation spectra of Co^{II}OEP diluted in the Ni^{II}OEP single-crystal with $\mathbf{B} // z$. Hamming window functions were applied to detect the original nutation spectra. Only the observed contour plot is given. The nutation frequencies show a subtle variation with respect to the nuclear spin transitions. The detailed analysis is underway.

9. Single-crystal ESR spectroscopy of a $\text{Re}^{\text{III,IV}}$ dinuclear complex

9.1 ESR experiments in the principal-axis system of the $\text{Re}^{\text{III,IV}}$ dinuclear complex

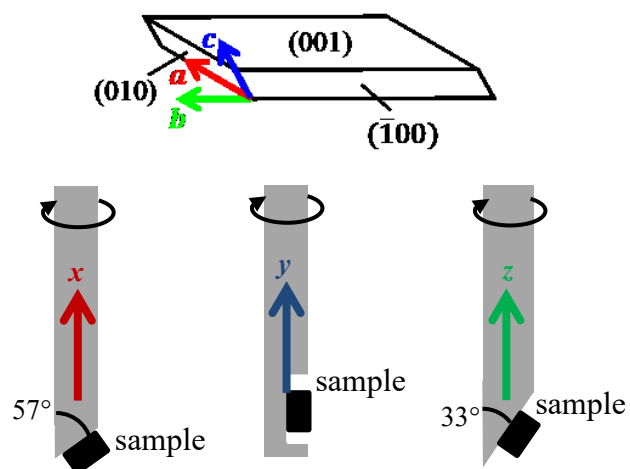


Figure S29 (Top) The outer shape of the single crystal of the $\text{Re}^{\text{III,IV}}$ dinuclear complex and Miller indexes. (Bottom) The angles of the designed wedges and the rotations around the principal axes. The plane angles were calculated from the X-ray crystallographic data and quantum chemical calculation for the principal axes of the magnetic tensors. The crystals were mounted on the (001) plane.

9.2 Angular dependence of the single-crystal ESR spectra of the $\text{Re}^{\text{III,IV}}$ dinuclear complex

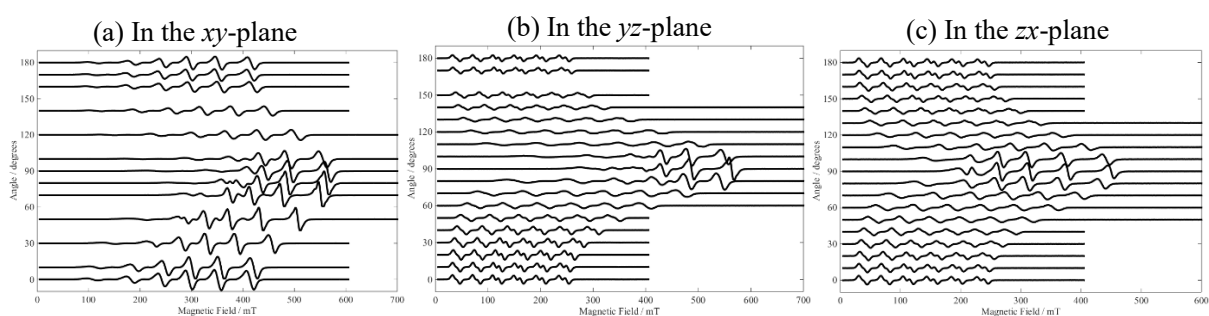


Figure S30 Angular dependence of the single-crystal ESR spectra of the $\text{Re}^{\text{III,IV}}$ dinuclear complex in the principal-axis (xyz) system. The principal axis was determined with the help of the theoretical calculations (Figure S34). In each plane, the angle giving the lowest resonance field is taken as the zero degree corresponding to $\mathbf{B} // x$ (in the xy -plane) and $\mathbf{B} // z$ (in the yz - and zx -planes), respectively. Frequency: 9.6369 GHz, noting that for each orientation the accurate frequency was measured during the measurements, temperature: 3.2 K.

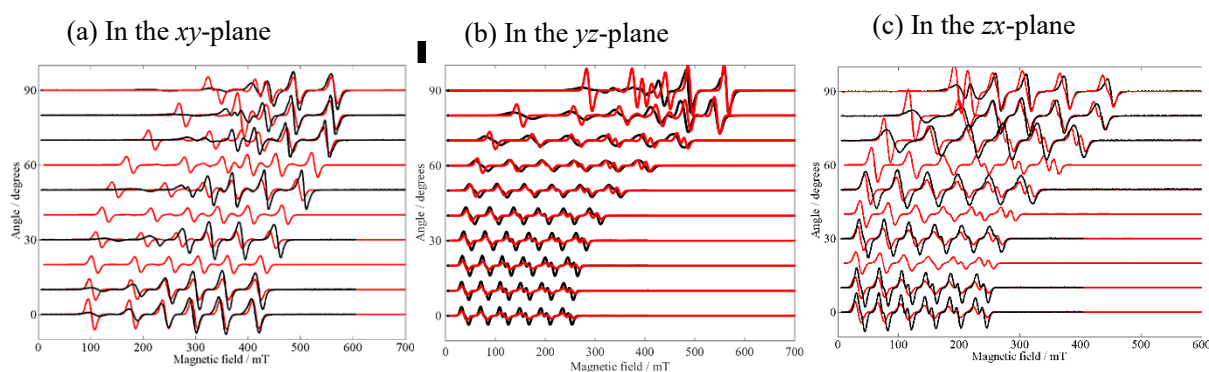


Figure S31 Simulated spectra of the single-crystal ESR of the $\text{Re}^{\text{III,IV}}$ dinuclear complex in the principal-axis system (simulated one in red). Magnetic parameters employed: $\mathbf{g}^{\text{true}} = [2.060, 2.260, 1.820]$ (component 1), $[2.060, 2.260, 1.720]$ (component 2), $\mathbf{A}^{\text{true}} = [-1290, -850, -990]$ MHz, $D = -350$ GHz (-11.7 cm^{-1}), $E = 97.23$ GHz, $E/D = 0.2778$. Any strain effect of the line width is not included. The simulated spectra were obtained by using EasySpin (ver. 5.1.10).

9.3 Magnetic measurement (M - H plot) for the $\text{Re}^{\text{III,IV}}$ dinuclear complex

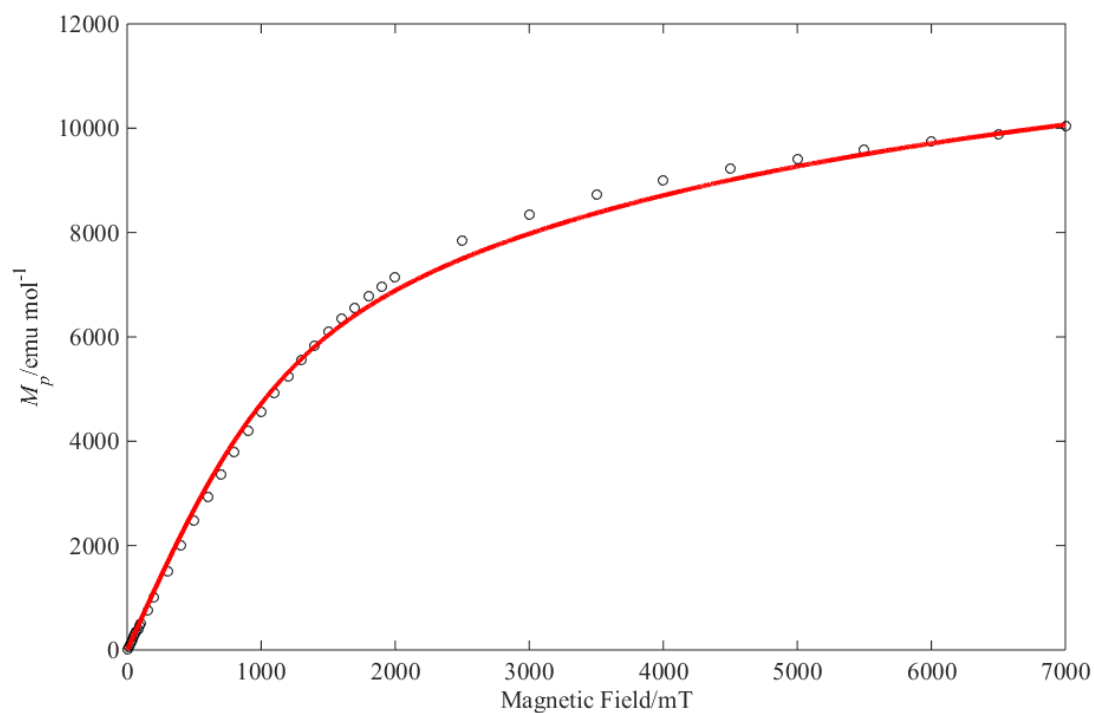


Figure S32 Experimental and simulated curves of the M - H plot for the $\text{Re}^{\text{III,IV}}$ dinuclear complex. Black circle: experimental, red line: simulated. The principal values of the \mathbf{g} -tensor ($g_x = 2.050$, $g_y = 2.240$, $g_z = 1.820$), and $E/D = 0.2778$ were used in this simulation, which were determined by the single-crystal spectroscopy. The value of $D = -350$ GHz (-11.7 cm^{-1}) was derived from the simulation.

10. Quantum chemical calculations for magnetic tensors

10.1 Quantum chemical calculations for the spin Hamiltonian parameters of Fe^{III}(Cl)OEP and Co^{II}OEP

Quantum chemical calculations of the spin Hamiltonian parameters including the **g**-tensor, **D**-tensor, **A**-tensor of ⁵⁷Fe, ⁵⁹Co, and ¹⁴N nuclei, and **Q**-tensor of ⁵⁹Co nuclei were carried out by means of DFT. Because the ruffled structure of the porphyrin ring of OEP plays an important role on their electronic structures, we used the solid state geometry of the diamagnetic Ni^{II}OEP host molecule as determined from the X-ray crystallography,^[S6] by substituting the Ni atom to Fe or Co. The position of the Cl atom in Fe^{III}(Cl)OEP was optimized at the UTPSS/Sapporo-DZP level, and the Cartesian coordinates of all other atoms were fixed during the geometry optimization. The optimized Fe–Cl bond length is 2.413 Å.

The magnetic tensors were calculated at the UTPSS/Sapporo-DZP level. In the **D**-tensor calculations the first order spin–spin dipolar contributions (**D**^{SS} terms) were calculated by using the natural orbitals constructed from the unrestricted Kohn–Sham determinant, in conjunction with the McWeeny–Mizuno equation.^[S7] The second order spin–orbit contributions (**D**^{SO} terms) were evaluated by using the natural orbital-based Pederson–Khanna (NOB-PK) method^[S8] with the one-electron spin–orbit Hamiltonian with effective nuclear charges. The NOB-PK method, which has recently been proposed by us, utilizes a single Slater determinant consisting of natural orbitals as the ground-state wavefunction in conjunction with the Pederson–Khanna (PK)-type determinant-based perturbation theory. The NOB-PK method gives more accurate **D**^{SO}-tensors in [Mn^{II}(terpy)X₂] (terpy = 2,2':6,2''-terpyridine, X = NCS, Cl, Br, and I), [Mn^{II}(tpa)X₂] (tpa = tris-2-picolylamine, X = Cl, Br, and I), and (NBu₄)₂[Re^{IV}X₄(ox)] (ox = oxalate, NBu₄ = tetra-*n*-butylammonium cation, X = Cl and Br) systems than the conventional PK^[S9] and quasi-restricted orbital (QRO)^[S10] approaches.

The **g**-, **A**-, **Q**-, and **D**^{SS}-tensors were calculated by using ORCA software (version 3.0.0),^[S11] and the **D**^{SO}-tensors were computed by means of GAMESS-US program suite^[S12] and our laboratory-made source code.

The electronic configuration in the spin-sextet ground state of Fe^{III}(Cl)OEP is (d_{xz})¹(d_{yz})¹(d_z²)¹(d_{x²-y²})¹(d_{xy})¹ without any ambiguity. However, determining the electronic configuration of the spin-quartet ground-state of Co^{II}OEP needs special care, because of the presence of low-lying excited electronic states arising from the ruffled structure of the porphyrin ring. In order to elucidate the electronic structure of the ground state of Co^{II}OEP, we have carried out 10 single point calculations with the different initial-guess 3d-electron configurations. According to the single point calculations the energy-lowest electronic configuration is (d_{xz})¹(d_{yz})¹(d_z²)²(d_{x²-y²})²(d_{xy})¹, but the electronic states having (d_{xz})²(d_{yz})¹(d_z²)¹(d_{x²-y²})²(d_{xy})¹ and (d_{xz})¹(d_{yz})²(d_z²)¹(d_{x²-y²})²(d_{xy})¹ configurations are calculated to be at 273 and 274 cm⁻¹, respectively, above the ground state. Here, we defined the *x* and *y* axes to be parallel to the direction connecting cobalt and *meso*-carbon atoms and the *z* axis to be

parallel to the pseudo- S_4 axis. The quasi-degeneracy of these two electronic states is rationalized from the pseudo- S_4 symmetry of $\text{Co}^{\text{II}}\text{OEP}$. The electronic state described as $(d_{xz})^2(d_{yz})^2(d_z)^1(d_{x^2-y^2})^1(d_{xy})^1$ configuration, expected from the crystal field of the square planar coordination, is calculated to be at 1909 cm^{-1} higher in energy than the ground state. Note that other spin-quartet electronic states are calculated to have higher energy ($\Delta E > 20\ 000\text{ cm}^{-1}$) than the ground state at the UTPSS/Sapporo-DZP level.

Because the low-lying electronic states are energetically very close to each other and it is hard to determine the ground state electronic configuration only from the DFT calculations, we also carried out the CASSCF(7e,5o)/6-31G* calculations for $\text{Co}^{\text{II}}\text{Por}$ (Por = porphyrin) molecule. The molecular geometry of $\text{Co}^{\text{II}}\text{Por}$ was prepared from the solid state geometry of $\text{Ni}^{\text{II}}\text{OEP}$, by substituting Ni to Co, and the ethyl groups to the H atoms. The CASSCF active space consists of valence 3d orbitals and electrons. During the SCF calculation state averaging is done for 10 spin-quartet states. According to the CASSCF calculation, the lowest quartet state is described mainly by the $(d_{xz})^2(d_{yz})^2(d_z)^1(d_{x^2-y^2})^1(d_{xy})^1$ configuration with the expansion coefficient $C = 0.99$. The first and second excited quartet states are located to be at 717 cm^{-1} and 718 cm^{-1} , respectively, higher in energy above the ground state. Both the first and second excited quartet states have multiconfigurational character and the main configurations are $0.80 [(d_{xz})^2(d_{yz})^1(d_z)^2(d_{x^2-y^2})^1(d_{xy})^1] + 0.58 [(d_{xz})^1(d_{yz})^2(d_z)^1(d_{x^2-y^2})^2(d_{xy})^1]$ and $0.81 [(d_{xz})^2(d_{yz})^1(d_z)^1(d_{x^2-y^2})^2(d_{xy})^1] - 0.58 [(d_{xz})^1(d_{yz})^2(d_z)^2(d_{x^2-y^2})^1(d_{xy})^1]$, respectively. The third excited quartet state is described mainly by the $(d_{xz})^1(d_{yz})^1(d_z)^2(d_{x^2-y^2})^2(d_{xy})^1$ configuration, which is the energy-lowest configuration in the UTPSS/Sapporo-DZP single point calculations. The excitation energy of the third excited quartet state is 2522 cm^{-1} at the CASSCF level. From the DFT and CASSCF calculations, we expect that the ground state electronic configuration must be $(d_{xz})^2(d_{yz})^2(d_z)^1(d_{x^2-y^2})^1(d_{xy})^1$ or $(d_{xz})^1(d_{yz})^1(d_z)^2(d_{x^2-y^2})^2(d_{xy})^1$ and we have carried out the magnetic tensor calculations for these two electronic configurations.

The spin density distributions of $\text{Fe}^{\text{III}}(\text{Cl})\text{OEP}$ and $\text{Co}^{\text{II}}\text{OEP}$ are plotted in [Figure S33](#) with an isosurface value is set to be 0.005, and Mulliken atomic spin densities on the metal center, chlorine, and nitrogen atoms are summarized in Table S6. In both molecules most of unpaired electrons are located on the metal center, and non-negligible amounts of spin densities are distributed onto the coordinated chlorine and nitrogen atoms.

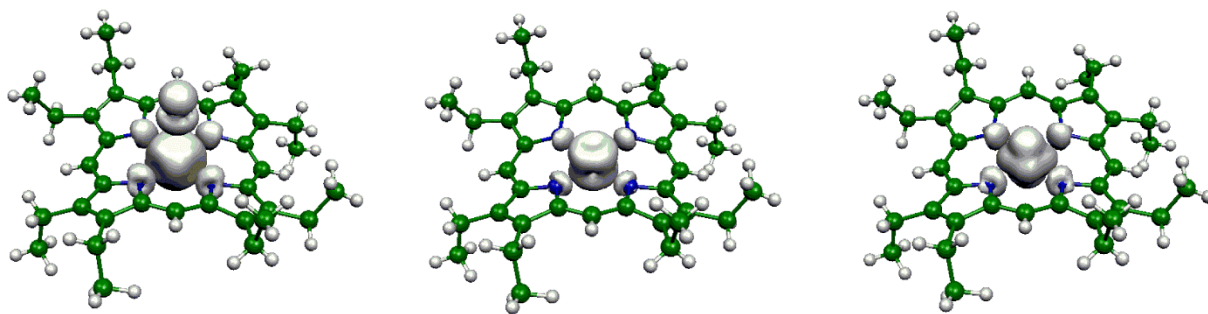


Figure S33 Spin density distributions of Fe^{III}(Cl)OEP (left) and Co^{II}OEP (center: $(d_{xz})^1(d_{yz})^1(d_z)^2(d_{x^2-y^2})^2(d_{xy})^1$ configuration, right: $(d_{xz})^2(d_{yz})^2(d_z)^1(d_{x^2-y^2})^1(d_{xy})^1$ configuration) calculated at the UTPSS/Sapporo-DZP level of theory.

Table S6 Mulliken atomic spin densities of Fe^{III}(Cl)OEP and Co^{II}OEP calculated at the UTPSS/Sapporo-DZP level

Molecule	Fe ^{III} (Cl)OEP	Co ^{II} OEP	
Electronic configuration	$(d_{xz})^1(d_{yz})^1(d_z)^1$ $(d_{x^2-y^2})^1(d_{xy})^1$	$(d_{xz})^1(d_{yz})^1(d_z)^2$ $(d_{x^2-y^2})^2(d_{xy})^1$	$(d_{xz})^2(d_{yz})^2(d_z)^1$ $(d_{x^2-y^2})^1(d_{xy})^1$
Metal center	3.966	2.522	2.668
Cl	0.329		
4N	0.376	0.205	0.331

The calculated magnetic tensors of Fe^{III}(Cl)OEP and Co^{II}OEP are summarized in Table S7. In Fe^{III}(Cl)OEP the **D**-, **g**-, **A**(⁵⁷Fe)-tensors are roughly coaxial. The D_{zz} axis is nearly parallel to the Fe–Cl bond. The D_{xx} axis is approximately parallel to the direction connecting Fe and the carbon atom at the *meso* position. The **D**^{SS} contribution to the D value is about 600 MHz and therefore the **D**^{SO} term is dominant. The analysis of the theoretical **D**^{SO}-tensor based on the orbital region partitioning technique (ORPT) revealed that the most important excitation on the **D**^{SO} contributions are $d_{x^2-y^2}(\alpha) \rightarrow d_{xy}(\beta)$ excitation, which raises the D_{zz} principal value by about 3×10^5 MHz. The $d_{x^2-y^2}(\alpha) \rightarrow d_{yz}(\beta)$ and $d_{x^2-y^2}(\alpha) \rightarrow d_{xz}(\beta)$ excitations contribute mainly to the D_{xx} and D_{yy} principal values, respectively, which act to decrease the D value by about 0.7×10^5 MHz. The **g**-tensor is slightly shifted positively from the g value of free electron (2.0023) but the shift is small compared with that of Co^{II}OEP. The **A**(⁵⁷Fe)-tensor has small anisotropy reflecting the d^5 high-spin electronic configuration.

In Co^{II}OEP of the $(d_{xz})^1(d_{yz})^1(d_z)^2(d_{x^2-y^2})^2(d_{xy})^1$ electron configuration, the negative D^{SS+SO} value is predicted. The D_{zz} axis is perpendicular to the porphyrin ring. According to the ORPT, the most important excited electronic configurations are $d_{xy}(\alpha) \rightarrow d_{yz}(\beta)$ and $d_{xy}(\alpha) \rightarrow d_{xz}(\beta)$. These excitations work to raise D_{xx} and D_{yy} principal values, as discussed in the **D**^{SO}-tensor analysis of Fe^{III}(Cl)OEP. The **A**(⁵⁹Co)-tensor has very small anisotropy reflecting the electronic configuration.

In the **D**^{SO}-tensor calculation of Co^{II}OEP in $(d_{xz})^2(d_{yz})^2(d_z)^1(d_{x^2-y^2})^1(d_{xy})^1$ electronic

configuration we have encountered difficulties in the DFT-based approach. In the single determinant comprised of natural orbitals the highest occupied spin- α (d_{xy}) orbital has higher energy than the lowest unoccupied spin- β ($d_{x^2-y^2}$) orbital ($\varepsilon(d_{xy})(\alpha) = -0.111576$ Hartree and $\varepsilon(d_{x^2-y^2})(\beta) = -0.114939$ Hartree). This means that the spin-doublet excited configuration has lower energy than the spin-quartet state, although in the CASSCF calculations the $(d_{xz})^2(d_{yz})^2(d_z)^1(d_{x^2-y^2})^1(d_{xy})^1$ spin-quartet state is the ground state. The theoretical D^{SO} value calculated based on the NOB-PK method is -5.496×10^6 MHz. However, the ORPT analysis revealed that the $d_{xy}(\alpha) \rightarrow d_{x^2-y^2}(\beta)$ excited configuration contributes dominantly to the D^{SO} value (-5.664×10^6 MHz), which has the abovementioned negative orbital energy difference. If this excited spin-doublet configuration has positive orbital energy difference like in the CASSCF energy orderings, the sign of the D^{SO} value becomes positive. We note that such orbital energy order inversion occurs in the Kohn–Sham orbital of both $Fe^{III}(Cl)OEP$ and $Co^{II}OEP$, and therefore the D^{SO} values of $Fe^{III}(Cl)OEP$ and $Co^{II}OEP$ of $(d_{xz})^1(d_{yz})^1(d_z)^2(d_{x^2-y^2})^2(d_{xy})^1$ configuration calculated by means of the conventional PK method has the opposite absolute sign to those calculated by NOB-PK.

In order to estimate \mathbf{D}^{SO} -tensor of $Co^{II}OEP$ in $(d_{xz})^2(d_{yz})^2(d_z)^1(d_{x^2-y^2})^1(d_{xy})^1$ configuration other than the DFT-based methods, we have adopted spin-orbit CI (SO-CI) based on the CASSCF(7e,5o)/6-31G* wavefunction in the $Co^{II}Por$ system. In the SO-CI calculations we used the 50-state-averaged (40 doublets and 10 quartets) CASSCF wavefunctions as the non-relativistic wavefunctions. The D^{SO} and E^{SO} values are calculated directly from the energy differences between spin sublevels. The obtained D^{SO} value is positive as expected ($D^{SO} = +2.174 \times 10^6$ MHz), and the E^{SO} value is less than 1 MHz. Note that at the SO-CI method the D^{SO} value of $(d_{xz})^1(d_{yz})^1(d_z)^2(d_{x^2-y^2})^2(d_{xy})^1$ configuration (the third excited quartet state) is -7.725×10^5 MHz, which is close to the NOB-PK-based theoretical value.

The $\mathbf{A}^{(59Co)}$ -tensor of $Co^{II}OEP$ in $(d_{xz})^2(d_{yz})^2(d_z)^1(d_{x^2-y^2})^1(d_{xy})^1$ configuration calculated at the UTPSS/Sapporo-DZP shows large axial anisotropy: $A_{xx} \sim A_{yy} > A_{zz}$, because two unpaired electrons occupy in-molecular-plane orbitals ($d_{x^2-y^2}$ and d_{xy} orbitals). Since the $d_{x^2-y^2}$ orbital is doubly occupied in $(d_{xz})^1(d_{yz})^1(d_z)^2(d_{x^2-y^2})^2(d_{xy})^1$ configuration and singly occupied in $(d_{xz})^2(d_{yz})^2(d_z)^1(d_{x^2-y^2})^1(d_{xy})^1$, the smaller \mathbf{Q} -tensor is obtained in $(d_{xz})^2(d_{yz})^2(d_z)^1(d_{x^2-y^2})^1(d_{xy})^1$ configuration than in $(d_{xz})^1(d_{yz})^1(d_z)^2(d_{x^2-y^2})^2(d_{xy})^1$ reflecting the occupation number.

Table S7 Magnetic tensors calculated at the UTPSS/Sapporo-DZP level.

Molecule	Fe ^{III} (Cl)OEP	Co ^{II} OEP	
Electronic configuration	(d _{xz}) ¹ (d _{yz}) ¹ (d _z ²) ¹ (d _{x²-y²}) ¹ (d _{xy}) ¹	(d _{xz}) ¹ (d _{yz}) ¹ (d _z ²) ² (d _{x²-y²}) ² (d _{xy}) ¹	(d _{xz}) ² (d _{yz}) ² (d _z ²) ¹ (d _{x²-y²}) ¹ (d _{xy}) ¹
D^{SS+SO}/MHz	$+2.301 \times 10^5$	-6.403×10^5	$+2.174 \times 10^6$ ^[a]
E^{SS+SO}/D^{SS+SO}	0.0481	0.0015	0.0000 ^[a]
g_{xx}	2.0149	2.0792	2.0948
g_{yy}	2.0166	2.0793	2.0947
g_{zz}	2.0075	2.0226	2.0093
g_{iso}	2.0130	2.0604	2.0663
$A_{xx}(\text{M})/\text{MHz}$	20.97	148.01	352.68
$A_{yy}(\text{M})/\text{MHz}$	22.24	148.08	352.66
$A_{zz}(\text{M})/\text{MHz}$	18.38	148.49	158.02
$a_{iso}(\text{M})/\text{MHz}$	20.53	148.19	287.79
$A_{xx}({}^{14}\text{N})/\text{MHz}$ ^[b]	11.20	15.88	17.17
$A_{yy}({}^{14}\text{N})/\text{MHz}$ ^[b]	7.95	12.04	12.85
$A_{zz}({}^{14}\text{N})/\text{MHz}$ ^[b]	9.00	12.40	13.80
$a_{iso}({}^{14}\text{N})/\text{MHz}$	9.38	13.44	14.61
$Q_{xx}({}^{59}\text{Co})/\text{MHz}$		-2.773	-0.768
$Q_{yy}({}^{59}\text{Co})/\text{MHz}$		-2.767	-0.764
$Q_{zz}({}^{59}\text{Co})/\text{MHz}$		5.540	1.532

[a] The spin-orbit CI result in Co^{II}Por using CASSCF(7e,5o)/6-31G* wavefunctions as the non-relativistic wavefunctions. [b] The $A_{xx}({}^{14}\text{N})$ axis is parallel to the M–N coordination bond, $A_{zz}({}^{14}\text{N})$ axis is perpendicular to the molecular plane.

10.2 Quantum chemical calculations for the spin Hamiltonian parameters of the Re^{IV}-monomer

In the Re^{III,IV} dinuclear mixed-valence complex under study the Re^{III} site (d⁴) is spin-singlet and we focused on the lowest spin-quartet ($S = 3/2$) state of the Re^{IV}-monomer for the magnetic tensor calculations. The DFT calculations of the **g**- and **D**-tensors, and **A**-tensor of the Re atom of the Re^{IV}-monomer were carried out by using TPSS exchange–correlation functional in conjunction with the Sapporo-DKH3-DZP-2012 and Sapporo-DZP-2012 basis sets for Re and the other atoms, respectively. We used the solid state geometry of the Re^{IV} monomer in the mixed-valence complexes determined from the X-ray crystallography. In the SCF procedure we used the second-order Douglas–Kroll–Hess Hamiltonian^[S13] to include relativistic effects. The **D**^{SS}- and **D**^{SO}-tensors were calculated using the same procedure as the calculations in Fe^{III}(Cl)OEP and Co^{II}OEP.

The electronic configuration of valence 5d orbitals in the ground state of the Re^{IV}-monomer is (d_{xz})¹(d_{yz})¹(d_{x²-y²})¹(d_{z²})⁰(d_{xy})⁰, as expected from the crystal field of the octahedral coordination. The definition of the axis (which is identical to the principal axis of the theoretical **D**^{SS+SO}-tensor) is given in Figure S34, together with the spin density distribution obtained from the single point calculation. Unpaired electrons distribute mainly onto the Re^{IV} center but delocalizes onto the Cl⁻ and bim²⁻ groups. According to the Mulliken population analysis the Re atom carries 2.342 of unpaired electrons, and the two Cl⁻ and bim²⁻ groups hold 0.325 and 0.374, respectively, of the delocalized spins. Spin densities on the PⁿPr₃ groups are very small (−0.041).

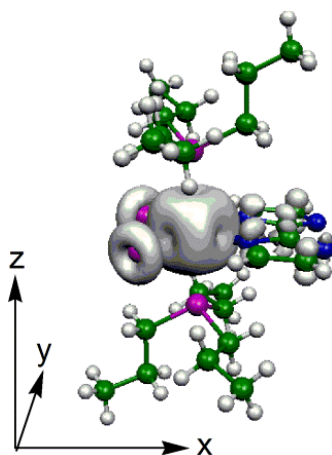


Figure S34 Spin density distributions of Re^{IV}-monomer.

The calculated $D^{\text{SS+SO}}$ value is -1.730×10^6 MHz, and the $|E^{\text{SS+SO}}/D^{\text{SS+SO}}|$ value is 0.205. As expected, the spin–orbit term dominantly contributes to the **D**-tensor and spin–spin dipolar contribution is about 0.2% in the **D**^{SS+SO}-tensor. The large E/D value indicates the departure from the axial symmetry. Such a large E/D value is also observed in [Re^{IV}X₄(ox)]²⁻ systems (X

= Cl and Br).^[S14]

The \mathbf{g} - and $\mathbf{A}({}^{187}\text{Re})$ -tensors are nearly coaxial to the $\mathbf{D}^{\text{SS+SO}}$ -tensor (deviations are less than 4°). At the present calculation the principal value of the \mathbf{g} -tensor is $g_{xx} = 1.9806$, $g_{yy} = 2.0138$, $g_{zz} = 2.0345$, ($g_{\text{iso}} = 2.0096$). The anisotropic nature of the \mathbf{g} -tensor is consistent with the non-symmetric spin-orbit coupling and hence non-axial-symmetric \mathbf{D} -tensor. By contrast, the $\mathbf{A}({}^{187}\text{Re})$ -tensor is rather symmetric ($A_{xx} = -3135.02$ MHz, $A_{yy} = -3119.34$ MHz, $A_{zz} = -3103.09$ MHz, $a_{\text{iso}} = -3119.15$ MHz), reflecting the $5d^3$ electron configuration and spin density distributions.

11. Experiments

Single-crystals of diamagnetic Ni^{II}OEP well incorporating Fe^{III}(Cl)OEP ($S = 5/2$) were prepared, in which actual guest/host concentration ratios were not determined. The detailed preparation process of the magnetically diluted sizable single-crystals will be given elsewhere. The Miller indexes of the single-crystal were assigned to the crystal planes of a square-bipyramidal structure.^[S6] Based on the assignment of the Miller indexes an oxygen-free copper wedge was designed and prepared for ESR/ENDOR experiments in the principal-axis coordinate systems. Fortunately, the bipyramidal plane coincides with the square plane composed of the four nitrogen nuclei of the porphyrin skeleton, and an angle between the crystal a -axis (or the b -axis) and the direction of the diagonal nitrogen nuclei is only 2 degrees, as shown in Figure S33. The error of the plane angles of the wedge was less than 0.2 degrees. All the experiments including pulsed ESR and electron spin transient nutation spectroscopy at X-band were carried out at liquid helium temperatures except otherwise specified.

Conventional CW ESR experiments were carried out with a Bruker ESP300/350 X-band ESR Spectrometer equipped with a dual mode resonator ER4116DM, in which the ESR measurements were achieved in a not only conventional perpendicular mode ($\mathbf{B} \perp \mathbf{B}_1$: \mathbf{B} denotes the static magnetic field and \mathbf{B}_1 the microwave oscillating field) but also a parallel excitation mode ($\mathbf{B} // \mathbf{B}_1$). The parallel mode allows the fine-structure/hyperfine forbidden transitions allowed. Temperature was controlled with an Oxford ESR910 helium-gas flow temperature controller system. CW X-band ENDOR measurements in the principal-axis coordinate systems were carried out with the ESP350 based spectrometer equipped with a single-circle goniometer.

Single-crystal X-band pulsed-ESR spectroscopy was carried out with ESP300/380E (BrukerBioSpin) spectrometer equipped with a 1 kW TWT microwave amplifier. The relative phase and the intensity of microwave pulses were adjusted by using a high speed oscilloscope 9450A, 300 MHz (Lecroy). The microwave frequency was monitored with a frequency counter R5373 (Advantest). The temperature was regulated with a helium-gas flow controller systems (Oxford). Echo-detected field-swept ESR spectra were obtained with the conventional pulse sequence: $\pi/2-\tau-\pi-\tau$ -echo with $\pi/2 = 30$ ns, $\pi = 60$ ns and $\tau = 300$ ns. Electron spin transient nutation spectroscopy for the metalloporphyrins was carried in the echo-detected scheme with a pulse sequence of the nutation pulse- $t_0-\pi/2-\tau-\pi-\tau$ -echo, where the nutation pulse was changed from 16 to 512 ns in the step of 4 ns with $\pi/2 = 30$ ns, $\pi = 60$ ns, $t_0 = 40$ ns and $\tau = 300$ ns.

Magnetic susceptibilities were measured with Quantum Design Superconducting Quantum Interference Device (SQUID) magnetometer MPMS-XL in the temperature range 1.9–298 K at an applied magnetic field of 100 mT.^[S15] Corrections for molecular diamagnetism, estimated from Pascal's constants, were applied.^[S15] In order to increase the accuracy of the data, the susceptibility measurements were carried out at 400 and 500 mT, and the susceptibility was obtained with the slope of these points. Calculations of M_p and χ_p were carried out with

laboratory-build programs on MATLAB R2014b. The accuracy of the calculation was examined by comparing with the analytical solution for $S = 3/2$.^[S16] Additional contributions from a thermally accessible excited (triplet, $S = 1$) state of the trivalent rhenium moiety were taken into account, where the principal values of the \mathbf{g} -tensor were taken from the theoretical values ($g_{xx} = 2.033$, $g_{yy} = 2.009$, $g_{zz} = 2.014$), and the D -value of the triplet state and the excitation energy J between the ground singlet and triplet state were optimized.

The host crystal of Ni(II)OEP is a tetragonal bipyramidal with the space group $I4_1/a$, $Z = 4$, $a = b = 1.493(1)$ nm, $c = 1.384(1)$ nm as determined by Mayer^[S6] and the crystal has a habit of well-developed planes with Miller indexes, (100) (minor), (010) (minor), (001) (minor), (-100) (minor), (0-10) (minor), (00-1) (minor), (101), (011), (0-11), (-101), (01-1), (10-1), (0-1-1), (-10-1).

The host Ni^{II}OEP molecule has a slightly ruffled structure of the porphyrin plane with S_4 symmetry. The molecular principal-axis system of the crystal nearly coincides with the crystallographic-axis system. It facilitates the spectral analyses for the observed ESR/ENDOR spectra, giving good accuracy of the determined tensors. The experimental error of setting the crystals of Ni^{II}OEP in the cavity was estimated within 0.5 degrees. The c -axis of the crystal is perpendicular to the porphyrin plane, while the N–N directions are nearly parallel to the a or b axis. An oxygen-free copper wedge was used for mounting the crystal.



Figure S35 The molecular structure and the principal axes used for the experiments. Note that the theoretical principal x - or y -axis is along the nearest neighboring N–N direction.

References

- [S1] B. Bleaney and K. D. Bowers, Anomalous Paramagnetism of Copper Acetate, *Proc. Roy. Soc. A*, 1952, **214**, 451–465.
- [S2] J. W. Orton, *Electron Paramagnetic Resonance: An Introduction to Transition Group Ions in Crystals*, Gordon and Breach, 1968.
- [S3] C. Rudowicz and R. Bramley, On Standardization of the Spin Hamiltonian and the Ligand Field Hamiltonian for Orthorhombic Symmetry, *J. Chem. Phys.*, 1985, **83**, 5192–5197.
- [S4] R. Kripal, D. Yadav, P. Gnutek and C. Rudowicz, Alternative Zero-Field Splitting (ZFS) Parameter Sets and Standardization for Mn^{2+} Ions in Various Hosts Exhibiting Orthorhombic Site Symmetry, *J. Phys. Chem. Solids*, 2009, **70**, 827–833.

- [S5] J. R. Pilbrow, Effective g Values for $S = 3/2$ and $S = 5/2$, *J. Magn. Reson.*, 1978, **31**, 479–490.
- [S6] E. F. Mayer, Jr. The crystal and molecular structure of nickel(II)octaethylporphyrin. *Acta Crystallogr., Sect. B*, 1972, **28**, 2162–2167.
- [S7] R. McWeeny, Y. Mizuno, The density matrix in many-electron quantum mechanics II. Separation of space and spin variables; spin coupling problems. *Proc. R. Soc. London, Ser. A*, 1961, **259**, 554–577; S. Sinnecker, F. Neese, Spin-spin contributions to the zero-field splitting tensor in organic triplets, carbenes, and biradicals—A density functional and ab initio study. *J. Phys. Chem. A*, 2006, **110**, 12267–12275.
- [S8] K. Sugisaki, K. Toyota, K. Sato, D. Shiomi, T. Takui, Quasi-restricted orbital treatment for the density functional theory calculations of the spin–orbit term of zero-field splitting tensors. *J. Phys. Chem. A*, 2016, **120**, 9857–9866.
- [S9] M. R. Pederson, S. N. Khanna, Magnetic anisotropy barrier for spin tunneling in Mn12O12 molecules. *Phys. Rev. B: Condens. Matter Mater. Phys.*, 1999, **60**, 9566–9572.
- [S10] F. Neese, Importance of direct spin–spin coupling and spin-flip excitations for the zero-field splittings of transition metal complexes: A case study. *J. Am. Chem. Soc.*, 2006, **128**, 10213–10222.
- [S11] F. Neese, The ORCA program system. *Wiley Interdiscip. Rev.: Comput. Mol. Sci.*, 2012, **2**, 73–78.
- [S12] M. W. Schmidt, K. K. Baldrige, J. A. Boatz, S. T. Elbert, M. S. Gordon, J. H. Jensen, S. Koseki, N. Matsunaga, K. A. Nguyen, S. J. Su, T. L. Windus, M. Dupuis, J. A. Montgomery, General atomic and molecular electronic structure system. *J. Comput. Chem.*, 1993, **14**, 1347–1363.
- [S13] B. A. Hess, Relativistic electronic-structure calculations employing a two-component no-pair formalism with external-field projection operators. *Phys. Rev. A*, 1986, **33**, 3742–3748.
- [S14] J. Martínez-Lillo, T. F. Mastropietro, E. Lhotel, C. Paulsen, J. Cano, G. De Munno, J. Faus, F. Lloret, M. Julve, S. Nellutla, J. Krzystek, Highly anisotropic rhenium(IV) complexes: New examples of mononuclear single-molecule magnets. *J. Am. Chem. Soc.*, 2013, **135**, 13737–13748.
- [S15] G. P. Bernardini, D. Borrini, A. Caneschi, F. Di Benedetto, D. Gatteschi, S. Ristori and M. Romanelli, EPR and SQUID Magnetometry Study of $\text{Cu}_2\text{FeSnS}_4$ (Stannite) and $\text{Cu}_2\text{ZnSnS}_4$ (Kesterite), *Phys. Chem. Minerals*, 2000, **27**, 453–461.
- [S16] R. Boča, *Current Methods in Inorganic Chemistry, vol. 1, Theoretical Foundations of Molecular Magnetism*, Elsevier, 1999.